REPORT DOCUMENTATION PAGE

Form Approved
OMB No. 0704-0188

The public reporting burden for this collection of information is estimated to average 1 hour per response, including the time for reviewing instructions, searching existing data sources, gathering and maintaining the data needed, and completing and reviewing the collection of information. Send comments regarding this burden estimate or any other aspect of this collection of information, including suggestions for reducing the burden, to the Department of Defense, Executive Service Directorate (0704-0188). Respondents should be aware that notwithstanding any other provision of law, no person shall be subject to any penalty for failing to comply with a collection of information if it does not display a currently valid OMB control number.

PLEASE DO NOT RETURN YOUR FORM TO THE ABOVE ORGANIZATION.

1. REPORT DATE *(DD-MM-YYYY)*	2. REPORT TYPE	3. DATES COVERED *(From - To)*
20-12-2011	Final	June 2010-Dec. 2011

4. TITLE AND SUBTITLE
Magnesium Aluminum Borides as Explosive Materials

5a. CONTRACT NUMBER

5b. GRANT NUMBER

5c. PROGRAM ELEMENT NUMBER

6. AUTHOR(S)
Whittaker, Michael L.
Cutler, Raymond A.

5d. PROJECT NUMBER
DOTC-10-01-INIT116

5e. TASK NUMBER

5f. WORK UNIT NUMBER

7. PERFORMING ORGANIZATION NAME(S) AND ADDRESS(ES)
Ceramatec, Inc.
2425 South 900 West
Salt Lake City, Utah 84119

8. PERFORMING ORGANIZATION REPORT NUMBER
RD-R-060-NB

9. SPONSORING/MONITORING AGENCY NAME(S) AND ADDRESS(ES)
Dr. Paul E. Anderson
ARDEC
Building 3028, Room 40
Picatinny Arsenal, NJ 07806-5000

10. SPONSOR/MONITOR'S ACRONYM(S)

11. SPONSOR/MONITOR'S REPORT NUMBER(S)

12. DISTRIBUTION/AVAILABILITY STATEMENT
Distribution unlimited

13. SUPPLEMENTARY NOTES

14. ABSTRACT

Metal borides and boron carbide reacted with Al were compared to B, Mg, Al, Mg-Al and Si as potential fuel additives. Stoichiometric physical mixtures of powders corresponding to unreacted boride compounds were also investigated in comparison to the compounds. Submicron boron was used, which resulted in very fine particle sizes for all materials studied. It was demonstrated that boride compounds were less sensitive to low-temperature oxidation in flowing air than the powder mixtures or metallic fuels. Compounds with high mole fractions of boron were generally less sensitive, but their high temperature oxidation behavior showed no improvement over boron. Cylinder expansion testing of MgAlB14 exposed its poor performance in an energetic mixture. However, aluminum and magnesium diborides had relatively low sensitivity and also exhibited mechanisms to increase the rate of boron oxidation at high temperatures, showing promise as insensitive high-energy-density fuel additives. Detonation calorimetry results suggest that AlB2 released approximately 50% more heat per gram than Al +2B and underwent complete reaction. These results warrant further testing of the diboride compounds in energetic formulations. Inexpensive B4C/Al mixtures also warrant testing.

15. SUBJECT TERMS

16. SECURITY CLASSIFICATION OF:			17. LIMITATION OF ABSTRACT	18. NUMBER OF PAGES	19a. NAME OF RESPONSIBLE PERSON
a. REPORT	b. ABSTRACT	c. THIS PAGE			Raymond A. Cutler
U	U	U	SAR	105	19b. TELEPHONE NUMBER *(include area code)* (801) 978-2126

Reset

Standard Form 298 (Rev. 8/98)
Prescribed by ANSI Std. Z39.18
Adobe Professional 7.0

Table of Contents

List of Figures

List of Figures (continued)

List of Tables

I. Introduction and Literature Survey

The most common compounds formed from boron are boron carbide (B_4C) and boron nitride (BN), which are generally not considered borides but which are included here since they are commercially available as high-quality powders. Borides are generally considered as compounds combining one, or more, metals with boron. Strong covalent bonding allows many of these borides to have high melting or decomposition temperatures, such that they can be used in reducing environments. LaB_6, for example, is used as a replacement for W in thermoionic emitters, such as the filaments for electron microscopes, due to its high melting point and low work function. BN is used as a crucible material in its hexagonal form and as a cutting tool in its cubic state. B_4C is used as an armor material due to its low specific gravity. A comprehensive survey of borides was performed by Cutler[1] based primarily on the earlier data of Samsonov and Vinitskii[2] and is still the best literature source for the properties of borides. Other excellent reviews include the work of Lundstrom[3] as well as information on ternary borides as discussed by Nowotny and Rogl[4]. Williams gives data on selected borides[5]. Borides are processed like other non-oxide ceramics, using methods well known in the literature[6-11].

Interest in boron as an energetic material is the result of its high heat of combustion per unit volume of reactants[12]. B has a lower heat of combustion than Al or Mg when compared on a volume basis. Hsia[12] tested a number of Li, Al, and Mg borides compared to pure B, showing that MgB_{12} and LiB_2 were completely oxidized with relatively short ignition delays compared to B. Diborides decompose into elemental metal and dodecaborides during the heating process, making the higher borides more attractive since the decomposition process is endothermic. Aluminum dodecaboride (AlB_{12}) is an interesting material since there is still some confusion over whether it melts congruently or incongruently and whether or not it undergoes a polymorphic transition at 1550ºC (see Figure 1). Hsia argued that compounds that do not undergo decomposition reactions are better choices for rocket propellants since the endothermic decomposition reaction is undesired. The endotherm for AlB_2 decomposition, however, is small[13], especially when compared to the heat of combustion such that this is not an issue.

Unfortunately, the choice of fuel is not as simple as just looking at the thermochemical data available since impurities, surface coatings, particle shape, degree of agglomeration, other components of the explosive mixture, and degree of mixing also affect combustion. For example, Yeh and Kuo[14] confirmed that combustion of fine boron particles in air occurs by two stages due to the oxide layer found on the surface of boron particles. The first stage corresponds to burning of the boron particle while it is still covered in a pre-existing oxide layer. Boron diffuses outward much faster than O_2 diffuses inward, and $B_2O_{3\,(l)}$ and dissolved boron form a vitreous polymeric complex $[BO]_n$ on the surface of particle. Through reactions with O_2 and H_2O, this complex is vaporized into BO_2 (g) and HOBO (g)[14]. The second stage is the combustion of the exposed, 'clean', boron particle. Removal of the liquid oxide layer plays an important role in ignition and combustion[14]. $B_2O_{3(l)}$ melts at 450°C, but doesn't boil until 2043°C. Elemental boron melts at 2075°C and sublimes at 2550°C. Because boron oxide boils at a lower temperature than boron itself, combustion occurs on the outside of the boron particle

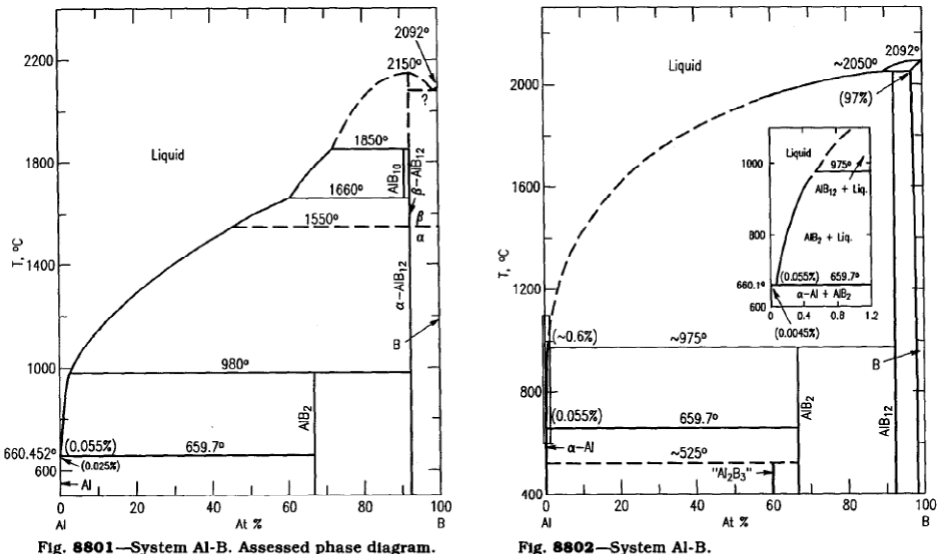

Fig. 8801—System Al-B. Assessed phase diagram.

Fig. 8802—System Al-B.

Figure 1. Comparison of two phase diagrams for the Al-B system[15]. Figure on left is from Carlson[16] and right-hand diagram is from Rogl and Schuster[17].

first. In contrast, the oxides of magnesium, lithium and aluminum boil at a higher temperature than the respective metal[12]. The $B_2O_{3(l)}$ layer on boron particles, in contrast to particles of aluminum, tends to be self-healing and almost no 'clean' boron is in contact with the gas phase until the oxide layer is completely removed[18]. Without added metals, boron ignites around 1200-1600°C[18], but the ignition temperature and burning rate of boron particles are dependent on many factors. Macek and Semple[19] showed that burning time is proportional to the square of the particle diameter. Li[20] found, based on light intensities that the particle size change is negligible in the first stage of combustion and decreases linearly with time during the second stage. Therefore, the second stage of combustion controls burning time of the particle. Increasing ambient gas temperature decreases ignition delay times[20]. It has been shown that the addition of water vapor to the gas surrounding a boron particle decreases the burning time substantially[13]. Crystalline boron is more difficult to ignite than amorphous boron[13].

Energetic materials, however, are composed of fuel and oxidizers with the metal component being a minor ingredient in many instances[21]. If one were changing an energetic formulation by substituting B for Al, for example, one would not add the same number of atoms. This is easily understood by thinking about substituting AlB_2 or AlB_{12} into a mix since substituting equal numbers of boride molecules for metal atoms makes no sense. It is tempting when making comparisons with energetic formulations to make substitutions on a mass basis. However, if one were to substitute heavy metals, such as W or Mo for light metals like B, Mg, and Al it would be obvious that this would not be the right approach either. For energetics with a fixed geometry, substitutions on the basis of volume make the most sense. Even this is problematic, however, since B is not atomized and fine particles pack very differently than atomized Al and Mg as they are currently used in most energetic formulations. The efficiency of burning must also be considered since many large metal powders are not completely consumed

in the reactions which occur. While the data presented compare materials on a mass or volume basis, it must be remembered that test results are much more important than predictions and it will be critical to this program that test results can guide this effort.

A common area of concern in energetic materials is making the formulation insensitive yet still allowing for short delay times and high energy once detonation occurs[22]. Formulations are considered sensitive if they are susceptible to electrostatic discharge or are too easy to ignite. It is for this reason that fine Al and Mg powders are not used in most formulations. Fine B is considered insensitive, but has a long delay. Early work by Hsia[12] showed that many metal borides can be ignited without ignition delays and that they ignite at lower temperatures than elemental boron. LiB_2 and MgB_{12} were able to be burned without ignition delay to near 100 % efficiency. Since these borides are much less sensitive then Li and Mg, it is clear that the direction of this development effort is to determine the advantages of using metal borides as compared to sensitive metals.

Methods for lowering the ignition temperature of boron particles include using a halogen containing environment, putting on a thin metallic or LiF coating[13]. Faeth[23] suggested LiF could be used as a coating on B, likely based on the earlier work of Schmotolocha and Edelman[24] who added Mg and LiF to boron slurry fuels. The use of LiF is based on the concept that it aids in the oxide removal as[13]

$$B_2O_{3(l)} + LiF_{(l)} \rightarrow LiBO_{2(l,g)} + BOF_{(g)} \quad (1)$$

Having metals such as Li and Mg intimately mixed with boron may therefore be advantageous and eliminate the need for a coating. The passivation which occurs due to oxide layers on particles may be advantageous in allowing fine particles to still be insensitive.

Crystal Structure

All crystalline boron is either rhombohedral or tetragonal, with large numbers of atoms ($12 \leq Z \leq 315$) making up a single unit cell. The high melting point comes as a result of the

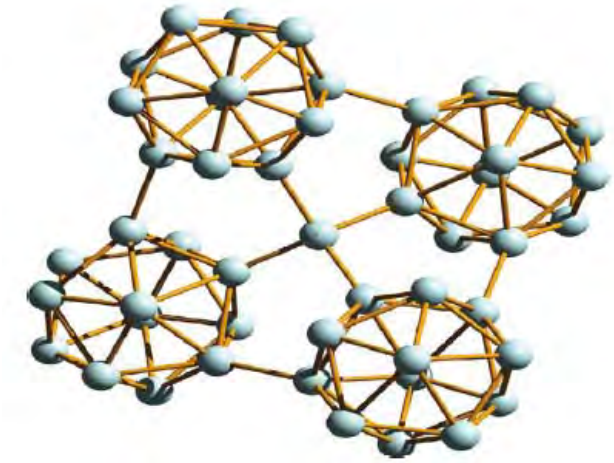

Figure 2. Structure of tetragonal boron composed of four icosahedra bonded by boron[25]. Boron has a high melting point due to the strong covalent bonding between atoms.

covalent bonding between atoms. One such structure contains 50 B atoms by connecting four icosehedra with boron atoms as shown in Figure 2[25]. Metal borides of the types M_2B, MB, MB_2, MB_4, MB_6, and MB_{12} account for 75 % of all borides[25]. Many of these are composed of the same type of icosahedra as shown in Figure 3 where $MgAlB_{14}$ has the same orthorhombic crystal structure as MgB_{12} or AlB_{12}.

The hexagonal crystal structure of materials like LiB[27,28], MgB_2, and AlB_2 is of interest since they are not composed of icosahedra but rather has alternating layers of boron and metal atoms as shown in Figure 4[26]. These layered structures do not have the same lubricity that hexagonal BN has, but decompose at relatively low temperatures. It is presently unclear whether there is a preferred crystal structure for energetic borides since the layered structures have the penalty of decomposition, which is endothermic, associated with them.

The largest deterrent to the use of boron in energetics is cost. Boron is not found free in nature but borates are extensive with large deposits of borax in Turkey. The mineral rasorite is found in the Mojave Desert of California. These hydrated sodium borates are reduced to form boron[29]. H. C. Starck's amorphous boron currently sells for $165-220/kg compared to $22/kg for Al (grade H-30 from Valimet) or $30/kg for atomized Mg (Hart Metals). Lower cost materials are available from China. The least expensive non-oxide source of boron is B_4C powder, which sells for about $20-40/kg. Any high value use of borides will result in a similar price if the same volume of market is developed. There is no production of MgB_2 or AlB_2 powders at the present time, which make such powders prohibitively expensive. This means that the performance of boron-based powders must be substantially better than metallic powders or non-oxide powders.

Lithium Substitutions

Lithium borides are the least studied of the borides in part due to the difficulty in making such compounds and their reactivity with water[30]. There is no phase diagram, but the literature mentions a number of compounds including LiB[27,28], Li_5B_4[31], LiB_2[12], Li_3B_{14}[32], $LiB_{12.93}$[33], and $Li_{1.8}B_{14}$[32], and LiB_{12}[12]. It is also possible to substitute Li for Mg making $LiAlB_{14}$[34, 35], an orthorhombic analog to $MgAlB_{14}$, making $Li_xMg_{1-x}AlB_{14}$ compounds a possibility. Synthesis of these compounds can be performed at relatively low temperatures[36-37].

Comparative Properties

In order to down select to a few compounds it is necessary to compare properties. Table 1 gives atomic weight, theoretical density, crystal structure, melting temperature and relative cost for selected metals, while Table 2 gives the heats of combustion (molar, mass, or volume basis) and heat capacities for these same materials based on data from Barin[38]. Boron has a low heat of combustion both on a volume and a weight basis. Silicon should be a better fuel than or comparable to Mg or Al when the same volume of material is substituted. The combustion reactions considered were sent to Dr. Paul E. Andersen of ARDEC as a spreadsheet.

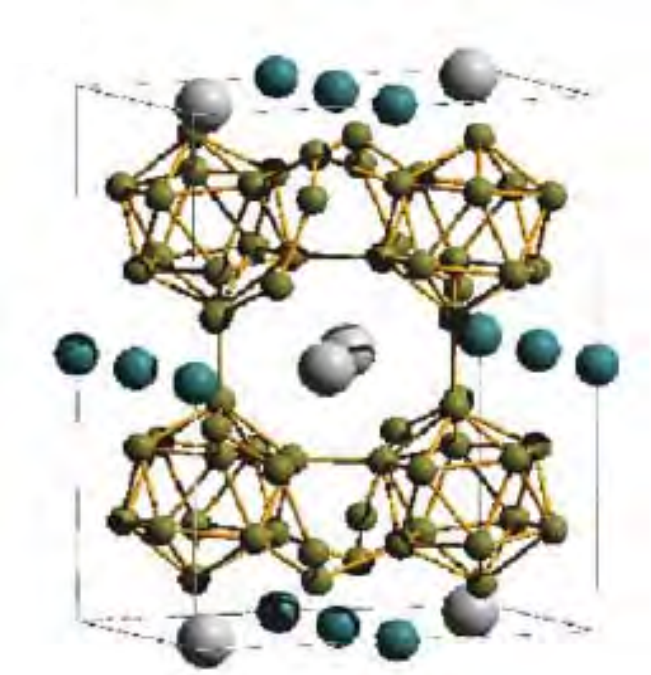

Figure 3. Unit cell of $MgAlB_{14}$ showing B which are mainly tied up as four B_{12} icosahedra with boron atoms connecting them. Al (large white atoms) and Mg (smaller blue-green atoms) occupy specific sites in this orthorhombic structure[25].

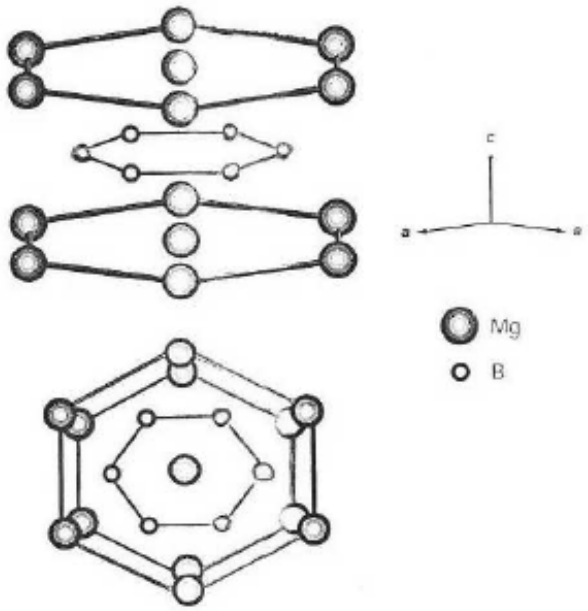

Figure 4. Hexagonal structure of MgB_2, which consists of a hexagonal close packed arrangement of B and Mg alternating layers with a P6/mmm space group[26].

Table 1
Physical Properties and Cost of Selected Metals

Metal	At. Wt. (g/mol)	Theoretical Density (g/cc)	Crystal Structure	Melting Temperature (°C)	Relative Cost
Al	26.98	2.70	Cubic	660	Low
B	10.81	2.34	Rhombohedral	2077	High
Co	58.93	8.90	Hexagonal	1768	Medium
Fe	55.85	7.87	Cubic	1495	Low
Li	6.94	0.53	Cubic	181	Medium
Mg	24.31	1.74	Hexagonal	649	Low
Ni	58.69	8.90	Cubic	1455	Medium
Si	28.09	2.42	Cubic	1412	Low
Ti	47.87	4.54	Hexagonal	1666	Medium
Zr	91.24	6.51	Hexagonal	1852	High

In order to do this same thing for boron-containing compounds, it was necessary to review a substantial body of literature[1-110]. Table 3 gives the corresponding data for borides that Table 1 gives for metals. Likewise, Table 4 is the analog to Table 3 with the exception that the heats of formation for the compounds are also given in this table. Unfortunately, reliable thermochemical data are not available for all of the compounds listed in Table 3. These data, however, allow one to compare the metals with the non-metals. In accord with the early work of Hsia[12] these comparisons (see Figure 5) suggest that metal borides are competitive with the metal powders relative to their heats of combustion. B and AlB_{12}, for example, both lie near the bottom of both charts, which is desirable since a low heat of combustion is preferred.

Table 2
Thermochemical Properties of Selected Metals at 1000 K

Metal	ΔH_c (kJ/mol)	ΔH_c (kJ/g)	ΔH_c (kJ/cc)	C_p (J/mol K)
Al	- 847.0	-31.4	- 84.7	31.8
B	- 618.5	-57.2	-135.5	25.0
Co	- 902.3	-15.3	-136.3	36.9
Fe	- 403.3	- 7.2	- 56.9	54.4
Li	- 302.2	-43.5	- 23.2	28.9
Mg	- 608.9	-25.1	- 43.6	32.6
Ni	- 235.0	- 4.0	- 35.6	33.0
Si	- 905.1	-32.2	- 75.1	26.3
Ti	- 750.0	-15.7	- 71.1	32.5
Zr	-1091.0	-12.0	- 77.9	31.1

Table 3
Physical Properties and Cost of Selected Compounds

Compound	Molecular Weight (g/mol)	Theoretical Density (g/cc)	Crystal Structure	Decomposition/Melting Temperature (°C)	Relative Cost
AlB_2	48.6	3.17	Hexagonal	1400	High
AlB_{10}	135.1	2.54	Orthorhombic	1850	High
AlB_{12}	156.7	2.58	Tetragonal	2150	High
B_4C	55.3	2.52	Rhombohedral	2470	Low
h-BN	24.8	2.26	Hexagonal	1927	Medium
CoB	69.7	6.77	Orthorhomcic	1460	High
Co_2B	128.7	8.06	Tetragonal	1280	High
Co_3B	187.6	8.17	Orthorhombic	>1200	High
$LiAlB_{14}$	185.3	2.50	Orthorhombic	---	High
MgB_2	45.9	2.63	Hexagonal	1545	High
MgB_4	67.5	2.8	Orthorhombic	1735	High
MgB_6	89.2	2.8	Tetragonal	---	High
MgB_7	100.0	2.7	Orthorhombic	2150	High
MgB_{12}	154.0	2.7	Orthorhombic	2071	High
$Mg_{.5}Al_{.5}B_2$	47.3	2.9	Hexagonal	---	High
$MgAlB_{14}$	190.5	2.75	Orthorhombic	---	High
NiB	69.5	7.2	Orthorhombic	1308	High
Ni_2B	80.3	8.05	Tetragonal	1398	High
Ni_3B	91.1	8.1	---	1429	High
Ni_4B_3	267.2	7.58	Orthorhombic	1853	High
SiB_3	60.5	---	---	---	High
SiB_4	71.3	2.42	Rhombohedral	---	High
SiB_6	93.0	2.17	Cubic	---	High
TiB	58.7	4.56	Orthorhombic	2190	High
TiB_2	69.5	4.52	Hexagonal	3225	Medium
Ti_3B_4	186.8	4.56	Orthorhombic	---	High
Ti_2B_5	149.8	4.63	Hexagonal	---	High
ZrB	102.0	6.48	Cubic	2800	High
ZrB_2	112.8	6.10	Hexagonal	3245	Medium
ZrB_{12}	221.0	3.63	Cubic	2250	High

As long as sensitivity is not an issue, one would also like the melting temperature to be low since this should aid in ignition. When a compound decomposes, this will only speed up diffusion if it decomposes into at least one molten component. For example, when MgB_2 decomposes, it forms Mg and MgB_4, but when MgB_4 decomposes, it only forms two solid forms (see Figure 6). In the case of MgB_4 decomposition, the endotherm only penalizes the material, whereas, MgB_2 decomposition allows a way for the reaction to initiate.

Table 4
Thermochemical Properties of Selected Compounds at 1000K

Compound	$\Delta H_f^{o}{}_{1000\ K}$ (kJ/mol)	$\Delta H_{c,1000\ K}$ (kJ/mol)	$\Delta H_{c,1000K}$ (kJ/g)	$\Delta H_{c,1000K}$ (kJ/cc)	$C_{p,\ 1000K}$ (J/mol K)
AlB_2	-165.2	-1919	-39.5	-125.1	78.2
AlB_{12}	-289.0	-7980	-50.9	-131.4	317.8
B_4C	- 73.1	-2796	-50.6	-127.5	114.3
h-BN	-254.8	- 529	-21.3	- 48.2	44.4
CoB	- 96.2	-1425	-20.4	-138.3	56.5
Co_2B	-128.7	-2295	-17.8	-143.7	89.3
MgB_2	-106.6	-1739	-37.9	- 99.6	71.7
MgB_4	-126.6	-2958	-43.8	-122.6	115.7
$Mg_{.5}Al_{.5}B_2$	-135.9	-1829	-38.7	-112.2	---
$MgAlB_{14}$	-395.6	-5390	-28.3	---	---
TiB	-162.0	-1207	-20.6	- 93.8	51.9
TiB_2	-326.7	-1660	-23.9	-108.0	77.1
ZrB_2	-325.4	-2003	-17.7	-108.3	72.0

One interesting observation is that boron carbide, a commercially available material, is similar in position to AlB_{12}, yet boron carbide is much less expensive. While there is no need to synthesize boron carbide, it is clear that this material should be included as a control, along with Al, Mg, and B. Similarly, Co is readily available due to its use in cemented carbides and should also be included in comparative testing.

Selection of Four Borides for Initial Testing

It is recommended that the four borides provided for initial testing be $MgAlB_{14}$, $Mg_{0.5}Al_{0.5}B_2$, AlB_{12}, and AlB_2-Al. In addition to testing these in comparison to Al, Mg, B, and Co, as mentioned above, they should also be compared to the respective chemistries of the elements in each of the four borides on a volume basis. $MgAlB_{14}$ and $Mg_{0.5}Al_{0.5}B_2$ represent icosohedrally-bonded orthorhombic and layered hexagonal structures, respectively. They both contain the same three elements, but one undergoes a low-temperature decomposition ($Mg_{0.5}Al_{0.5}B_2$) and the other one is believed to melt congruently. The $Mg_{0.5}Al_{0.5}B_2$ compound is a solid solution of MgB_2 and AlB_2 and should represent these two compounds. One would expect it to appear in between the magnesium and aluminum diborides in Figure 5. AlB_{12} is included since it allows a good comparison with the $MgAlB_{14}$ and also connects back to the early work of Hsia[12]. Finally, it is believed that having free Al metal may be advantageous for the diborides since melting of the Al may help with the combustion reaction prior to decomposition.

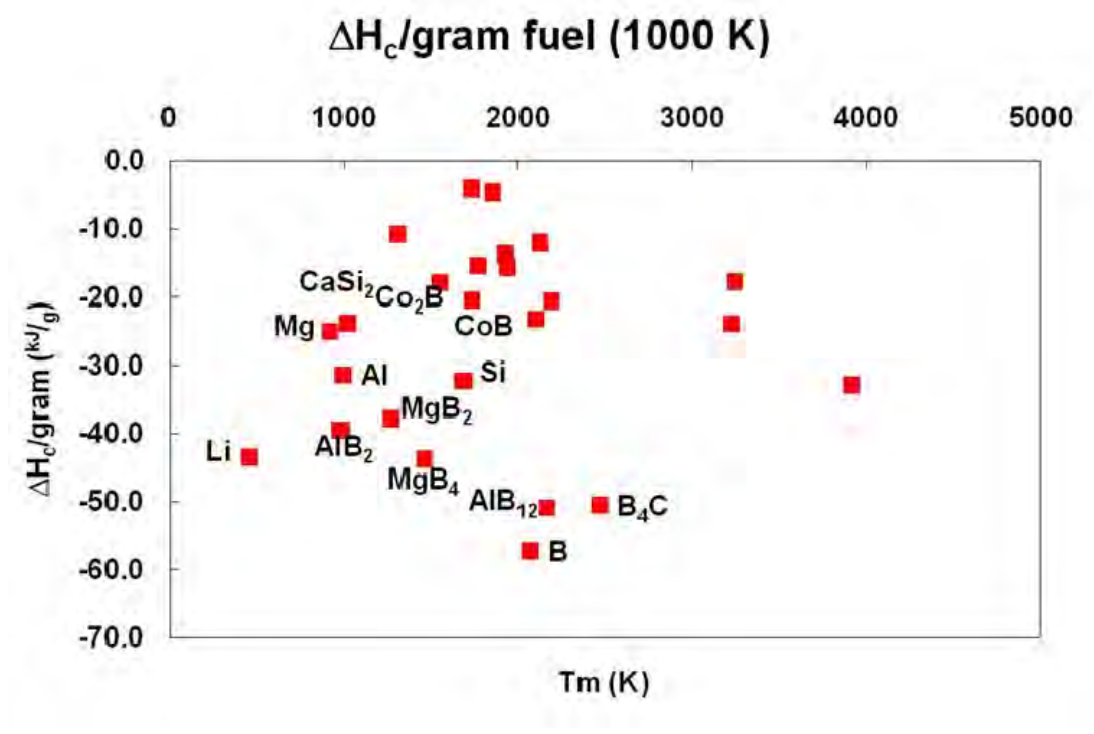

(a)

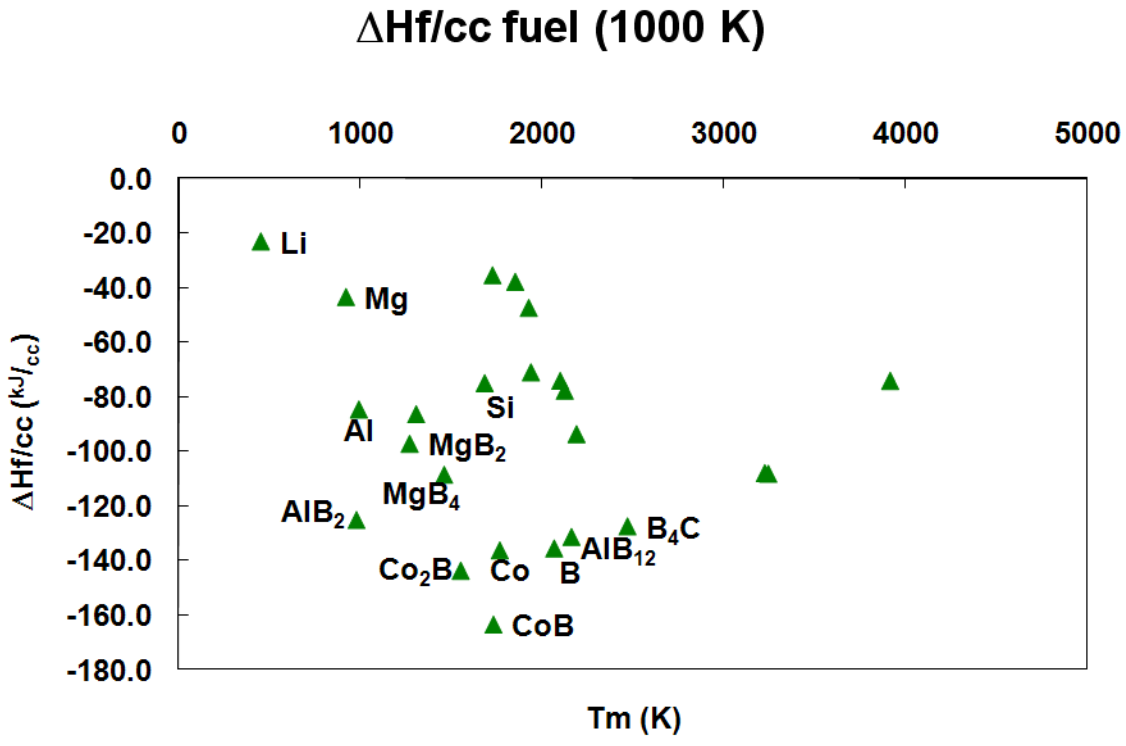

(b)

Figure 5. Heats of combustion on a (a) mass or (b) volume basis for selected metals and boron-containing compounds as a function of their melting or decomposition temperature.

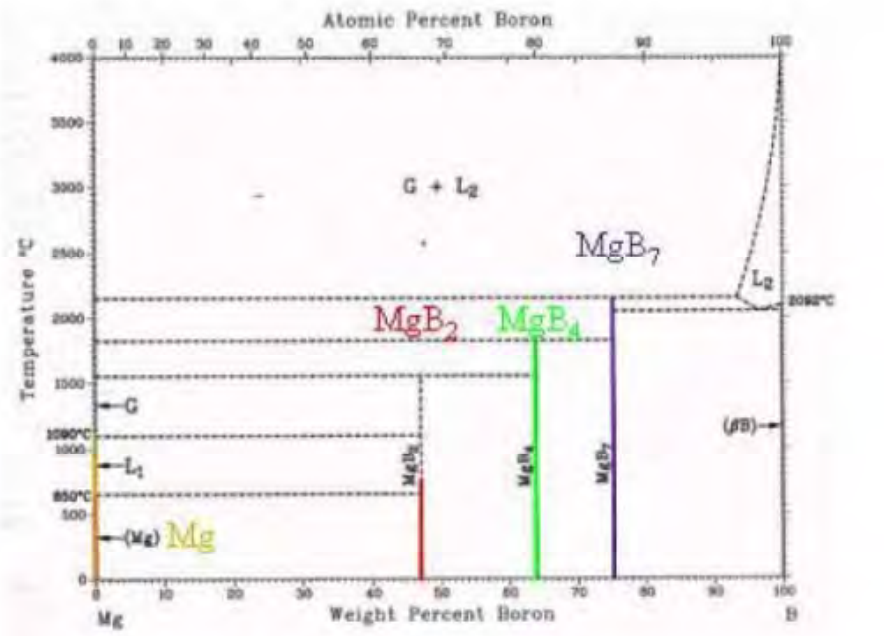

Figure 6. Mg-B phase diagram showing MgB_2, MgB_4, and MgB_7[39].

The reason for not including $LiAlB_{14}$, for example, is that it is unknown at the present time if ignition delay is an issue. If it is, then incorporation of lithium can be pursued. If not, there is no need to add a metal that is known to have sensitivity issues.

An important issue is that ARDEC establish a fast way to evaluate samples supplied by Ceramatec and that a methodology for screening be established. Ceramatec can likely supply more candidate materials if there is a way to get fast feedback from the Army. It is necessary in this first stage to determine if metal borides are advantageous over boron carbide. It is also possible that boron carbide-metal (or metal boride) fuel mixtures can be explored.

II. Characterization of Initial Borides Delivered to ARDEC

Four materials were selected from the prospective materials investigated in the literature survey. These four materials were prepared in two particle sizes and were shipped to ARDEC on October 5, 2010, along with their constituent raw powders and starting mixes. Characterization data included composition, crystal structure, particle size, particle surface area, particle morphology and oxidation characteristics by thermal gravimetric analysis and differential thermal analysis. The four materials selected in conjunction with Dr. Paul Anderson of ARDEC were AlB_2, MgB_2, $Al_{0.5}Mg_{0.5}B_2$ and $AlMgB_{14}$. Each of these materials was milled and screened to produce two particle sizes, labeled -230 mesh and -325 mesh.

X-ray diffraction of AlB_2 (Figure 7) shows that the powder sent to ARDEC contained two major phases, AlB_2 and excess aluminum. Note that Ceramatec has been able to make AlB_2 powder with varying amounts of free aluminum. It is thought that this free aluminum aids the oxidation of AlB_2 by initiating a liquid phase at a temperature (660°C) lower than the

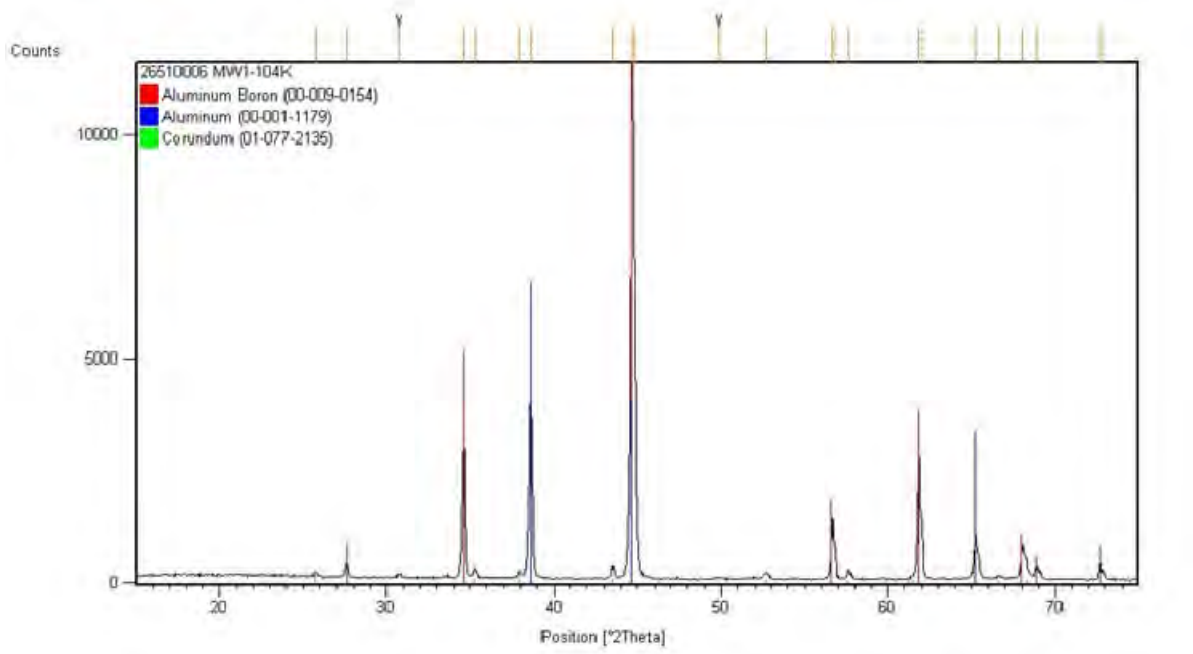

Figure 7. X-ray diffraction of AlB_2. The sample delivered to ARDEC contains approximately 10 wt % free Al. Red lines mark AlB_2, blue lines Al, and green lines Al_2O_3.

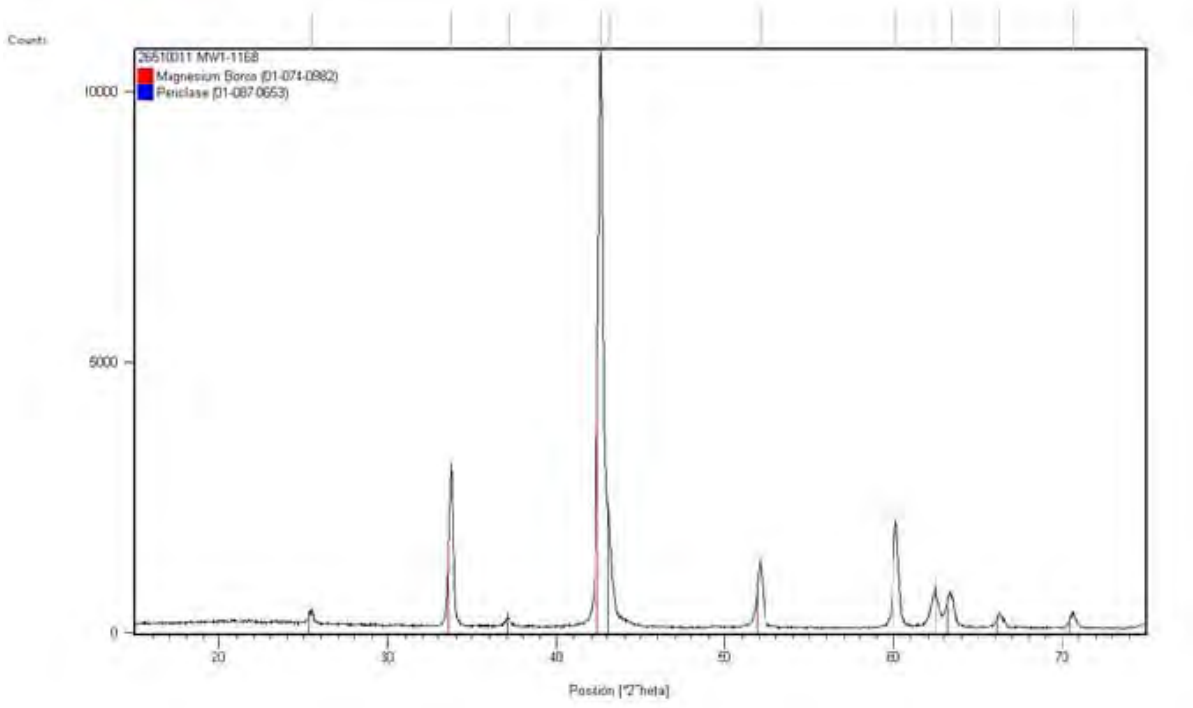

Figure 8. X-ray diffraction pattern for MgB_2, which has the same crystal structure as AlB_2. Red lines mark MgB_2 while blue lines mark MgO.

decomposition temperature of AlB_2 (980°C). It has been suggested that the oxidation of boron and metal borides is kinetically limited by the formation of a viscous B_2O_3 layer on the surface of boron or boride particles [12,14,18] which may be reduced by the presence of liquid aluminum. MgB_2 has a similar XRD pattern (see Figure 8), with peak locations shifted slightly due to small differences in lattice parameters from AlB_2. There is no free Mg detected in this pattern and very little MgO. Rietveld fitting estimates that MgO is about 6 wt. %. $Mg_{0.5}Al_{0.5}B_2$ has the same hexagonal structure as AlB_2 and MgB_2. Figure 9 shows this XRD pattern, which fits in between the AlB_2 and MgB_2 patterns since all three materials are isostructural. The $Mg_{0.5}Al_{0.5}B_2$ powder supplied had a small amount of free aluminum.

The only non-hexagonal boride supplied was $MgAlB_{14}$. The large number of peaks in Figure 10 is a result of the orthorhombic crystal structure, which is comprised of B_{12} icosahedra with metal atoms bonded between the icosahedra. In addition to $MgAlB_{14}$, secondary phases included $MgAl_20_4$ free Al. Rietveld fitting gave these amounts as 4% and 2%, respectively.

Particle size and surface area measurements were preformed on each powder and the results are summarized in Table 5. Samples were measured by laser light scattering using a Coulter LS230 particle analyzer and were dispersed in 2-propanol using 0.25 wt. % of a commercial phosphate ester (RE-610) made by Rhodia (Cranbury, NJ) and calculated using Fraunhofer optical diffraction[111]. Despite using the dispersant in combination with ultrasonic energy the laser light measures agglomerate size if particles adhere. The particle size distributions are shown in the appendix.

Surface area measurements are a more reliable indicator of the ultimate particle size since they are not influenced by the choice of dispersant, the dispersing medium, or the operator technique. Multipoint BET measurement is insensitive to operator error. A calculation of particle size was made based on the surface area of the particles using the equation

$$d = \frac{6}{\rho \cdot SA} \quad (2)$$

where d is the particle diameter, ρ is the density of the material in g/cc and SA is the surface area in m^2/g. Equation (2) assumes that all particles are spherical and monosized, which is a poor assumption. However, it is a better estimate of the particle size than the laser light scattering, which measures agglomerates instead of ultimate particles. Based on the SEM images of the reacted powders, Equation (2) seems to be a more accurate approximation of the true particle size. This would suggest that there are only slight differences in average particle size between the -230 and -325 mesh and that all of the powders are less than 10 μm in diameter.

Particle size and surface area data (see Table 5) show that the boron starting powder is submicron in size. Consequently, powder mixes with the boron powder were also very fine (see Figure 11). Milling primarily mixed powders without changing particle size. The powder mixes provided are therefore a distribution of metal powders in a boron matrix, as shown in Figure 11. The Al and MgAl powders are made by atomization and are spherical in nature, whereas the Mg is flake-like in its features, allowing these particles to be readily distinguished from the B.

SEM images show that the average particle size is < 10 μm for all reacted powders (see Figure 12). The images also show that these small particles tend to form large agglomerates,

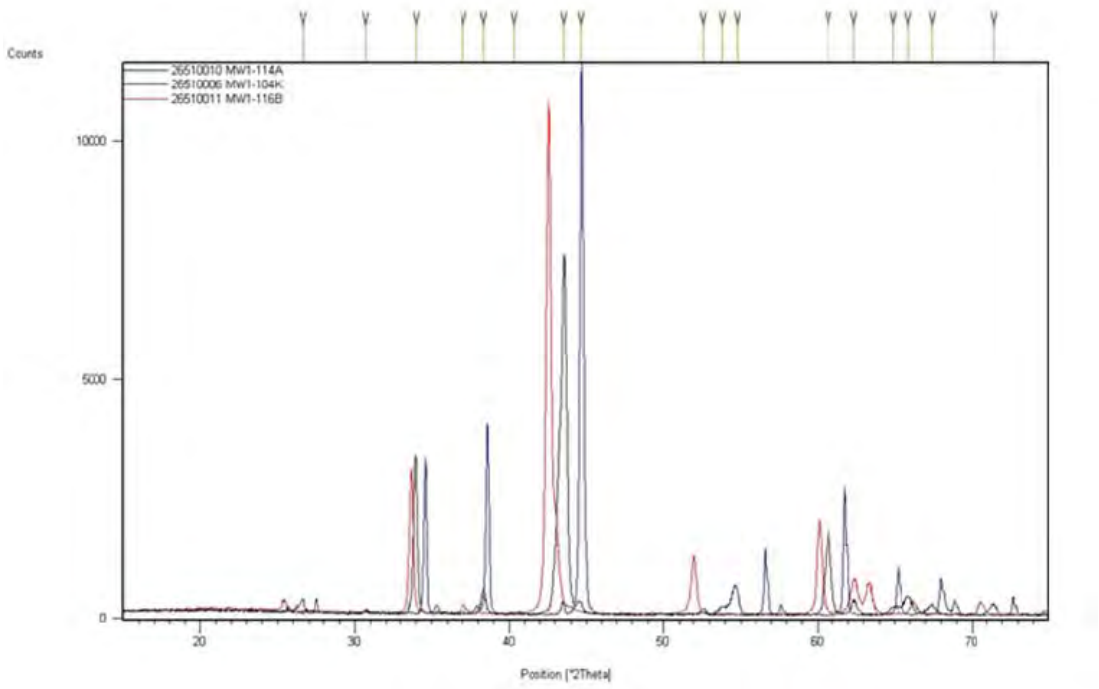

Figure 9. X-ray diffraction patterns of $Al_{0.5}Mg_{0.5}B_2$ (black), AlB_2 (blue), and MgB_2 (red). These materials are isostructural, with only slight differences in atom spacing.

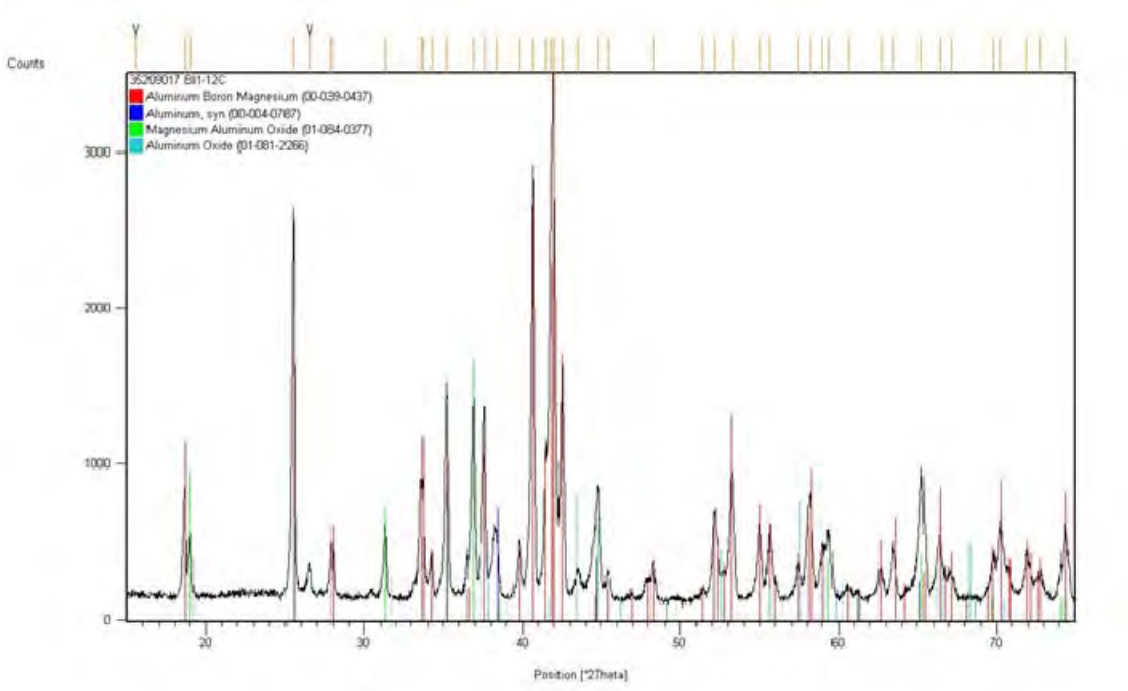

Figure 10. X-ray diffraction pattern of $MgAlB_{14}$. This material contains some $MgAl_20_4$ and free Al.

Table 5
Boride Powder Characteristics

Material	Surface Area (m^2/g)	Particle Size (μm) d_{10}	d_{50}	d_{90}	Mean	Calculated* Average (μm)
B	10.88	0.1	0.2	3.2	1.2	0.2
Al	1.39	0.2	2.9	7.8	3.4	1.6
Mg	0.82	11.9	38.2	66.5	38.6	3.9
Mg-Al	0.40	2.0	10.0	25.9	12.4	6.8
Al + 2B	6.23	0.2	2.3	6.5	2.8	0.4
AlB_2 -230	1.64	0.5	8.4	28.8	11.9	1.2
AlB_2 -325	2.10	0.4	5.4	21.9	8.7	0.9
Mg + 2B	6.73	0.3	8.6	65.4	24.0	0.4
MgB_2 -230	4.78	0.7	9.2	46.0	17.4	0.5
MgB_2 -325	5.55	0.5	1.6	2.9	1.6	0.4
½ MgAl + 2B	5.85	0.1	1.6	5.1	2.0	0.4
$Mg_{0.5}Al_{0.5}B_2$ -230	2.30	0.9	7.3	27.5	11.4	0.9
$Mg_{0.5}Al_{0.5}B_2$ -325	3.15	0.5	1.6	2.9	1.6	0.7
Mg + Al + 14B	7.75	0.1	1.3	4.4	1.8	0.3
$Mg_{0.78}Al_{0.75}B_{14}$ -230	0.55	4.8	14.7	28.2	16.0	4.1
$Mg_{0.78}Al_{0.75}B_{14}$ -325	1.29	0.4	7.5	17.1	8.4	1.8

*Based on Equation (2).

over 100 μm in size. Coupled with the particle size histograms (see Appendix A), this would suggest that screening the reacted powders through a mesh screen with an opening size of 63 μm (230 mesh) or 44 μm (325 mesh) is separating agglomerates of different sizes but the average particle size in each distribution is relatively close. The ultimate particle size of the diboride powders is smaller than $MgAlB_{14}$ due to a lower processing temperature and therefore, less particle growth.

Particle morphology is similar for the three diborides. A range of particle sizes and aspect ratios can be observed. The $MgAlB_{14}$ is more homogeneous in size, with more spherical particles and aspect ratios approaching unity. In all powders it is obvious that the metal powders have melted and wetted the boride particles to some extent. The powders provided are different from metal fuels, such as Al, in that the agglomerates are porous. For this reason is it is very important to compare metal non-porous fuels, such as Al and MgAl to the agglomerated fuels, which include B, Mg, and the synthesized borides. One way to do this is to look at oxidation without an intimate mixture of a polymeric fuel, as occurs in an energetic device. This limits volatility and allows one to see how the particles react with oxygen in air. This was performed using a Netzsch (Burlington, MA) model STA 409 with simultaneous DTA.

Table 6 gives oxidation characteristics of energetic powders after heating in flowing air (≈50 cc/minute) at 10°C/minute to 1500°C, holding for 10 minutes, and cooling at the same rate. Note that from Table 5 the surface area of the powders is not constant and therefore these data

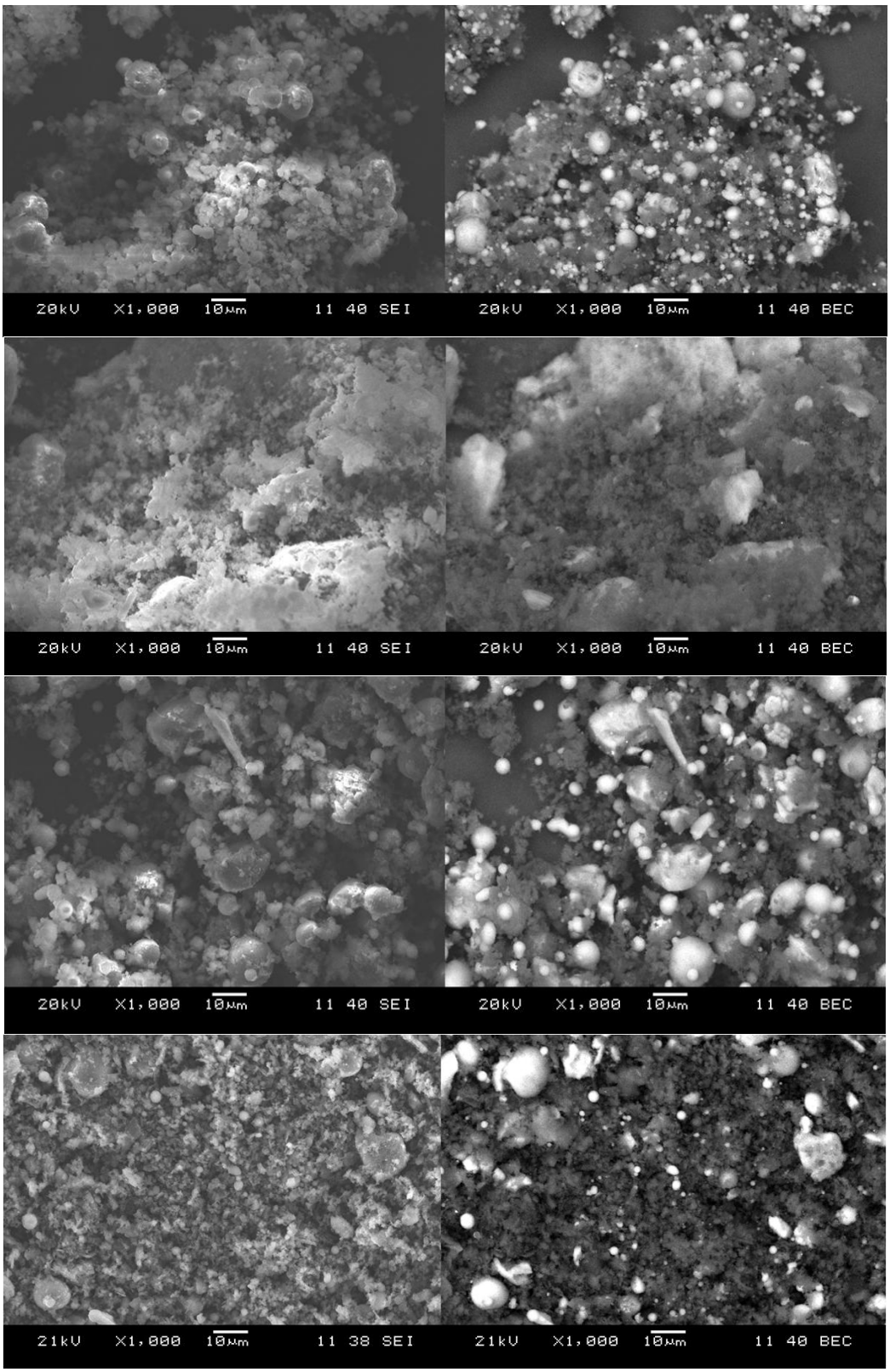

Figure 11. SEM images of starting powders. Top to bottom: AlB_2, MgB_2, $Al_{0.5}Mg_{0.5}B_2$, and $AlMgB_{14}$. Markers are 10 μm with secondary images on left and backscattered images on right.

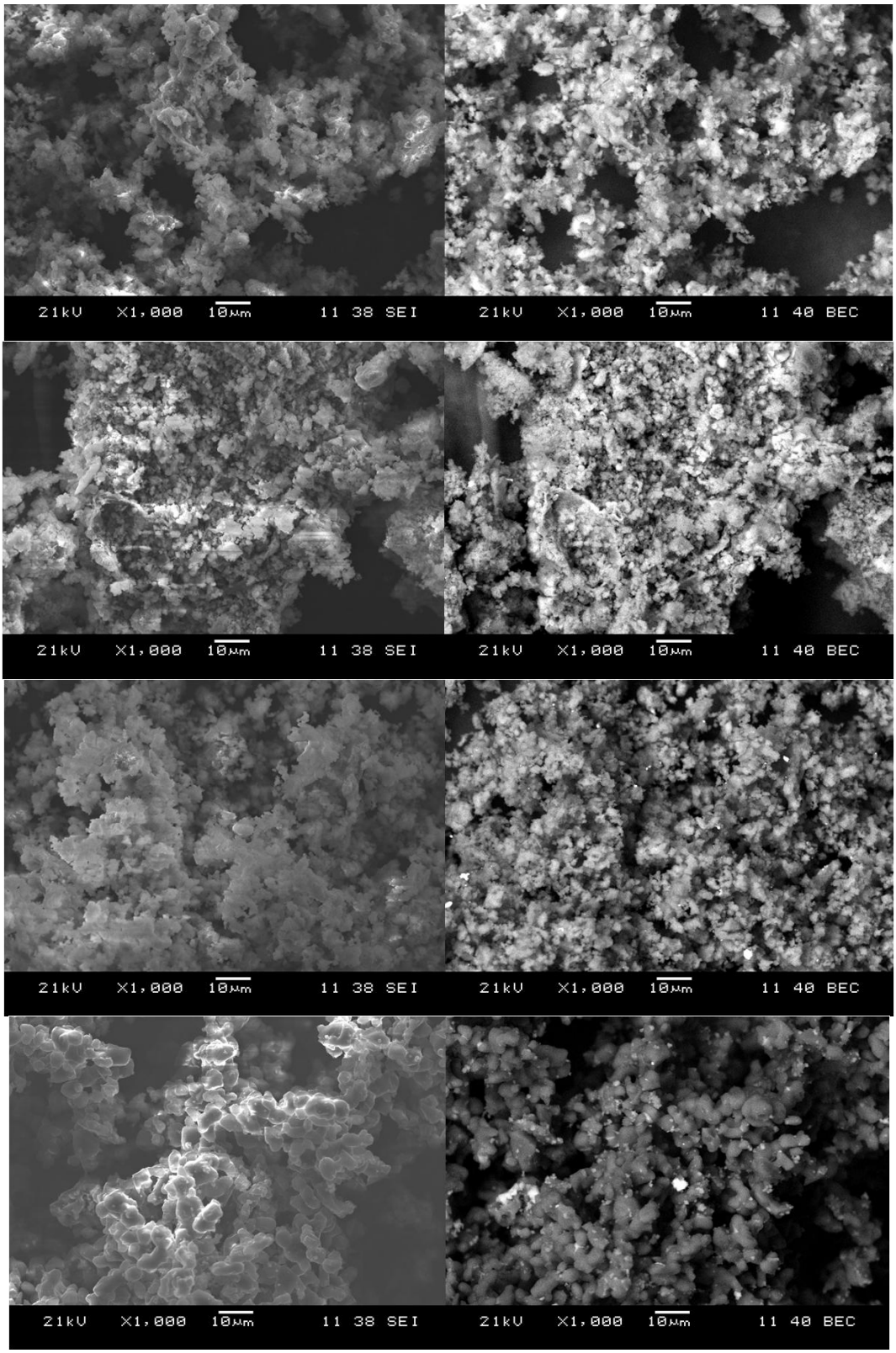

Figure 12. SEM images of reacted powders. Top to bottom: AlB_2, MgB_2, $Al_{0.5}Mg_{0.5}B_2$, and $AlMgB_{14}$. Markers are 10 μm with secondary images on left and backscattered images on right.

Table 6
Boride Powder Oxidation Characteristics

Material	% Actual Mass Change	% Theoretical Mass Change	% of Theoretical	Initiation Temp (C)*	Oxidation Range**
(C)					
B	152	222	69	548	905
Al	89	89	100	583	804
Mg	51	66	77	534	292
Mg-Al	78	77	102	527	520
Al + 2B	141	149	95	577	473
AlB_2 -230	145	149	98	755	505
AlB_2 -325	140	148	95	746	509
Mg + 2B	126	139	91	597	480
MgB_2 -230	126	139	90	673	705
MgB_2 -325	118	139	85	679	628
½ MgAl + 2B	122	146	83	596	765
$Mg_{0.5}Al_{0.5}B_2$ -230	126	146	86	753	726
$Mg_{0.5}Al_{0.5}B_2$ -325	119	146	82	723	748
Mg + Al + 14B	141	186	76	573	927
$MgAlB_{14}$ -230	135	186	73	890	608
$MgAlB_{14}$ -325	109	186	59	740	760

* Initiation temperature is reported as the temperature at 5% mass gain.
** Temperature range in which material goes from 5% to 90% mass gain.

should be discussed in light of their ultimate particle sizes. It must be stated at the onset that these data may have no correlation with what happens in an explosive device.

A number of observations can be drawn from the data in Table 6. Boron, because of its low initial mass, has the highest weight change of any material. For the purposes of calculations it is assumed that weight change can be ascribed solely to oxidation, in which case more weight change translates to more heat released (per unit mass). Therefore, these data reaffirm the thermodynamic calculations presented previously (see Figure 5) in which boron was the best material in terms of ΔH_c per gram. This is expected from a gravimetric measurement like TGA. Following this trend, $MgAlB_{14}$ should have a ΔH_c per gram intermediate to B and AlB_2, in the range of -40 to -50 kJ/g. With a density of 2.58 g/cc, that gives a ΔH_c per cc of -103 to -129 kJ/cc, putting it in the top 5 candidates based on volume. It should be noted that the materials for which thermodynamic data was found (B, Al, Mg, AlB_2 and MgB_2) followed the predicted trend of ΔH_c per gram.

Although boron looks promising in terms of actual weight gain (see Figure 13(a)), its weight gain as a percent of theoretical is the lowest of all materials tested. This can likely be attributed to the amount of oxide on the surface of the fine boron particles initially, which, as previously discussed, inhibit further oxidation at the boron particle surface as temperatures increase and the oxide layer becomes viscous. However, when aluminum is added to boron (in

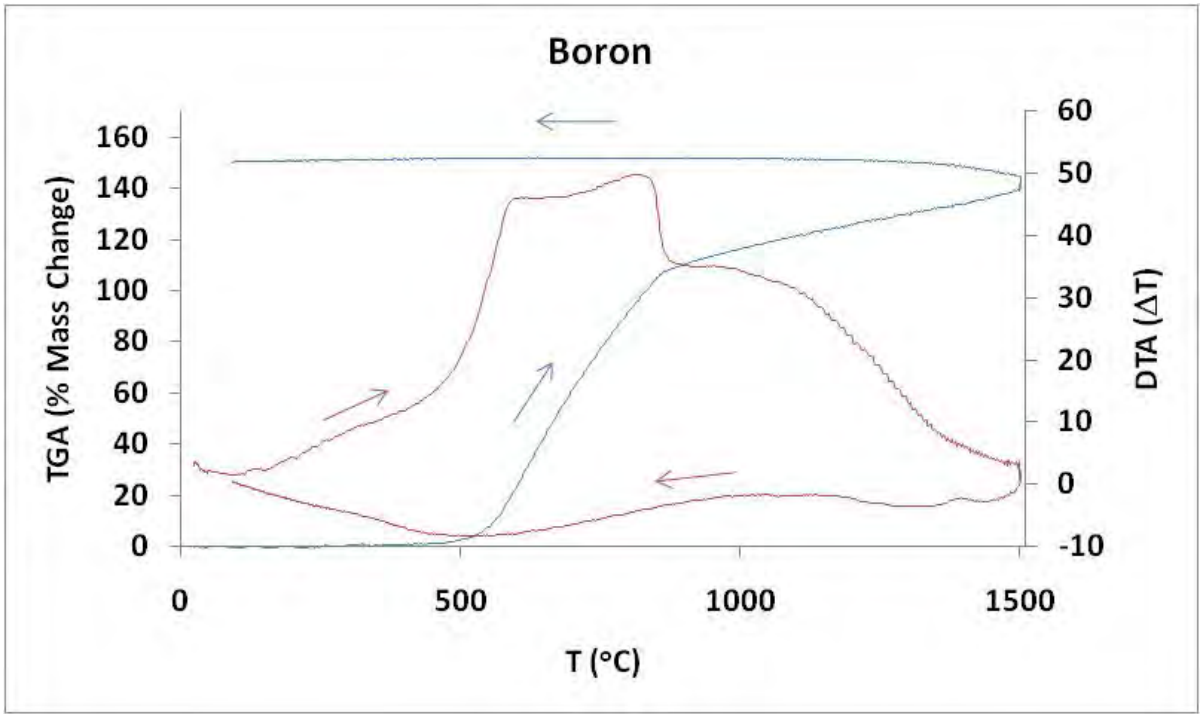

(a)

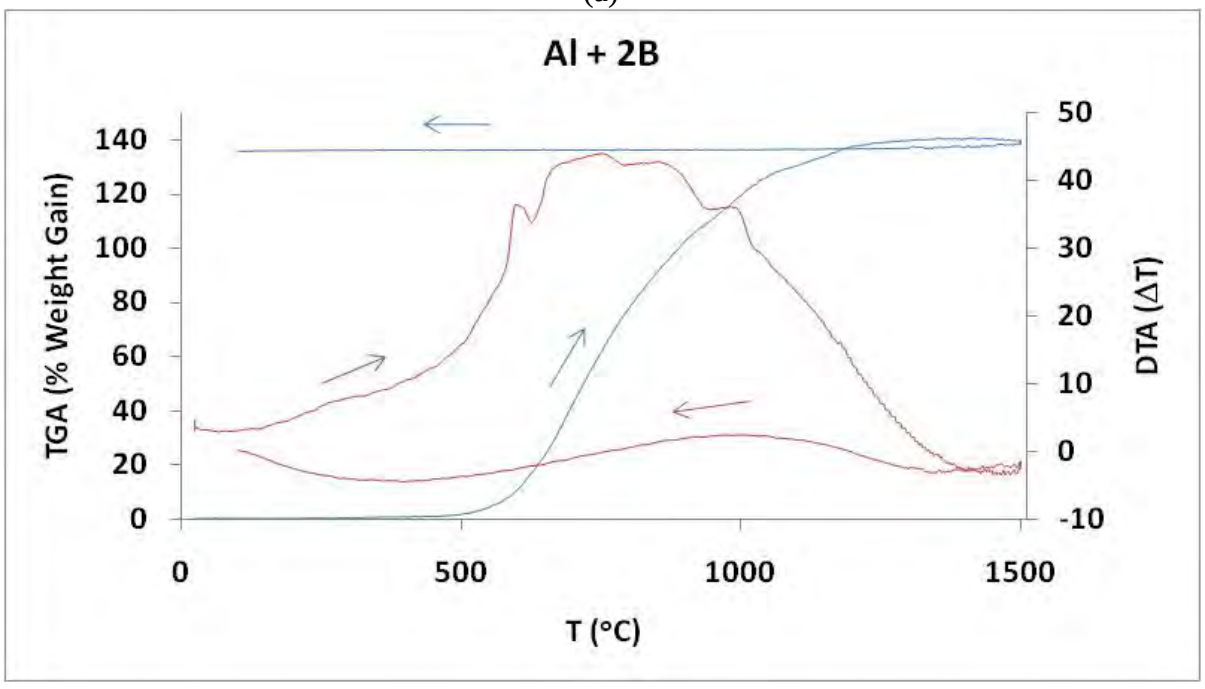

(b)

Figure 13. TGA (blue) and DTA (red) for (a) boron and (b) Al + 2B powders. The loop at the top of the TGA curve is attributed to the competing processes of weight gain due to oxidation and weight loss due to vaporization of boron oxide. The addition of Al allows the attainment of nearly complete oxidation by 1500°C for the Al-2B mixture.

the case of Al + 2B), the percent of theoretical weight gain increases from 78% for pure boron to 95% for the mixed system. If boron and aluminum were oxidizing independently, a weight gain of 77% would be expected. Therefore, aluminum is acting as an aid to oxidation for the boron particles (see Figure 13(b)). Magnesium has a similar effect on boron, increasing the percent of theoretical weight gain to 91%, compared to 71% for independent oxidation of magnesium and boron. The benefits for magnesium could likely be increased if a powder with less surface oxide or higher surface area were used. When magnesium and aluminum are both mixed with boron in the case of MgAl + 2B the weight gain reaches 83% of theoretical, compared to 78% for independent oxidation. In the case of $MgAlB_{14}$, it reaches 76% compared to 71% for independent oxidation.

This demonstrates that aluminum is in fact aiding in the removal of the boron oxide layer from the surface of boron particles. Magnesium has a similar effect, suggesting that a liquid that can wet the boron particle surface will increase the rate of boron oxidation. It is unclear if this is due to dilution or removal of the liquid oxide layer, colligative effects that reduce the vaporization temperature of the oxide, or other effects. It is interesting to note, however, that a combination of aluminum and magnesium is not as effective in aiding in boron oxidation. This may be the result of the formation of a spinel, $MgAl_2O_4$, early in the oxidation process. If this is the case, it is surprising, since the spinel would likely remove the B_2O_3 and would be expected to allow the remaining AlMg alloy to readily react. It might be argued that the larger particle size of the $MgAlB_{14}$ material slows the reaction, but the data suggest just the opposite. Larger particles of the same composition show earlier initiation (see Figure 14), but do not oxidize to the same extent. This is tied to the higher amount of oxygen in the starting powder. It would be worthwhile for ARDEC to measure the oxygen content of all of the powders. As Table 6 shows, the -325 mesh materials gained less weight than the -230 mesh materials. This trend holds true for all four materials. As mentioned previously, the surface area of the -325 mesh powder was slightly higher than that of the -230 mesh, which makes oxidation on the surface of these particles a likely explanation. Some additional oxidation on the surface of the reacted materials apparently occurred during the preparation of the finer size fraction. As the surface effects may change with differing energetic mixtures, multiple particle sizes should be tested. The first tests, however, should involve the -230 mesh and not the -325 mesh particles.

AlB_2 oxidizes to nearly the same percent weight gain as Al + 2B but it initiates at a higher temperature (see Figure 14 and Table 6). A higher initiation temperature will have implications for sensitivity, making the reacted compounds less sensitive than the powder mixes, as expected. The increase in initiation temperature for reacted compounds is seen most prominently for $MgAlB_{14}$ (see Figure 14(g)).

However, there may be an added benefit to forming a diboride compound over a physical mixture of boron and aluminum. Bonding in boron (both amorphous and crystalline) is through B_{12} icosahedra[25], in which each boron atom is participating in five covalent bonds, sharing its five electrons with five other boron atoms. Boron bonding in AlB_2 (as well as MgB_2 and $Mg_{0.5}Al_{0.5}B_2$) is trigonal planar, with boron atoms forming a graphite-like sheet in between metal

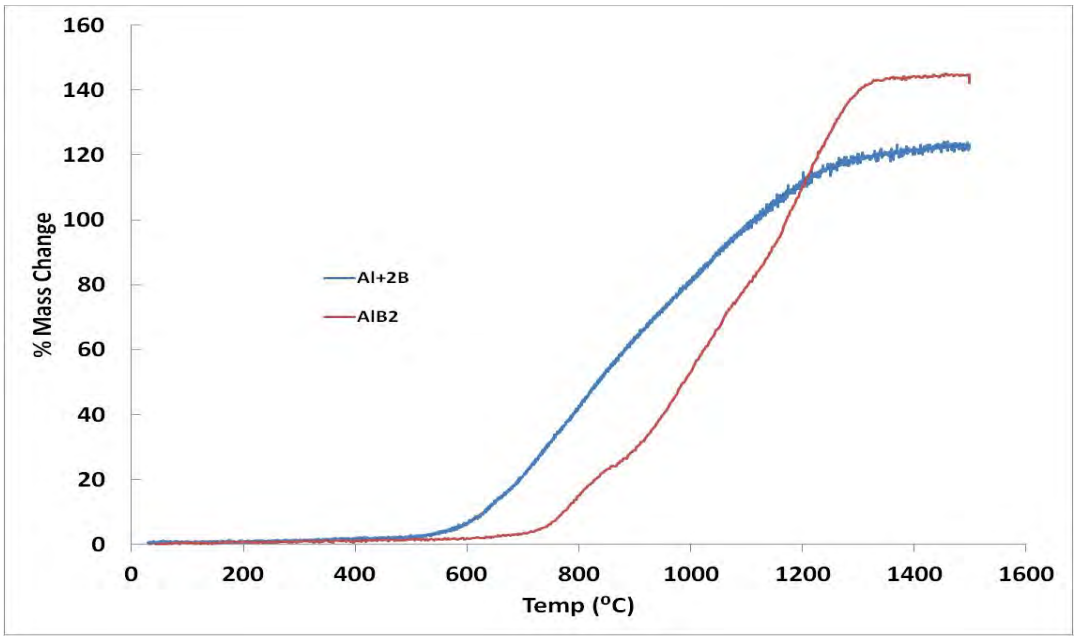

(a)

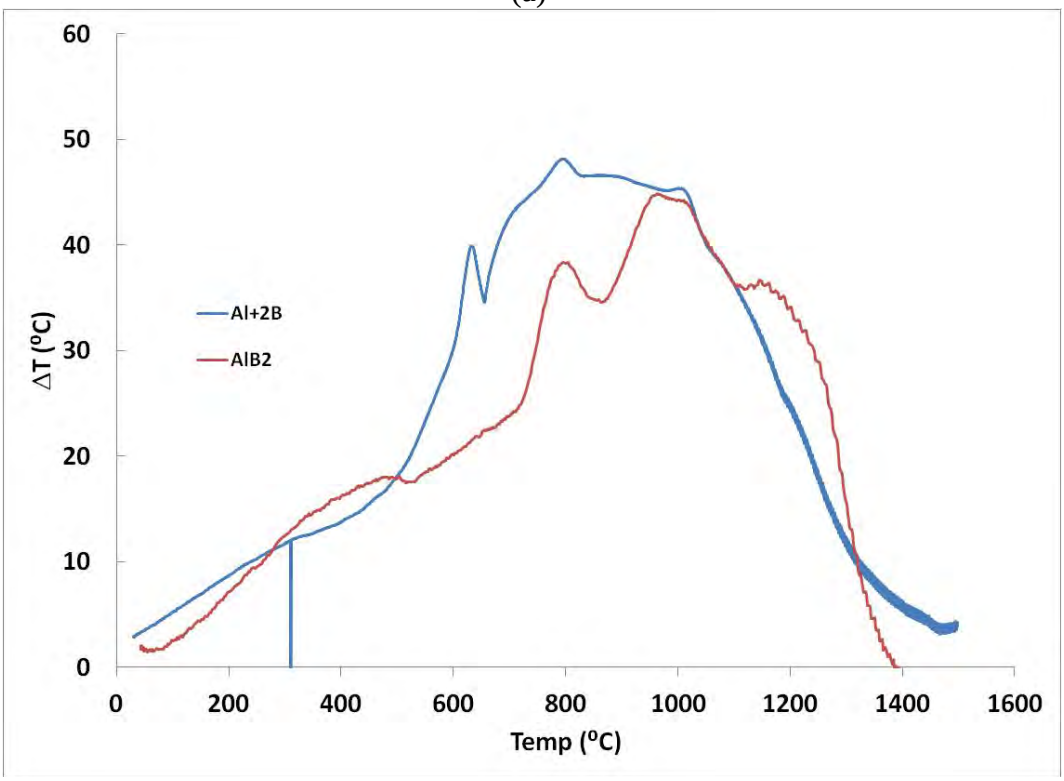

(b)

Figure 14. TGA and DTA patterns for selected samples. Comparison of Al + 2B to AlB_2 for (a) TGA and (b) DTA. AlB_2 achieves a similar weight change to Al + 2B, but it initiates at higher temperatures due to its much coarser particle size (see Figures A5 and A6).

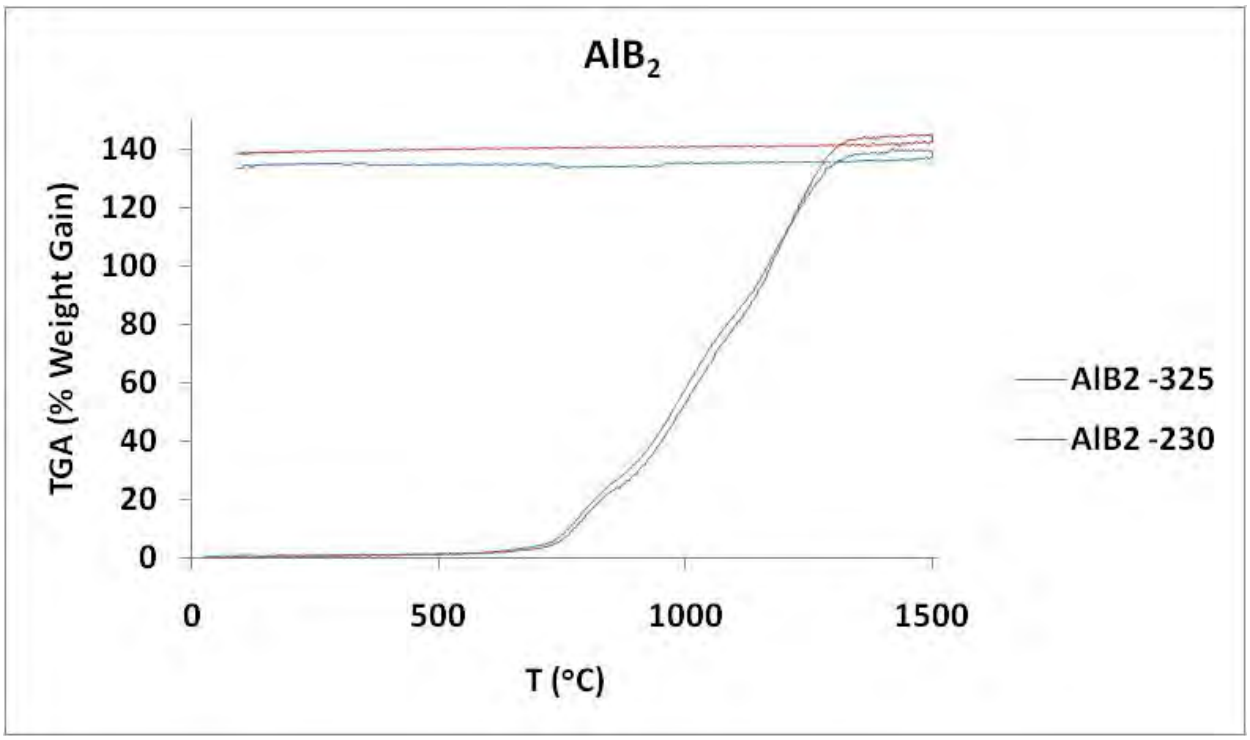

(c)

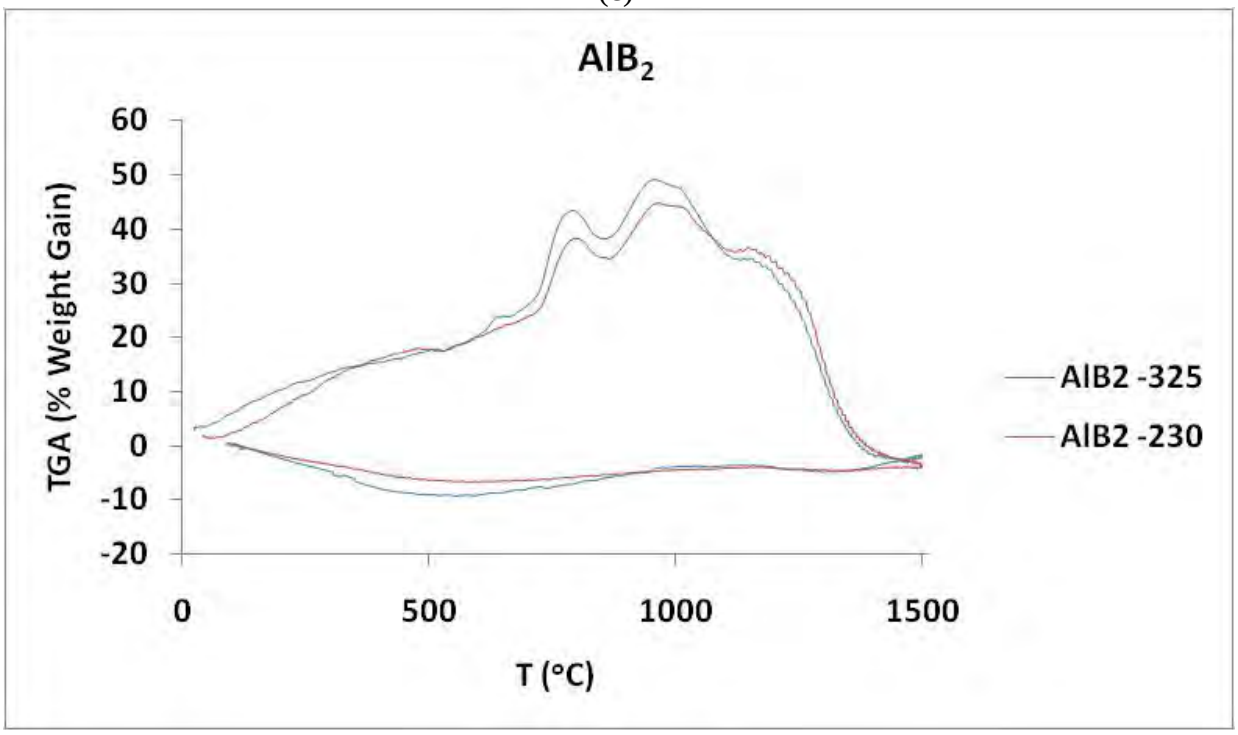

(d)

Figure 14 (continued). AlB_2 compared at two particle sizes for (c) TGA and (d) DTA. Note that there is little difference in performance since differences in particle size distributions are minor (see Figures A6 and A7).

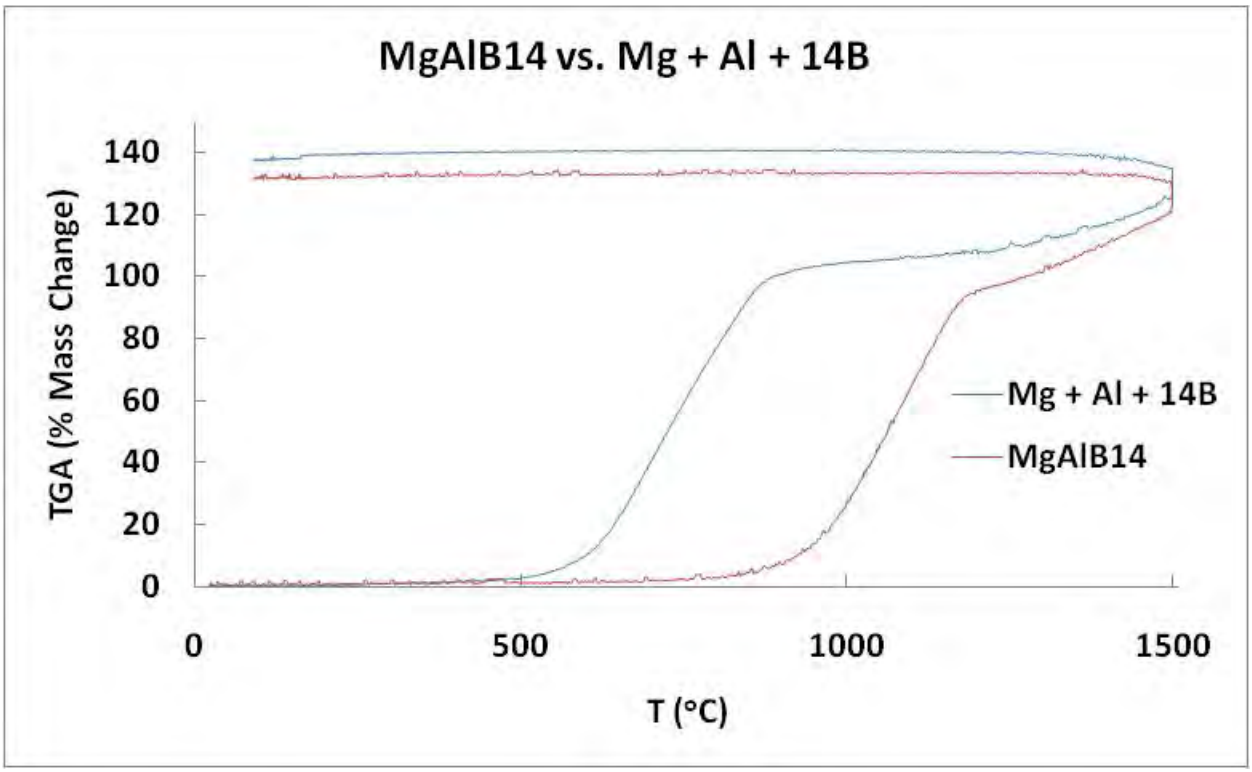

(e)

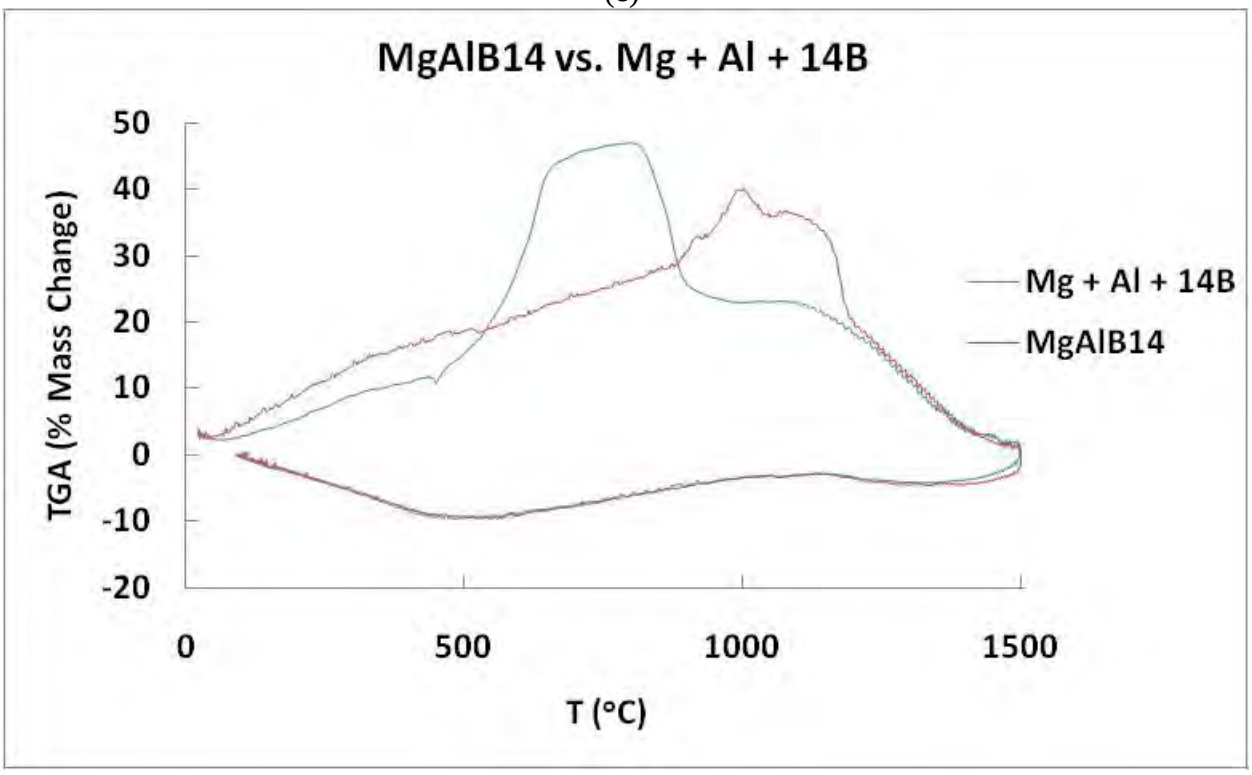

(f)

Figure 14 (continued). Comparison of Mg + Al + 14B to $MgAlB_{14}$ for (e) TGA and (f) DTA.

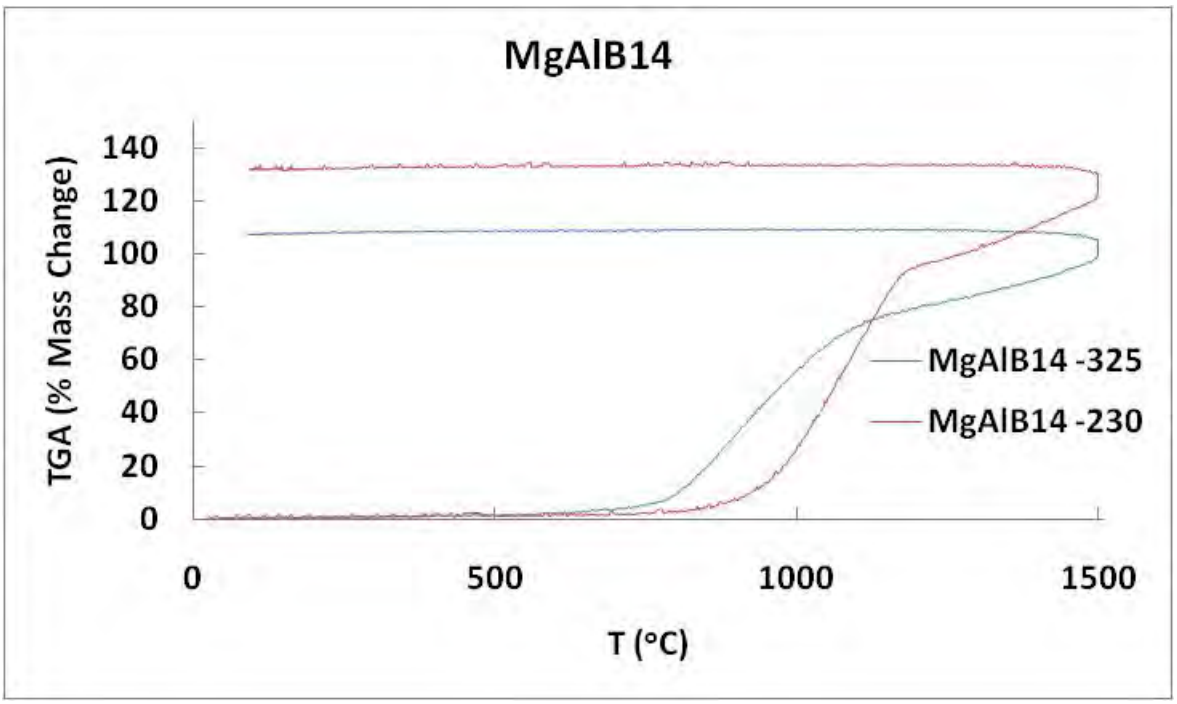

(g)

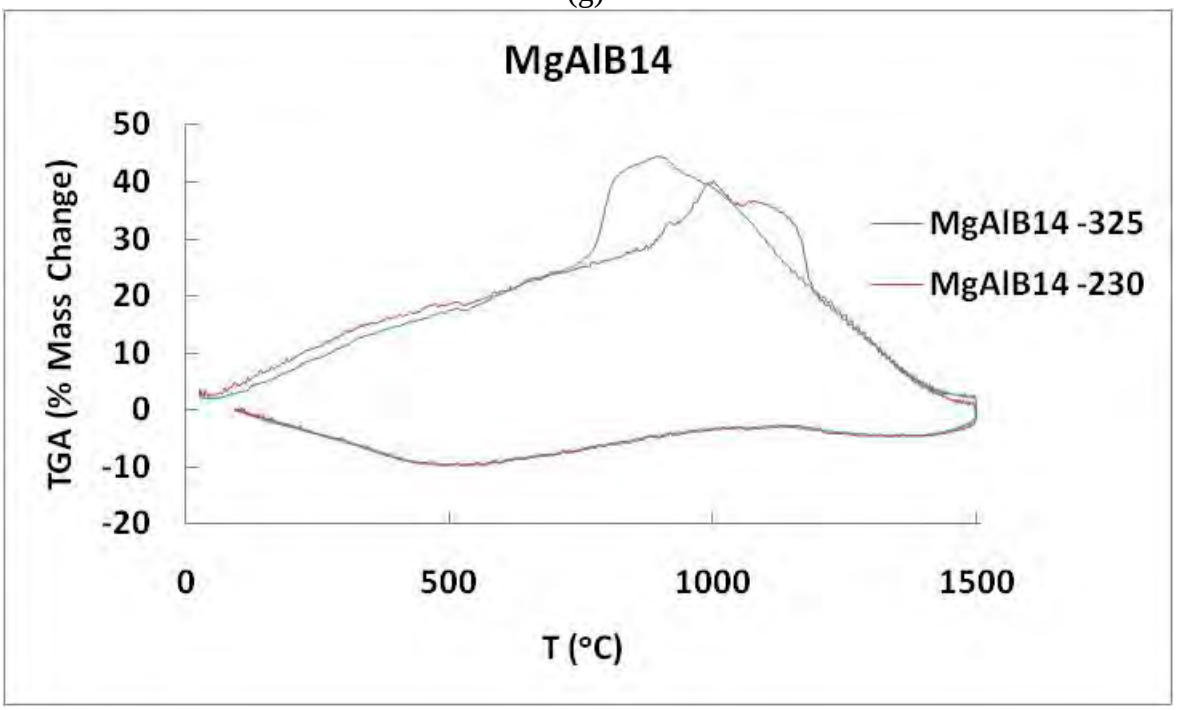

(h)

Figure 14 (continued). $MgAlB_{14}$ compared at two particle sizes for (g) TGA and (h) DTA. Note that there is a large difference in performance since differences in particle size distributions (see Figures A15 and A16) and surface areas (see Table 5) are significant.

atom sheets. In this case each boron atom is participating in three covalent bonds with three neighboring boron atoms and van der Waals forces between the sheets maintaining interplanar separation. The oxidation state of this hexagonal boron is the same as that in boron oxide, in which 3-coordinate boron is bound to 2-coordinate oxygen in a planar fashion. It is possible that this bonding may result in faster reaction kinetics once oxidation has initiated. The DTA graphs of Al + 2B and AlB_2 may suggest this, although DSC measurements would make the position and extent of the exotherms more obvious than the DTA data, which were collected with a system that allowed a limited number of data points to be collected thereby obscuring some of the thermodynamic transitions.

Figure 15 compares all four reacted materials on the same plot as well as gives a corresponding plot for the unreacted powders. For the four reacted materials, AlB_2 is clearly the best material since it maintains its rate of oxidation at higher temperatures. The Al + 2B mixture shows this same characteristic, which suggests that this has nothing to do with the hexagonal bonding and is related to the way Al reacts with B or B_2O_3. No Al-B_2O_3 phase diagram was found, but it is surprising that the reaction initiates at temperatures far below the melting point of Al, where diffusion would be increased. More surprising, in light of the many reports of delayed reaction for boron, was the low-temperature and fast reaction of B. The change in reaction rate does not correspond to the melting point of B_2O_3. Furthermore, the present results clearly show that the enhancement with Al is not dependent on volatilization, as has been postulated[112,113]. It is clear that the thermodynamic driving force for oxidation is delayed until the kinetics allow oxidation to proceed, which at this rate of heating is about 500°C. The reaction to form borides increases the initiation of the reaction, suggesting that particle size and free metal content enhance the kinetics.

If these results turn out to have some predictive ability for explosives, it would suggest that the $MgAlB_{14}$ offers no advantage over AlB_2 other than sensitivity, if it is indeed an issue. It is very possible that the dilution of Al with B is all that is needed to make the materials less sensitive such that mixtures can be used instead of borides. The Al + 2B mixture should be compared to the AlB_2 relative to sensitivity.

The largest deterrent to the use of boron in energetics is cost. Boron is not found free in nature but borates are extensive with large deposits of borax in Turkey. The mineral rasorite is found in the Mojave Desert of California. These hydrated sodium borates are reduced to form boron. SB Boron (Bellwood, IL) is the largest U.S. Supplier of boron, with costs ranging from $110/kg for their lowest purity (grade 86) and $139/kg for their most popular material for military use (grade 90) to $266/kg for their high purity (grade 95) boron. These costs are for quantities exceeding 225 kilograms. Surprisingly, the German supplier H. C. Starck is competitive in price and offers a higher quality product. H. C. Starck's amorphous boron currently sells for $165-220/kg compared to $22/kg for Al (grade H-30 from Valimet) or $30/kg for atomized Mg (Hart Metals). Lower cost materials are available out of China. The least expensive non-oxide source of boron is B_4C powder, which sells for about $20-40/kg. Any high value use of high-temperature borides will result in a similar price if the same volume of market

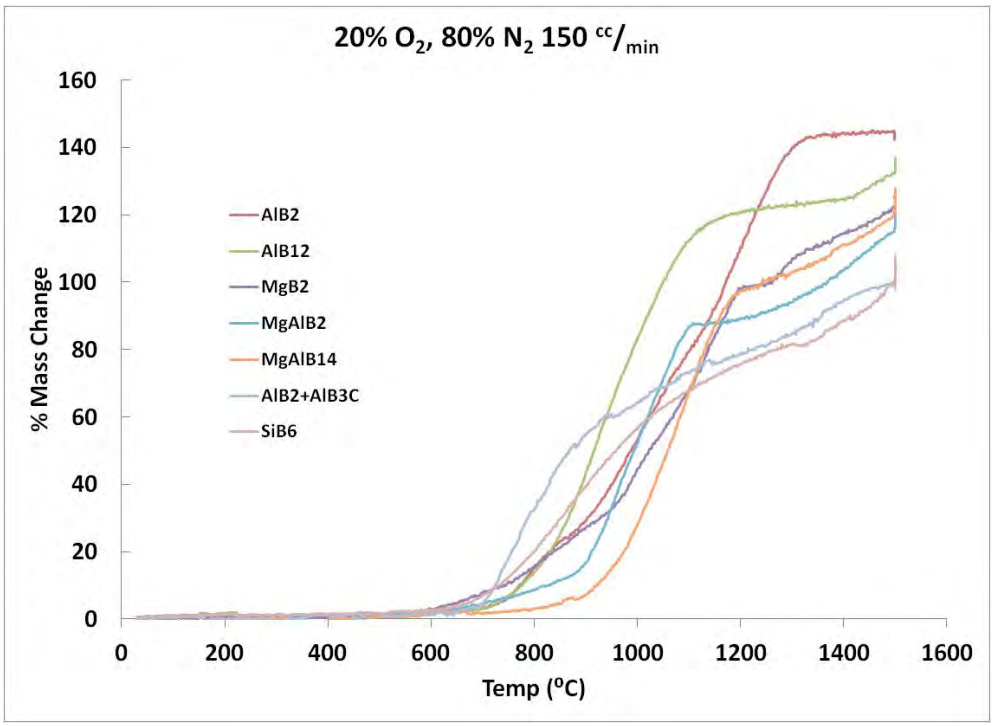

(a)

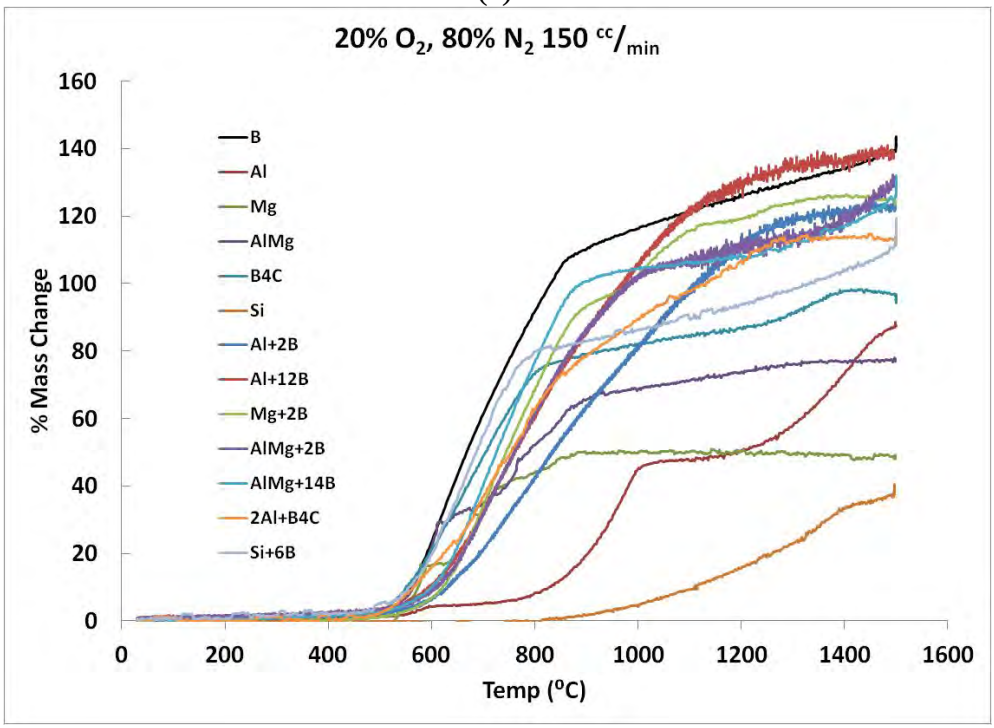

(b)

Figure 15. TGA data for (a) reacted compounds and (b) unreacted elements and mixtures. Note that the rate of oxidation begins to slow for all materials except AlB_2.

is developed. There is no production of MgB_2 or AlB_2 powders at the present time, which make such powders prohibitively expensive. This means that the performance of boron-based powders must be substantially better than metallic powders or non-oxide powders.

The cost to make Al + 2B as a mixture would be in the range of $100-150/kg in large quantities as an intimately mixed material. The cost to make the boride, however, would likely be in the $200-250/kg range for similar quantities. Costs for small quantities can be much higher. This drives one towards looking at less expensive materials. It is recommended that B_4C, B_4C + 2Al, Si, Si + 6B, SiB_6, Al + 12B, and AlB_{12} be made for evaluation.

Conclusions

Characterization of the four powders delivered to ARDEC, along with their starting mixes and raw starting materials included XRD, particle size and surface area, SEM images, TGA and DTA. These data provide a better understanding of the material systems involved in these energetic powders. While the relative energetic capabilities of these materials can only be determined through calorimetry and in situ testing, a combination of characterization and testing will give insight into what, if any, properties correlate with high performance in these metal borides. Below are the key results of the boride characterization.

- Surface area data and SEM images show that the average particle size of all powders is less than 10 μm, although particle size data suggests that the small particles tended to coalesce into larger agglomerates. This is a result of the fine boron powder used.
- The surface areas of the -325 mesh borides are higher than the -230 mesh borides, as expected, indicating that some size reduction occurred. This did not result in increased weight gain, suggesting that there must be some optimum between increased particle size and decreased oxygen content. The smaller particles tended to react earlier, but their rate of reaction was not higher than the larger particles with less surface oxygen.
- Boron gained the most weight per unit mass, but reached the lowest percent of its theoretical value of any material tested. Both aluminum and magnesium helped raise the weight gain of boron, but when mixed together didn't have as large of an impact. The Al + 2B and AlB_2 were the best materials based on the TGA data since they reacted quickly to nearly their full extent. Surprisingly, the fine boron powder used in this study reacted readily at low temperatures but the formation of a liquid oxide layer resulted in slow diffusion and volatilization at high temperatures.
- The extent of reaction TGA data correlated well to thermodynamic calculations made for ΔH_c/g.
- The DTA data were inadequate to flush out the integrated area of exotherms. Calorimetry and DSC measurements at ARDEC are essential.
- The high cost of boron is an impediment to the implementation of borides until demand is large. Boron carbide, which sells for similar prices to Al, shows that it will be possible in the long term to get pricing down if a large demand for borides exists. In the shorter-term, these materials are likely to be in the $200/kg to $1,000/kg range.

III. Characterization of 500 gram Samples

After receiving the four boride materials shipped on 10-5-10 and characterized on 11-11-10, Dr. Paul Anderson requested that 500 grams of AlB_2 and 500 grams of Al + 2B be prepared in a similar manner to the same samples shipped in 50 gram quantities. The new powders have the Ceramatec codes of MW1-113I (AlB_2) and MW1-113G (Al + 2B).

Figure 16 compares the X-ray diffraction patterns of the previous materials with those of the scaled up versions, showing them to be nearly identical. Figure 17 compares particles size distributions of the scaled up versions compared to the materials sent previously. There is good agreement between the 50 gram and 500 gram powders. Table 7 compares surface areas and particle size data showing that the 500 gram samples are similar to 50 gram batches.

IV. Characterization of Alternative Borides

The characterization of four boride powders and their respective starting materials suggested that Al + 2B and AlB_2 would likely be the best candidates for an insensitive energetic formulation. While the performance of these materials can only truly be characterized by in situ testing, TGA and DTA in flowing air suggest that these two materials exhibit the best oxidation kinetics of the materials tested. If Al + 2B or AlB_2 are in fact viable candidates, the cost of manufacturing these materials on a large scale would become an important issue to address. Boron carbide (B_4C) is a much cheaper alternative to boron, as it is widely used for a number of industrial applications. Currently, the price of boron powder from SB boron ranges from $110/kg for their lowest purity (grade 86) and $139/kg for their most popular material for military use (grade 90) to $266/kg for their high purity (grade 95) boron. These costs are for quantities exceeding 225 kilograms. Boron carbide costs $20-40/kg and is comparable to the cost of aluminum.

Silicon is an inexpensive metal that could be used to assist boron oxidation, making SiB_6 a material of interest. Since SiB_6 contains three times as much B as AlB_2, a higher aluminum boride (AlB_{12}) was also synthesized for comparison purposes.

The use of B_4C is predicated on comparable performance to B. Table 8 lists the powder characteristics of B_4C, as well as other boride mixes and powders synthesized. The B_4C used has

Table 7
Powder Characteristics Comparing 50 and 500 Gram Samples

	Surface Area	Particle Size (μm)				Calculated*
Material	**(m^2/g)**	**d_{10}**	**d_{50}**	**d_{90}**	**Mean**	**Average (μm)**
Al + 2B (MW1-90A (50 g))	6.23	0.2	2.3	6.5	2.8	0.4
Al + 2B (MW1-113G (500 g))	5.37	0.2	2.2	12.2	4.7	0.5
AlB_2 -230 (MW1-104K (50 g))	1.64	0.5	8.4	28.8	11.9	1.2
AlB_2 -230 (MW1-113I (500 g))	1.96	0.5	5.7	18.6	8.9	1.0

*Based on Equation (2).

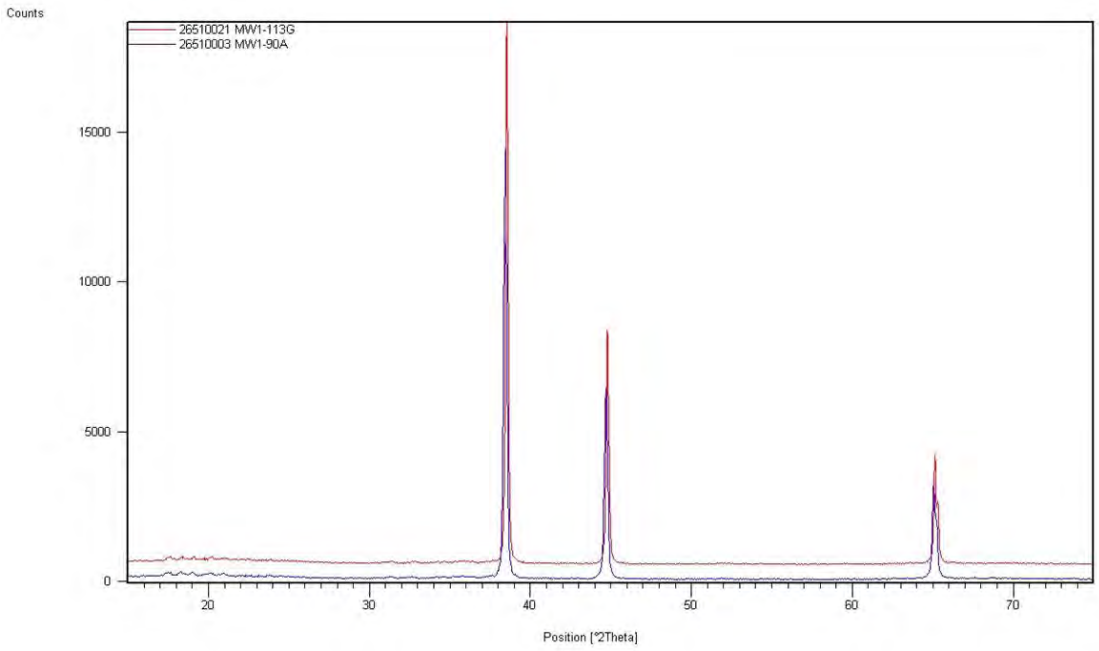

(a)

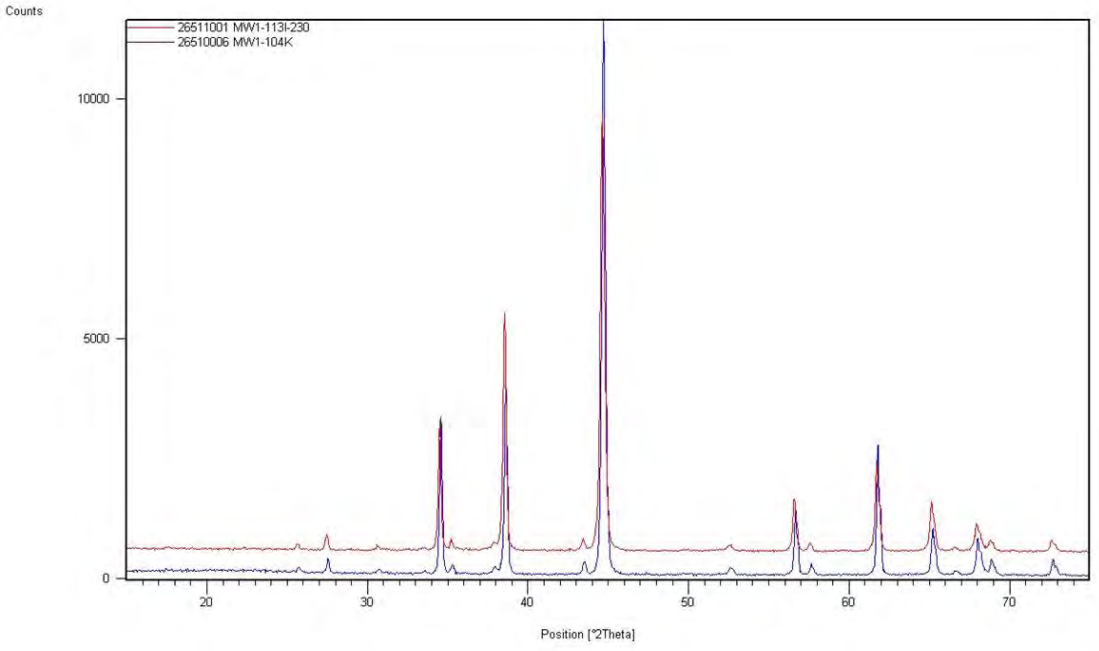

(b)

Figure 16. X-ray diffraction patterns comparing scaled-up 500 gram sample (red) to 50 g powder (blue) showing similar phases present in scaled-up versions. (a) Al + 2B (red=MW1-113G and blue=MW1-90A), and (b) AlB_2 (red=MW1-113I and blue=MW1-104K.

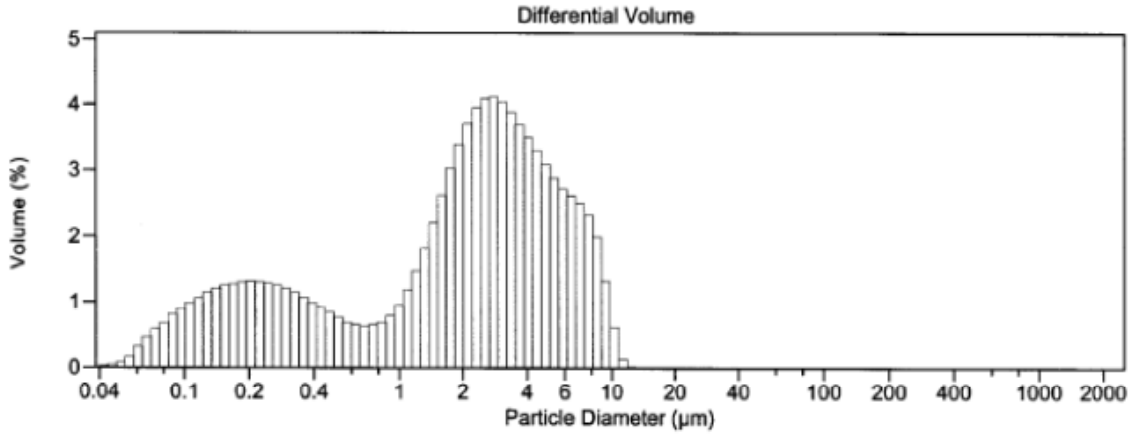

Volume Statistics (Arithmetic) 10015.$02

Calculations from 0.040 µm to 2,000 µm

Volume	100.0%		
Mean:	2.782 µm	S.D.:	2.444 µm
Median:	2.256 µm	C.V.:	87.8%
D(3,2):	0.542 µm		
Mode:	2.787 µm		

% <	10	25	50	75	90
Size µm	0.165	0.583	2.256	4.089	6.522

(a)

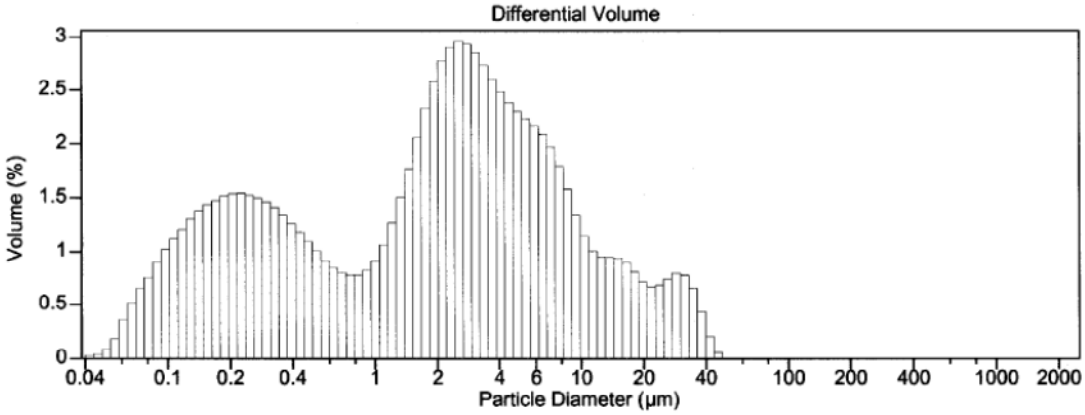

Volume Statistics (Arithmetic) 11001.$02

Calculations from 0.040 µm to 2,000 µm

Volume	100.0%		
Mean:	4.655 µm	S.D.:	7.060 µm
Median:	2.197 µm	C.V.:	152%
D(3,2):	0.491 µm		
Mode:	2.539 µm		

% <	10	25	50	75	90
Size µm	0.152	0.394	2.197	5.264	12.24

(b)

Figure 17. Particle size distributions measured in isopropanol. (a) 50 gram Al + 2B (MW1-90A) and (b) 500 gram Al + 2B (MW1-113G).

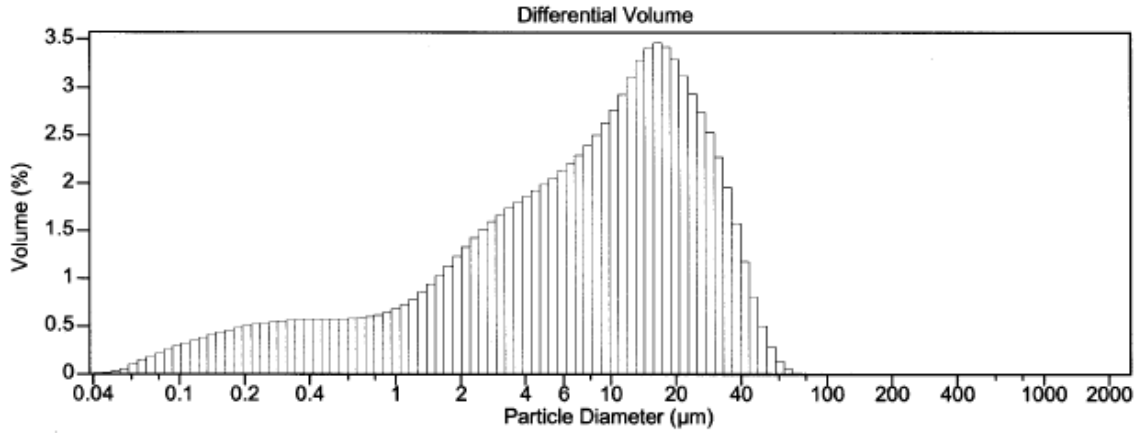

Volume Statistics (Arithmetic) 10023.$02

Calculations from 0.040 µm to 2,000 µm

Volume	100.0%		
Mean:	11.92 µm	S.D.:	11.56 µm
Median:	8.437 µm	C.V.:	97.0%
D(3,2):	1.310 µm		
Mode:	16.40 µm		

% <	10	25	50	75	90
Size µm	0.528	2.590	8.437	18.08	28.78

(c)

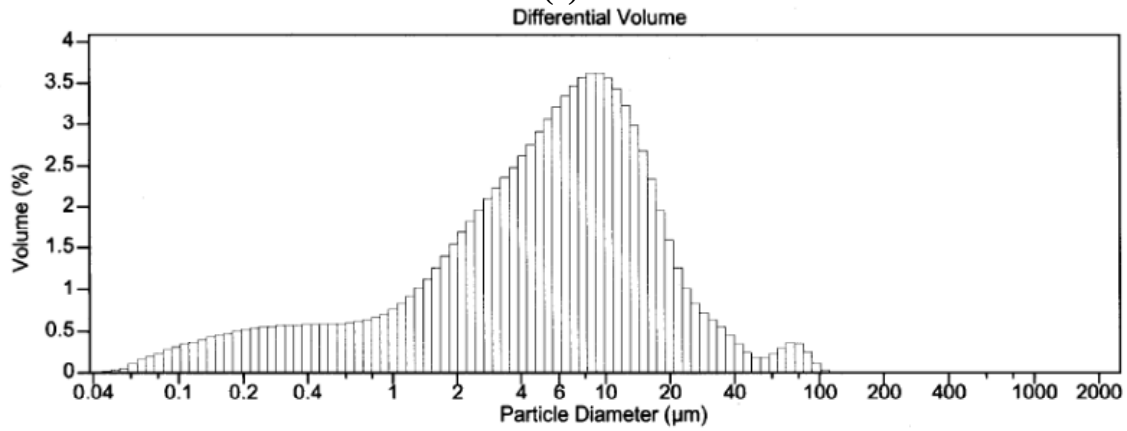

Volume Statistics (Arithmetic) 11002.$05

Calculations from 0.040 µm to 2,000 µm

Volume	100.0%		
Mean:	8.914 µm	S.D.:	11.80 µm
Median:	5.725 µm	C.V.:	132%
D(3,2):	1.213 µm		
Mode:	9.371 µm		

% <	10	25	50	75	90
Size µm	0.497	2.206	5.725	11.17	18.56

(d)

Figure 17 (continued). (c,d) -230 mesh AlB_2 (MW1-104K). (c) 50 gram (MW1-104K) and (d) 500 gram (MW1-113I).

Table 8
Powder Characteristics Comparing Initial and Alternative Materials

Material	Surface Area (m^2/g)	Particle Size (μm) d_{10}	d_{50}	d_{90}	Mean	Calculated Average (μm)
B	10.88	0.1	0.2	3.2	1.2	0.2
Al	1.39	0.2	2.9	7.8	3.4	1.6
Mg	0.82	11.9	38.2	66.5	38.6	3.9
Mg-Al	0.40	2.0	10.0	25.9	12.4	6.8
Al + 2B	6.23	0.2	2.3	6.5	2.8	0.4
AlB_2 -230	1.64	0.5	8.4	28.8	11.9	1.2
AlB_2 -325	2.10	0.4	5.4	21.9	8.7	0.9
Mg + 2B	6.73	0.3	8.6	65.4	24.0	0.4
MgB_2 -230	4.78	0.7	9.2	46.0	17.4	0.5
MgB_2 -325	5.55	0.5	1.6	2.9	1.6	0.4
½ MgAl + 2B	5.85	0.1	1.6	5.1	2.0	0.4
$Mg_{0.5}Al_{0.5}B_2$ -230	2.30	0.9	7.3	27.5	11.4	0.9
$Mg_{0.5}Al_{0.5}B_2$ -325	3.15	0.5	1.6	2.9	1.6	0.7
Mg + Al + 14B	7.75	0.1	1.3	4.4	1.8	0.3
$Mg_{0.78}Al_{0.75}B_{14}$ -230	0.55	4.8	14.7	28.2	16.0	4.1
$Mg_{0.78}Al_{0.75}B_{14}$ -325	1.29	0.4	7.5	17.1	8.4	1.8
B_4C	6.92	0.1	1.4	3.8	1.7	0.3
Si	3.56	0.2	2.7	5.9	2.7	0.7
Al + 12B	9.11	0.1	0.4	3.2	1.3	0.3
AlB_{12} -230	1.38	1.3	6.4	17.5	8.6	1.8
AlB_{12} -325	1.42	0.5	4.8	12.1	5.8	1.6
B_4C + 2Al	4.30	0.2	2.0	5.4	2.4	0.6
AlB_3C + AlB_2 -230	2.60	0.3	4.3	17.7	7.2	0.9
Si + 6B	9.10	0.1	0.4	2.6	0.9	0.3
SiB_6 -230	0.71	3.2	14.9	38.4	20.8	3.9

a high surface area and small particle size such that it is relatively comparable to the B powder. The B_4C was mixed with aluminum in a 2:1 B to Al ratio, similar to Al + 2B. This power was also reacted under similar conditions to Al + 2B. This resulted in an aluminum boron carbide (AlB_3C) as well as AlB_2, as evidenced by the XRD pattern in Figure 18. Figures 19 and 20 show that the SiB_6 and AlB_{12} phases formed as desired. Table 8 also shows data for samples prepared previously, so it is easy to see that the surface areas were low for all reacted powders, as expected. However, the particle size of the SiB_6 was much larger than the other two powders, being comparable in size to the $MgAlB_{14}$ prepared previously. Comminution, of course, could be used to reduce particle size. Appendix B contains particle size distributions of the alternative borides as measured in isopropanol.

Figures 21 and 22 show the TGA and DTA curves for the reacted powders as well as mixtures of the starting elements in these compositions. Figures 23-26 provide comparisons

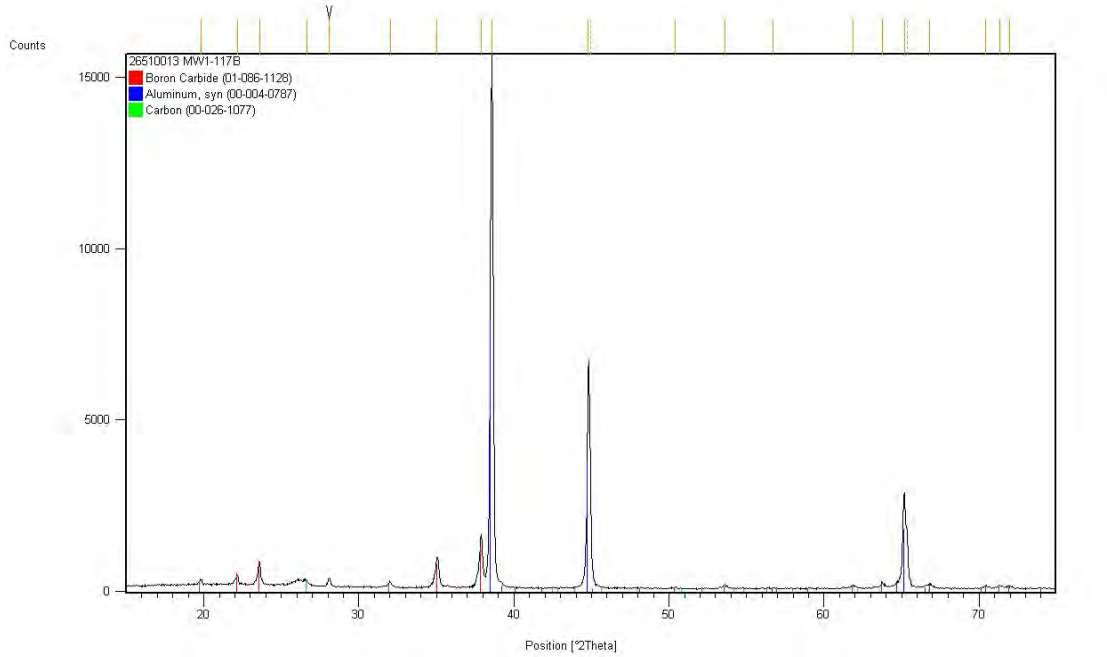

(a)

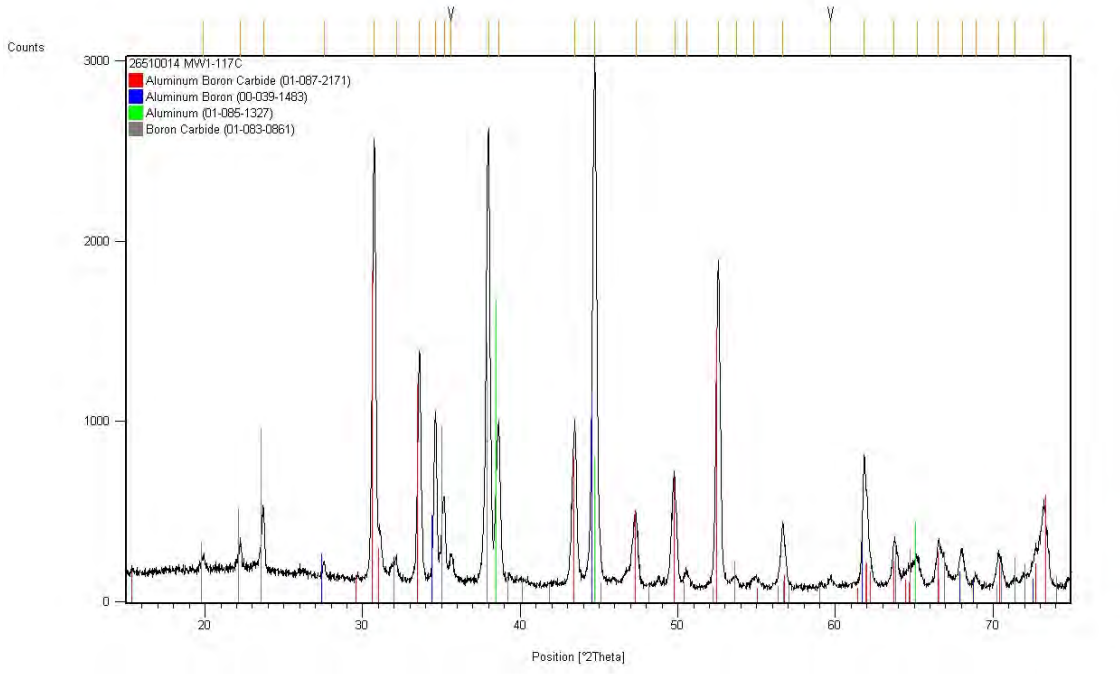

(b)

Figure 18. XRD pattern for B_4C + 2Al (a), and reacted B_4C + 2Al (b). The reacted powder contains AlB_3C and AlB_2 as major phases as well as some unreacted Al and B_4C.

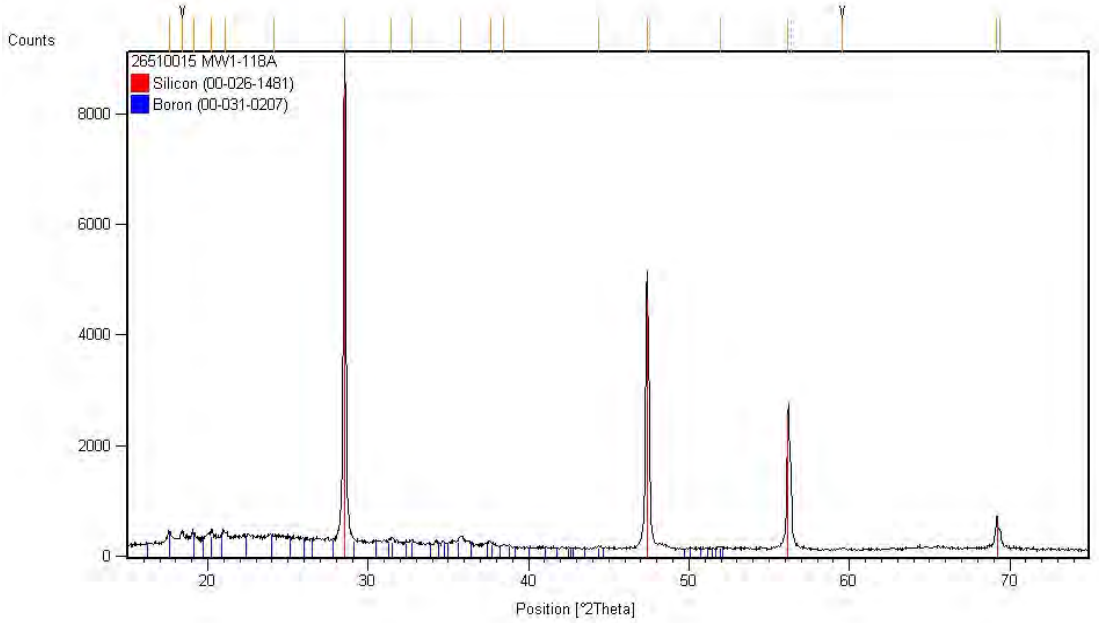

(a)

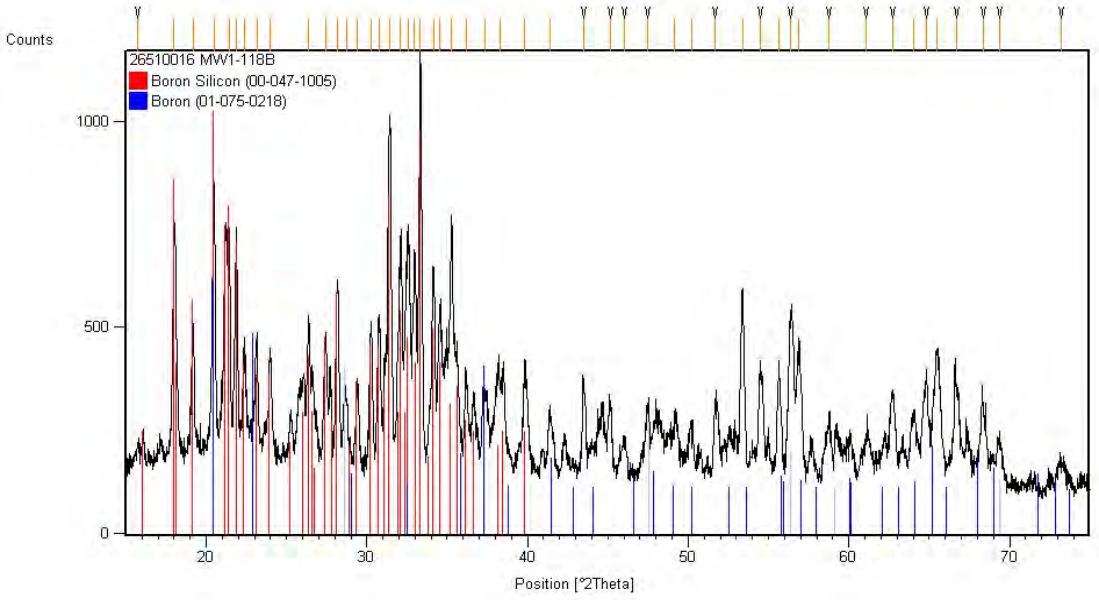

(b)

Figure 19. XRD pattern for Si + 6B (a) and SiB_6. The software only contained peaks indexed up to 40° 2θ for SiB_6, but it was a very good match up to that point.

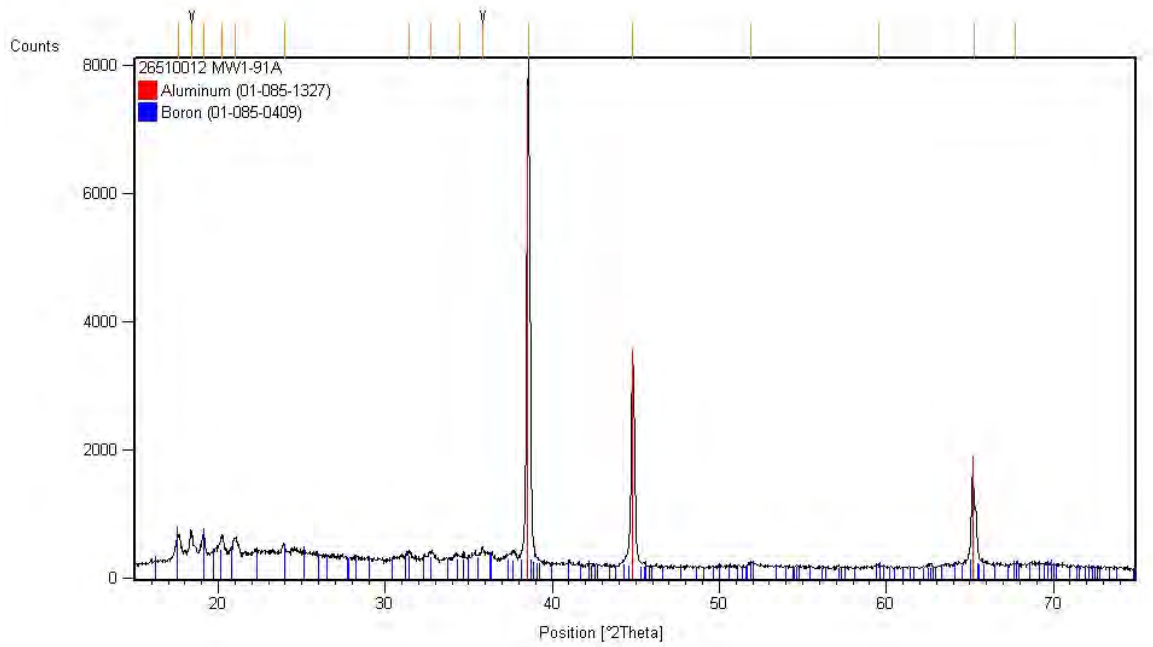

(a)

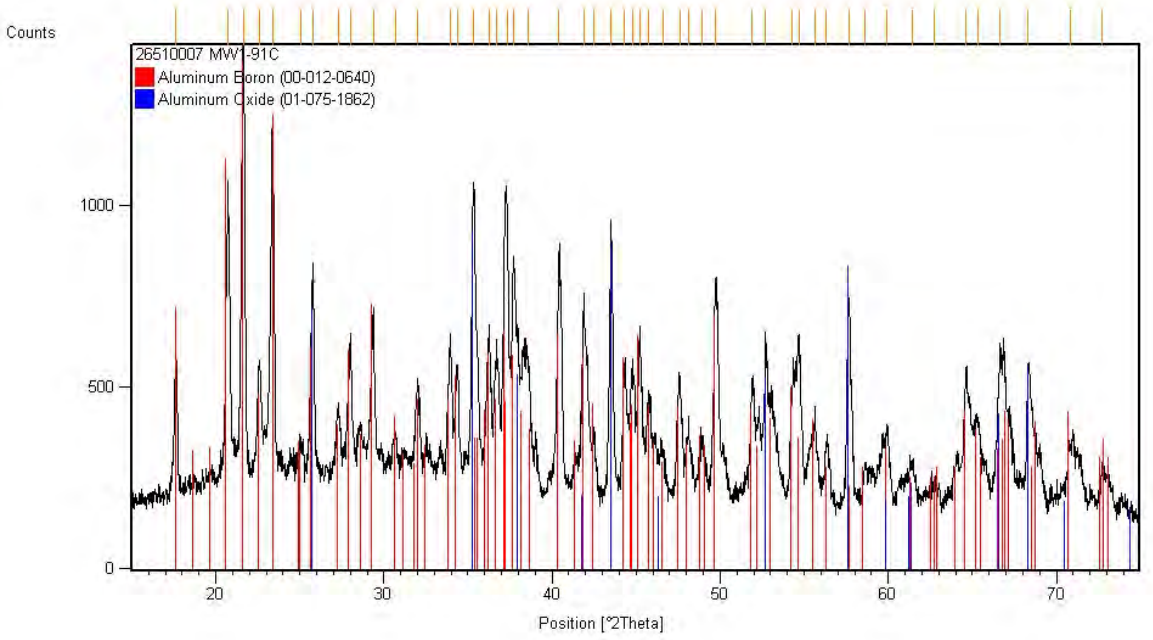

(b)

Figure 20. XRD scans of (a) Al + 12B and (b) AlB_{12}. As seen previously, amorphous boron is difficult to detect but the large amount of boron makes the minor crystalline phase easier to detect. When reacted, Al + 12B formed AlB_{12} with some Al_2O_3 as an impurity.

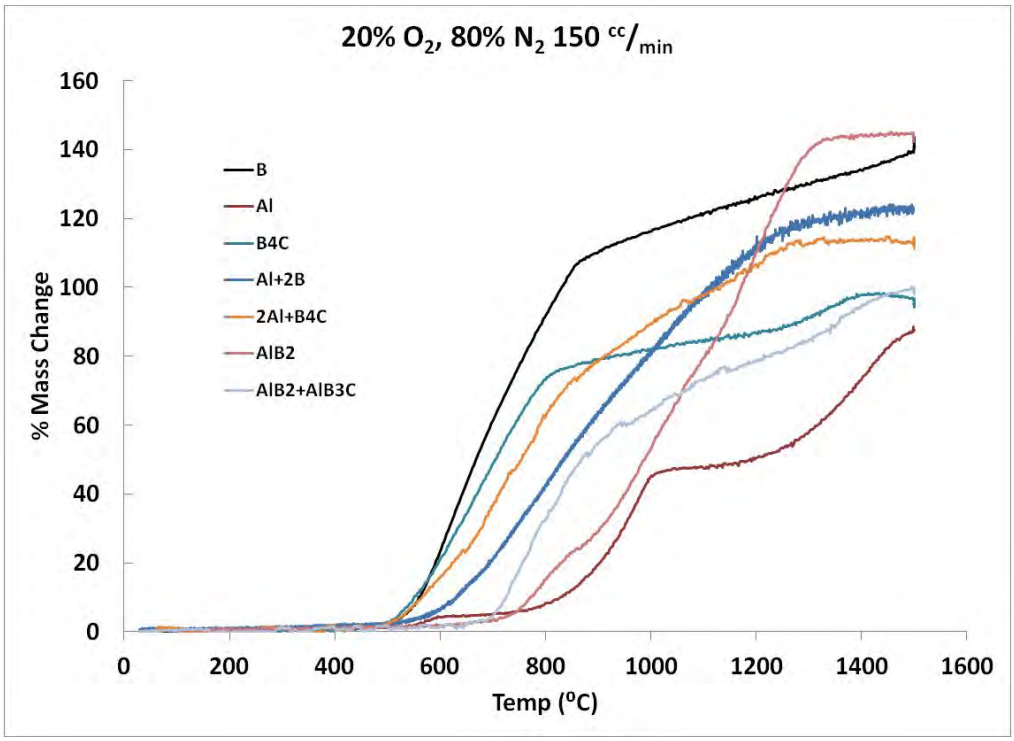

Figure 21. TGA of boron and boron carbide starting and reacted powders. Boron remained the best material in terms of mass gain, with both Al + 2B and AlB_2 within 20%. B_4C, B_4C + 2Al and reacted B_4C + 2Al all gained significantly less weight than Al + 2B, AlB_2, and boron.

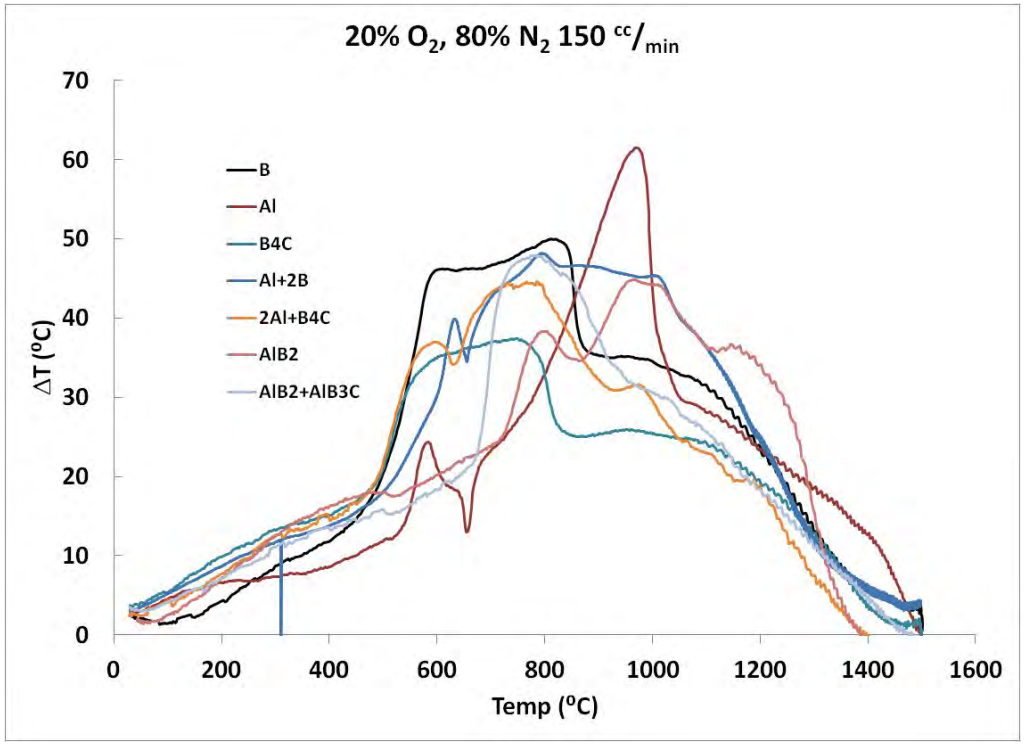

Figure 22. DTA of boron and boron carbide starting and reacted powders. The exotherms for the boron carbide materials are comparable to those of Al + 2B and AlB_2.

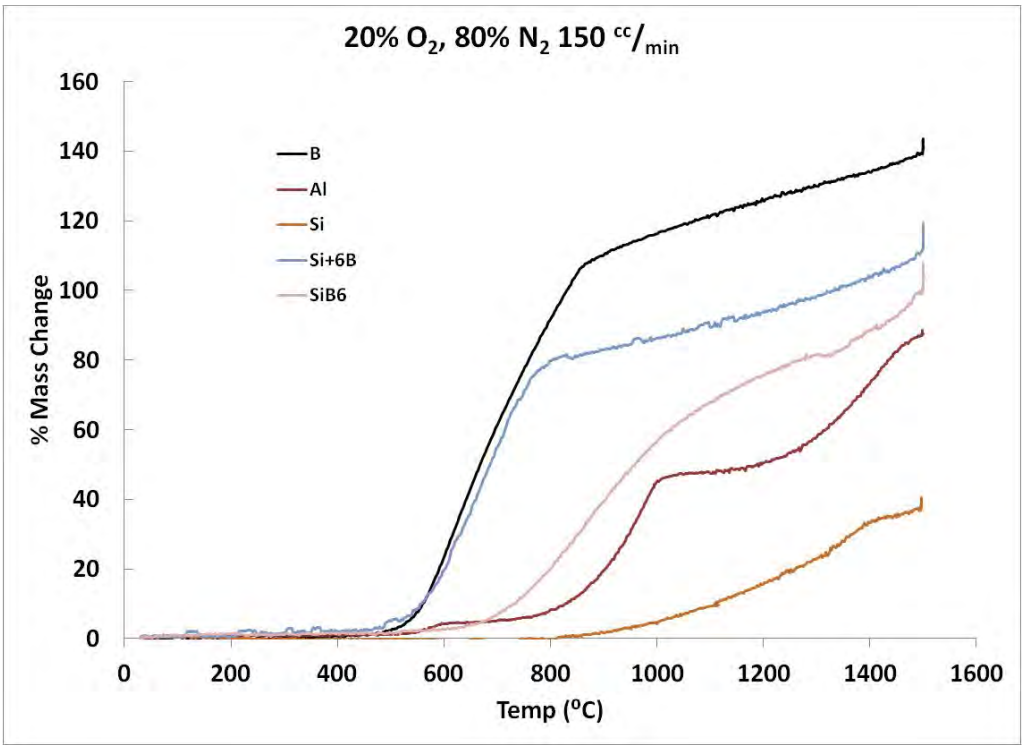

Figure 23. TGA of silicon borides vs. aluminum borides.

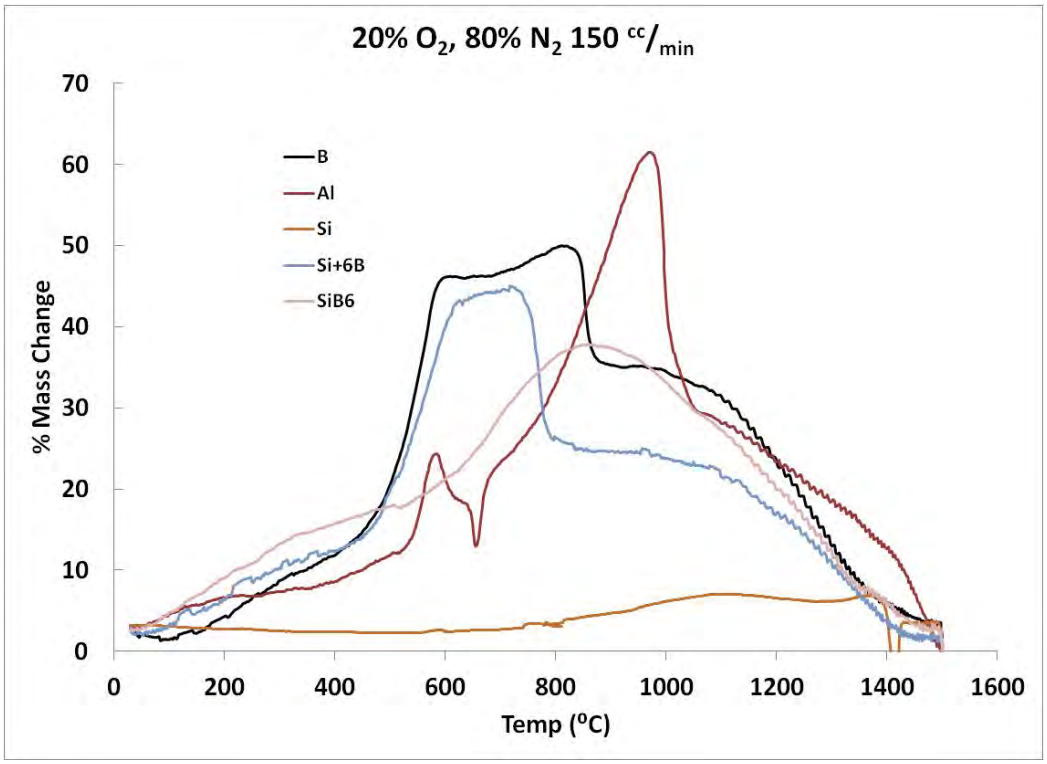

Figure 24. DTA of silicon borides vs. aluminum borides.

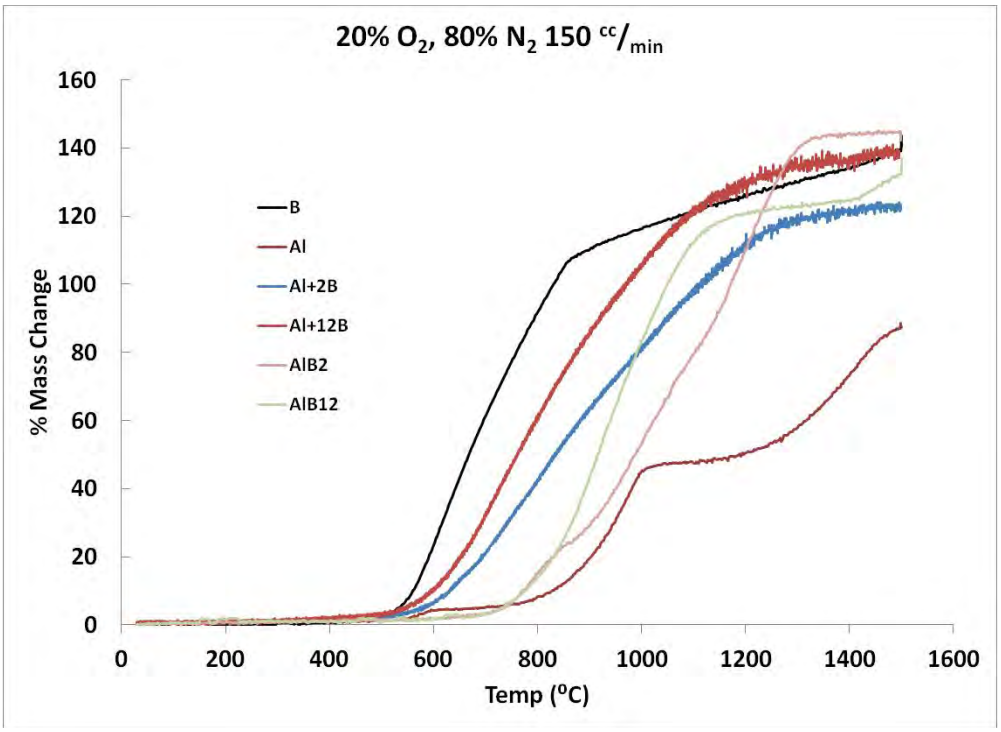

Figure 25. TGA comparing Al:B ratios of 1:2 and 1:12. The amount of aluminum had little impact on the actual weight change of the powders, but the 1:2 ratio had a much higher extent of oxidation suggesting that adding more aluminum helps boron oxidation.

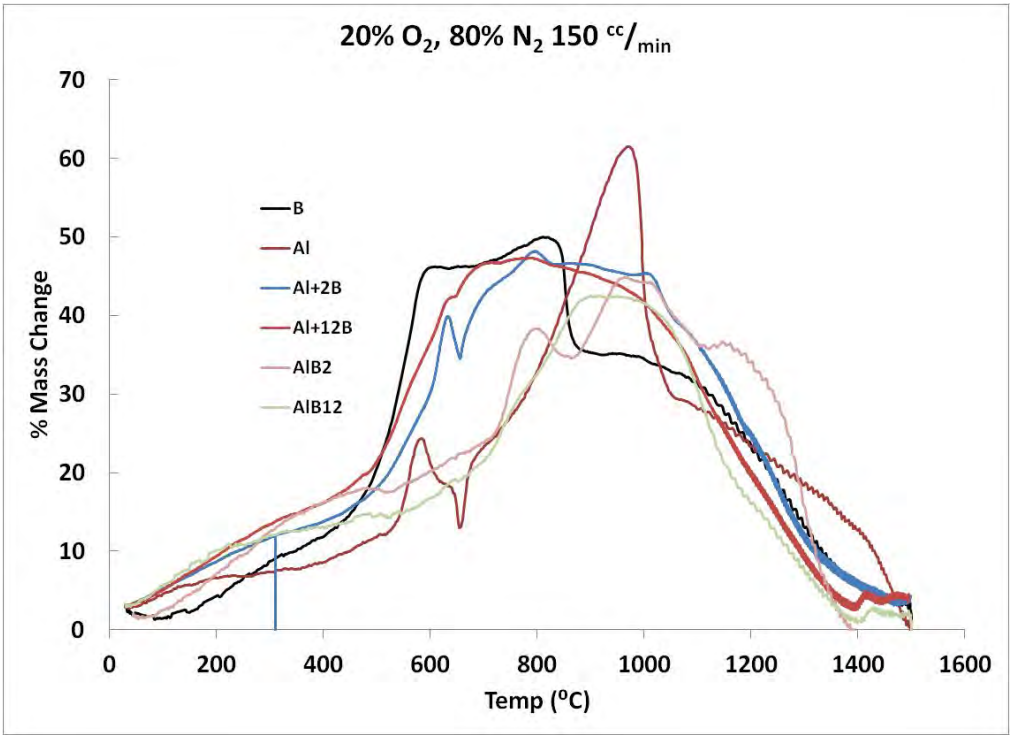

Figure 26. DTA comparing Al:B ratios of 1:2 and 1:12. Neither Al + 12B nor AlB_{12} seem to provide any advantage from an exothermic reaction standpoint.

between materials. Table 9 summarizes the oxidation characteristics of materials provided previously as well as the materials shown in Figures 21 and 22. The lighter the material the easier it is to show a high mass gain upon oxidation. A better way to compare these materials is relative to their theoretical mass gain. It is assumed that B_4C oxidizes to B_2O_3 and CO, such that the final weight gain assumes that all of the C has volatilized. The boron carbide is therefore fairly comparable to boron on the basis of oxidation (see Table 9). The TGA curves (see Figure 21) show that both B and B_4C start to oxidize at the same temperature and the DTA curves are fairly similar, with B showing more heat released than B_4C as shown in Figure 22. B_4C + 2Al was very similar to Al + 2B (Figure 22 and Table 9) and performed the best of the B_4C powders. Reacted B_4C + 2Al showed different oxidation behavior from AlB_2, with rapid oxidation around 650°C. Figure 22 suggests that this material would be worth comparing to AlB_2 using a bomb calorimeter with a polymeric source of oxygen and nitrogen.

Si + 6B and SiB_6 did not gain as much mass as Al + 2B or AlB_2. Both Si + 6B and SiB_6 were not fully oxidized at 1500°C, as indicated by the TGA data in Figure 23. SiB_6 does not decompose until 1380°C, at which point much of the oxidation has already taken place and no liquid metal exists to assist the reaction. The slow oxidation of this material may also be due to the relatively large particle size of the material. Furthermore, silicon does not exhibit good reaction kinetics and was the worst of all materials tested. Surprisingly, the reaction kinetics slowed down when the Si was molten whereas the other materials seemed to speed up when a liquid phase was present.

Al + 12B and AlB_{12} were also investigated in order to clarify the role of aluminum in boron oxidation (for the starting powders) and compare the oxidation behavior of AlB_2, SiB_6, and AlB_{12}. The weight gain of these powders was also similar, as seen in Figure 25. However, Al + 2B reached 98% of its theoretical mass gain while Al + 12B only got to 74% (Table 9). This suggests that the presence of aluminum enables boron to react more completely, and that increasing the amount of aluminum increases the fraction of boron that is oxidized. It is therefore clear that higher borides are not desirable due to the high cost of boron. The fact that AlB_{12} reacts quickly (has a high slope (see Figure 25) or a small oxidation range (see Table 9), however, is of interest and suggests that it deserves further characterization in at least a detonation calorimeter test. DTA (Figure 26) verifies these data in that Al + 12B give high heat output like boron but with a smaller ΔT. Interestingly, AlB_{12} achieves the same extent of oxidation as AlB_2. This is surprising because it was thought that the unreacted aluminum in the AlB_2 powder assisted oxidation of that powder. The similar extents of reaction for Al + 2B and AlB_2 weren't surprising because free aluminum existed in both cases. AlB_{12}, however, did not contain any free aluminum, based on XRD or DTA, and oxidized to the same extent as its starting powder. A more thorough study of oxidation behavior will need to be conducted to determine the role of aluminum in boron oxidation; specifically, the nature of the interaction between B_2O_3 and aluminum.

As it has been stated before, TGA and DTA may not be indicators of energetic performance and in situ tests must be performed, not only to determine the performance of

Table 9
Powder Oxidation Characteristics Comparing Initial and Alternative Materials

Material	Actual % Mass Change	Theoretical % Mass Change	% of Theoretical	Initiation Temp (°C)*	Oxidation Range** (°C)
B	152	222	69	548	905
Al	89	89	100	583	804
Mg	51	66	77	534	292
Mg-Al	78	78	100	527	520
Al + 2B	141	149	83	577	473
AlB_2 -230	145	149	98	755	505
AlB_2 -325	140	149	95	746	509
Mg + 2B	126	139	91	597	480
MgB_2 -230	126	139	90	673	705
MgB_2 -325	118	139	85	679	628
½ MgAl + 2B	122	146	83	596	765
$Mg_{0.5}Al_{0.5}B_2$ -230	126	146	86	753	726
$Mg_{0.5}Al_{0.5}B_2$ -325	119	146	82	723	748
Mg + Al + 14B	141	186	76	573	927
$MgAlB_{14}$ -230	135	186	73	890	608
$MgAlB_{14}$ -325	109	186	59	740	760
B_4C	100	152	66	522	749
Si	46	87	53	919	581
Al + 12B	147	199	74	543	566
AlB_{12} -230	146	199	74	746	484
AlB_{12} -325	143	199	72	751	706
$2Al + B_4C$	115	121	95	535	627
$AlB_3C + 2Al$ -230	100	121	83	699	658
Si + 6B	128	144	89	528	972
SiB_6 -230	116	144	81	683	818

* Initiation temperature is reported as the temperature at 5% mass gain.
** Temperature range over which material goes from 5% to 90% mass gain.

specific materials but more importantly to determine if any preliminary tests conducted here will correlate in any way with energetic performance. Aluminum is a common energetic additive, yet the TGA scan of Valimet H3 aluminum shows relatively little mass gain compared to the boride compounds. This is simply a result of the scale, which favors lighter materials. Although this aluminum is smaller than the standard aluminum used, it reacted almost completely, so larger aluminum could not gain more mass. Therefore, DTA scans may be more indicative of actual performance. The large exotherm exhibited by aluminum separates it from the other materials tested for this milestone although constant volumes of material should be compared. The temperatures at which the exotherms occur are probably more closely related to sensitivity than the apparent initiation temperature as extrapolated from a TGA curve. This reaffirms the importance of in situ testing.

Table 10
Calculated vs. Actual Mass Change for Starting Powders

Starting Powder	Calculated % Mass Gain	Actual % Mass Gain	Efficiency Increase (Δ%)
Al + 2B	118	141	23
½Al-Mg + 2B	113	122	9
Mg + 2B	99	126	27
Al + 12B	142	147	5
Al-Mg + 14B	134	141	7
2Al + B_4C	83	115	32
Si + 6B	121	128	7

An expected mass gain can be calculated for each of the starting powders based on the TGA of the raw powders. Comparing these calculations with the actual weight gain gives an idea of how the additional metal is affecting boron oxidation (see Table 10). All metals aided B or B4C oxidation. Since Al aids in B_4C oxidation, it would be worthwhile to test this powder mixture to see how it reacts when a polymer is added to aid in oxidation.

As the performance and sensitivity of these powders are analyzed, the cost of these powders must also be taken into consideration. While B_4C does not oxidize as well as B, it may be less sensitive and it is a fraction of the cost. It may be worthwhile to investigate methods to improve boron carbide powders to increase their performance. Si + 6B and SiB_6 do not show promise as viable candidates in the particle sizes tested based on low extents of reaction and relatively small heat outputs. This is not surprising in light of the poor performance of Si.

SEM images of the newly prepared powders are shown in Figures 27 and 28. These powders look similar to the initial borides. The reacted powders appear to be uniform with respect to distribution of the phases present.

Al + 12 B and AlB_{12} are not low cost alternatives, but provide a point of comparison with respect to metal-boron ratio and crystal structure (in the case of AlB_{12}). As addressed above, a higher metal to boron ratio increases the extent of reaction of boron and therefore this precludes Al + 12B from being a viable candidate. AlB_{12}, like AlB_2, oxidizes to the same extent as its starting powder and exhibits less sensitivity than B, Al + 2B and Al + 12B. However, it does not look better than AlB_2, a less expensive alternative, so its use is not recommended if these tests are predictive.

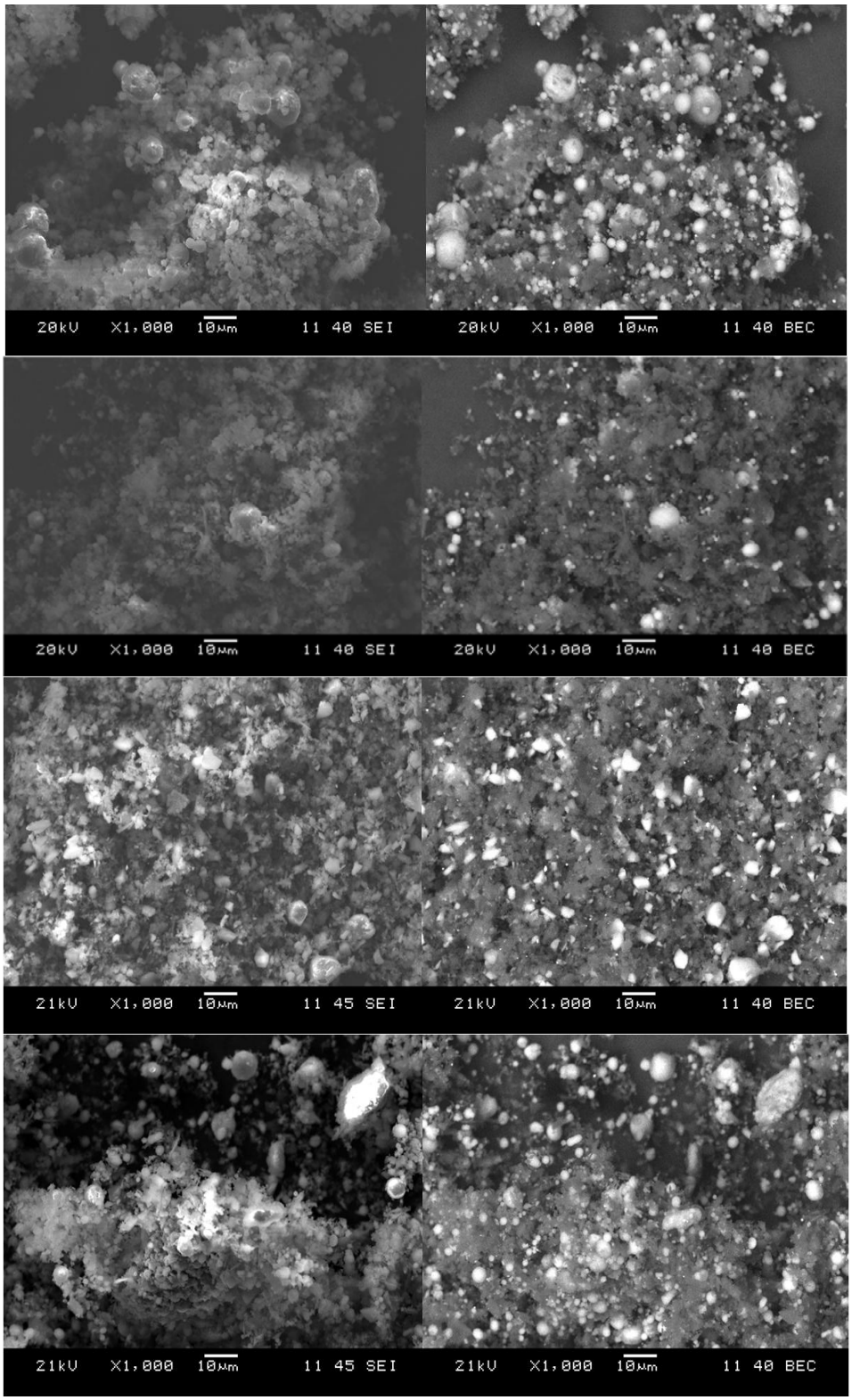

Figure 27. SEM images of starting powders (backscattered images on right and secondary images on left). From top to bottom: Al + 2B, Al + 12B, Si + 6B and 2Al + B_4C. Markers are 10 μm.

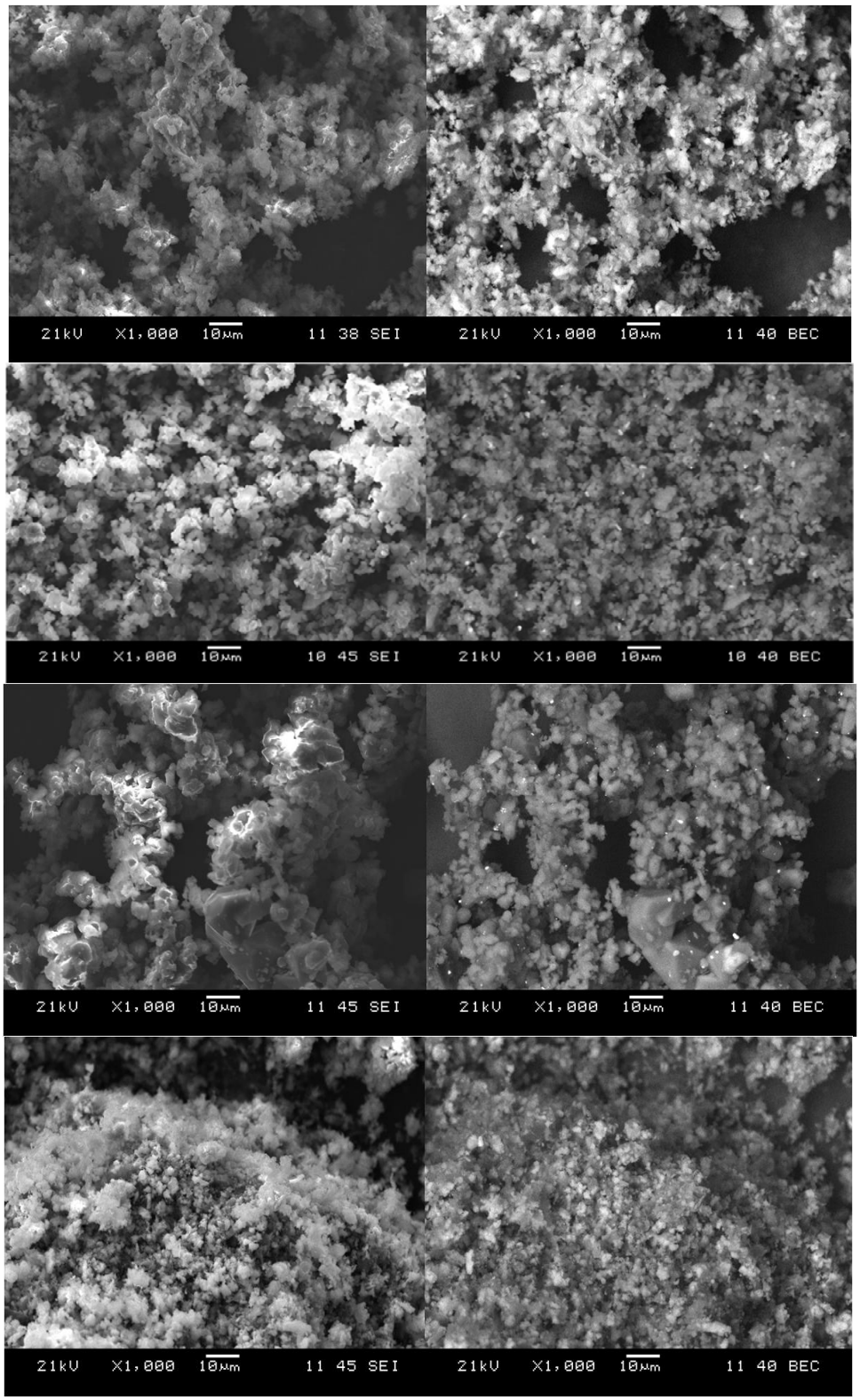

Figure 28. SEM images of reacted powders (backscattered images on right and secondary images on left). From top to bottom: AlB_2, AlB_{12}, SiB_6 and AlB_3C + AlB_2. Markers are 10 μm.

Conclusions

- B_4C is much cheaper than boron and like B is aided in its oxidation by the reaction with Al. When this powder is reacted it is more insensitive and deserves to be tested in comparison to AlB_2. If sensitivity is not an issue, a mixture of boron carbide and aluminum may be a good way to improve the heat output of an explosive mixture on a volume basis.
- A mixture of B_4C and Al in the same stoichiometric ratio as Al + 2B greatly increased the extent of oxidation of B_4C. Both B_4C + 2Al and Al + 2B reached 95% of their theoretical mass change.
- Unlike AlB_2, once the B_4C + 2Al was reacted its extent of oxidation decreased by 10%. Because the reacted composition was composed partially of AlB_2, this suggests that the AlB_3C does not oxidize well.
- Silicon does not provide an advantage over aluminum in aiding boron oxidation and does not oxidize well. The Si + 6B powder mixture showed an abrupt decrease in the rate of oxidation at around 800°C as seen by TGA and DTA. SiB_6 did not show promise either.
- The Al:B ratio in the starting powders Al + 2B and Al + 12B is related to the extent of oxidation. More aluminum corresponded to higher extent of reaction for these two mixes. Given the high cost of boron, the use of Al + 12B or AlB_{12} is difficult to justify if these results are predictive of explosive mixtures.
- Calorimetry data are needed to determine how the structural, morphological, and/or oxidation characteristics of the powders affect their performance.

V. Effect of Aluminum and Boron on AlB_2 Oxidation in Air

Effect of Free Boron and Aluminum

Powders with the nominal composition 'AlB_2' have been synthesized, but in all cases the reaction between aluminum and boron has been incomplete. Because the molar ratio of boron to aluminum is 2:1 and the mass ratio of boron to aluminum is about 1:2, the mass percents of aluminum and boron that remained unreacted are approximately the same. Therefore, the effect of both free aluminum and free boron on the oxidation of AlB_2 could be studied as a function of the percent free aluminum and boron remaining after reaction (see Figure 29 and Table 11). Figure 30 illustrates that having higher amounts of free aluminum and boron caused a sample to oxidize at lower temperatures. There was also more hysteresis in weight loss at high (>1250°C) temperatures for samples with more free boron and aluminum. The surface area of these powders may be, and probably is, different, which may impact the magnitude of differences seen between these powders. To determine the cause of these phenomena (aluminum, boron or something else), samples were prepared with varying amounts of free boron and aluminum.

Effect of Free Aluminum

Three powders were made to test the effect of free aluminum on the oxidation behavior of AlB_2. The first powder, 162F, was a stoichiometric mixture of aluminum and boron heated to 900°C for 1 hour in He-6%H_2. This powder had 9.4% free boron and 9.7% free aluminum by weight. Aluminum was then added to this powder and it was reacted again at 900°C for 1 hour in He-6%H_2 in an attempt to react all of the free boron, resulting in powder 169B1. This powder had less free boron than 162F but more free Al. The aluminum was then removed by washing in HCl and a powder with a composition around 95% AlB_2 – 5% B – 5%Al_2O_3 (165E) was formed.

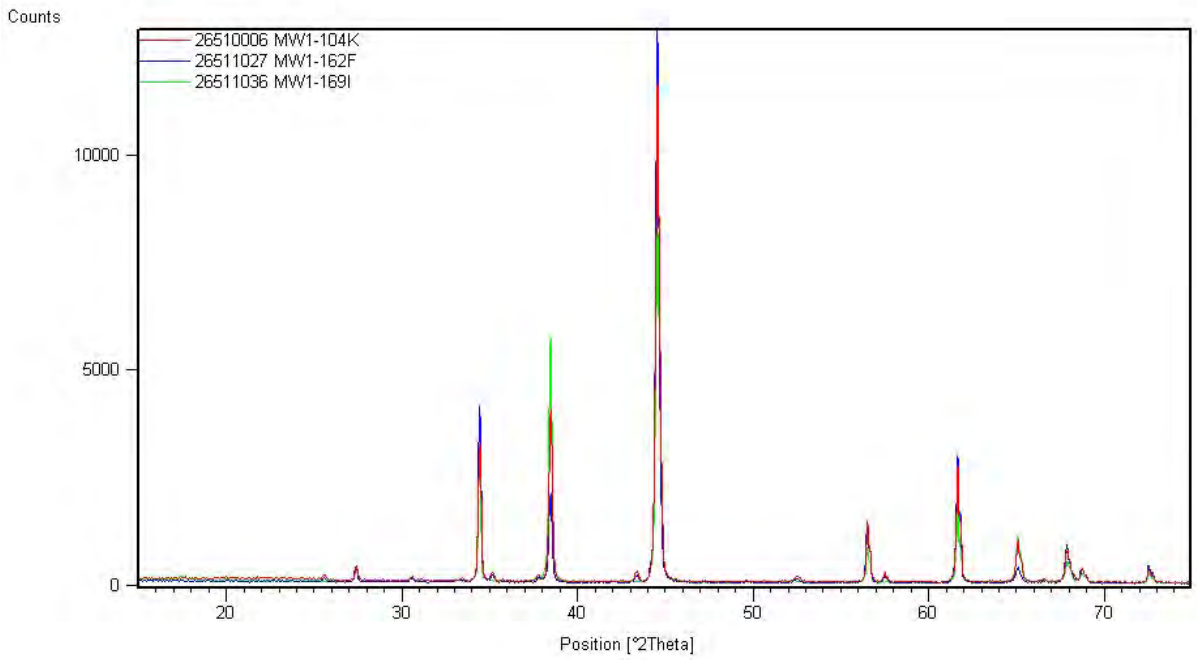

Figure 29. XRD patterns for three different "AlB_2" samples made starting with one mole of aluminum and two moles of boron. Free boron does not show up by XRD but the amount of free Al is very discernable increasing as 169I > 104K > 162F (see Table 11).

While Rietveld analysis suggests that the boron was not completely removed by the addition of aluminum, the aluminum peak went down after aluminum was added (Figure 31), showing that free boron existed, which reacted with the aluminum. TGA (Figure 32) showed that excess aluminum does not affect the initiation of oxidation, but does slow down the rate of oxidation at higher temperatures.

Table 11
Powders with Free Aluminum and Boron

	Rietveld Analysis (Weight %)				Adjusted Rietveld* (Weight %)				
Sample	AlB_2	Al	Al_2O_3	Al_3BC	AlB_2	Al	B	Al_2O_3	Al_3BC
162F	84.9	10.7	2.9	1.4	76.9	9.7	9.4	2.6	1.3
104K	76.0	19.1	3.8	1.1	64.8	16.3	14.7	3.2	0.9
169I	65.4	32.3	0.4	2.0	51.7	25.5	20.9	0.3	1.6

* Rietveld analysis adjusted for undetectable (by XRD) free boron.

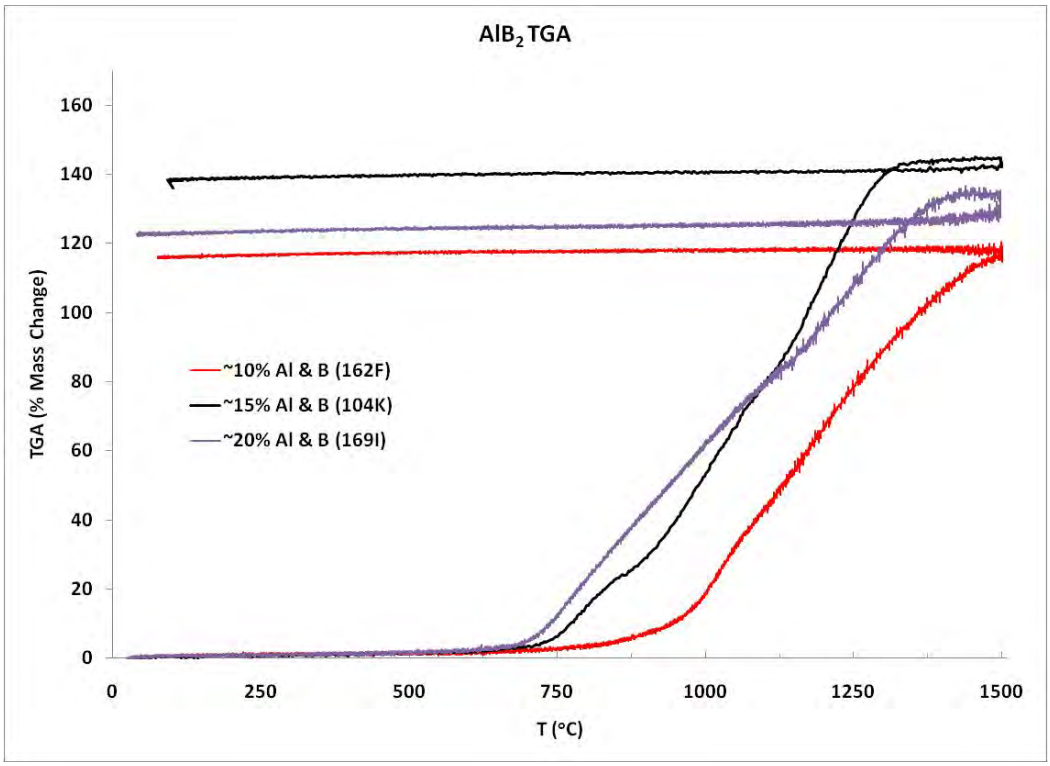

Figure 30. TGA of reacted AlB_2 samples containing different amounts of free Al & B (see Table 11). The oxidation initiation temperatures change as well as the % mass change and hysteresis.

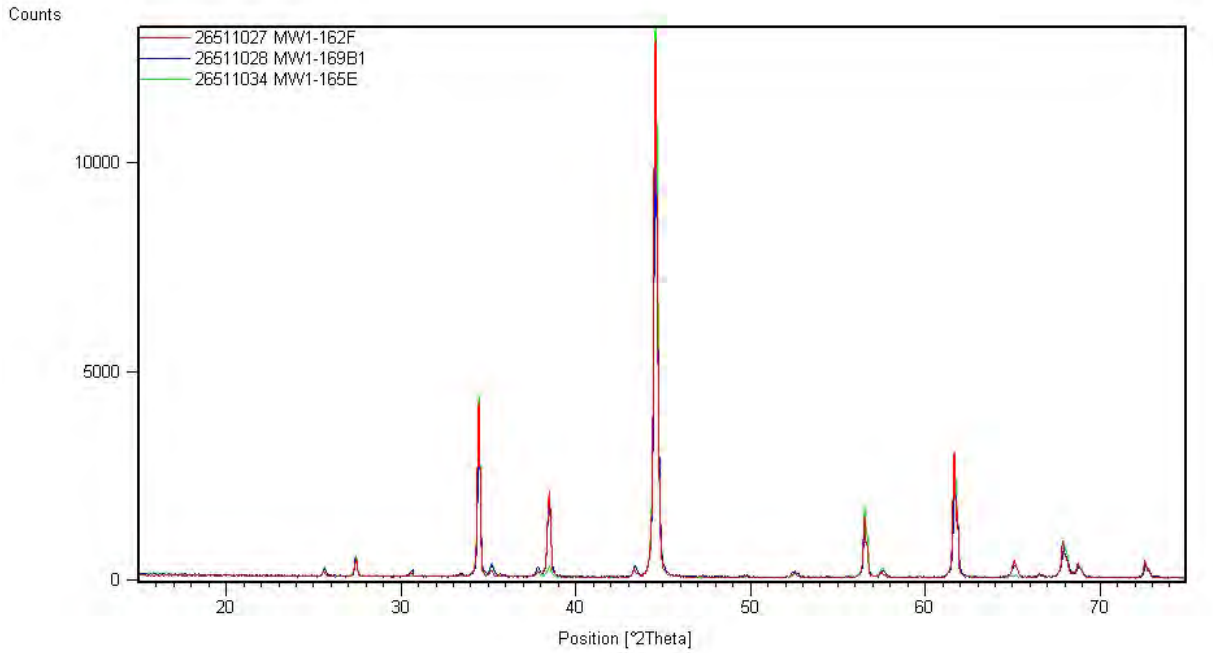

Figure 31. XRD patterns for 162F (reacted AlB_2), 169B1 (Al added to react with free B) and 165E (acid-washed 169B1). The acid-washed powder increased the AlB_2 content to 93 %.

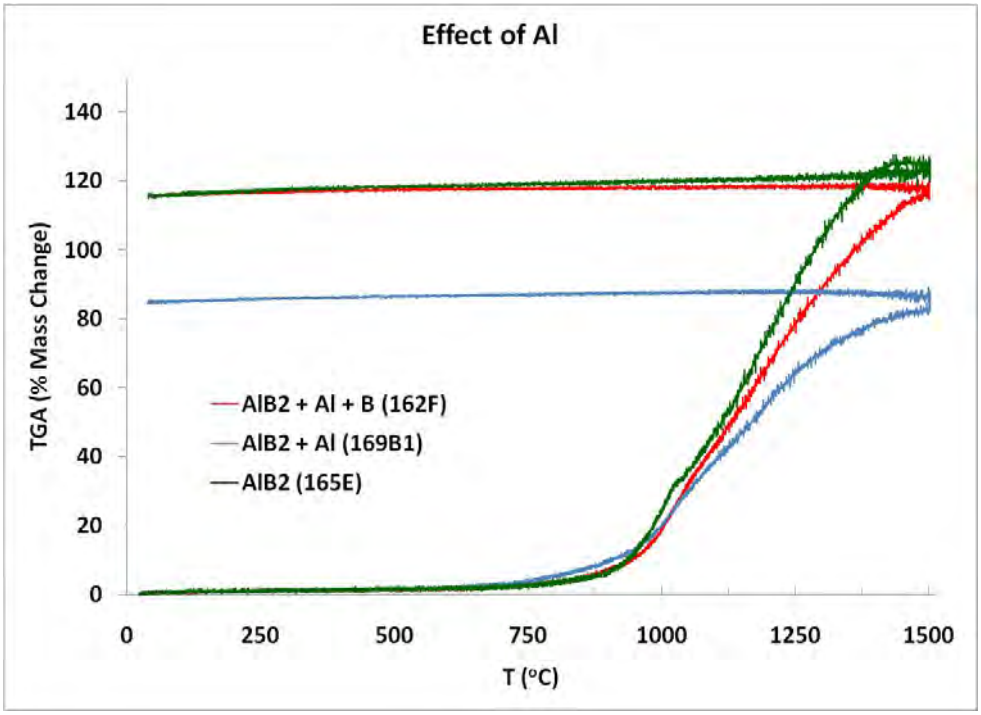

Figure 32. TGA of as reacted (162F (red)), with excess Al (169B1 (blue)) and acid washed powder (165E (green)). Excess Al does not change the oxidation initiation temperature but does slow down the kinetics of oxidation at higher temperatures.

Effect of Boron

The effect of free boron on AlB_2 oxidation was examined by acid washing three different samples. By acid washing samples with different amounts of free aluminum and boron, powders with almost no aluminum and different amounts of free boron were produced. Powders 142A and 163A were made by washing powders 104K and 158C, respectively. X-ray patterns for these three acid-washed powders are shown in Figure 33. The acid washing has essentially removed the Al with slightly higher aluminum oxide. Oxidation in air (see Figure 34) shows that the mass gains are higher for powders with more boron, as expected. However, reducing the amount of free boron increases the ability to oxidize to a higher percent of the theoretical value. Reducing the amount of free boron increases the initiation of oxidation without substantially affecting the rate of oxidation. The AlB_2 with 15% and 20% free boron began to oxidize around 750°C, but the boride powder with ~5% B did not oxidize readily until higher temperatures. The high-temperature hysteresis appears to be due to volatility of B_2O_3 produced by oxidizing the free B. When AlB_2 oxidizes, it forms an aluminum borate, which has a lower vapor pressure than B_2O_3.

Improvement in Purity

While it was not possible to make phase-pure AlB_2, as had been expected, recently synthesized powders have shown a much higher purity than the powder delivered previously to ARDEC. The free aluminum accompanying the AlB_2 in these powders has been nearly

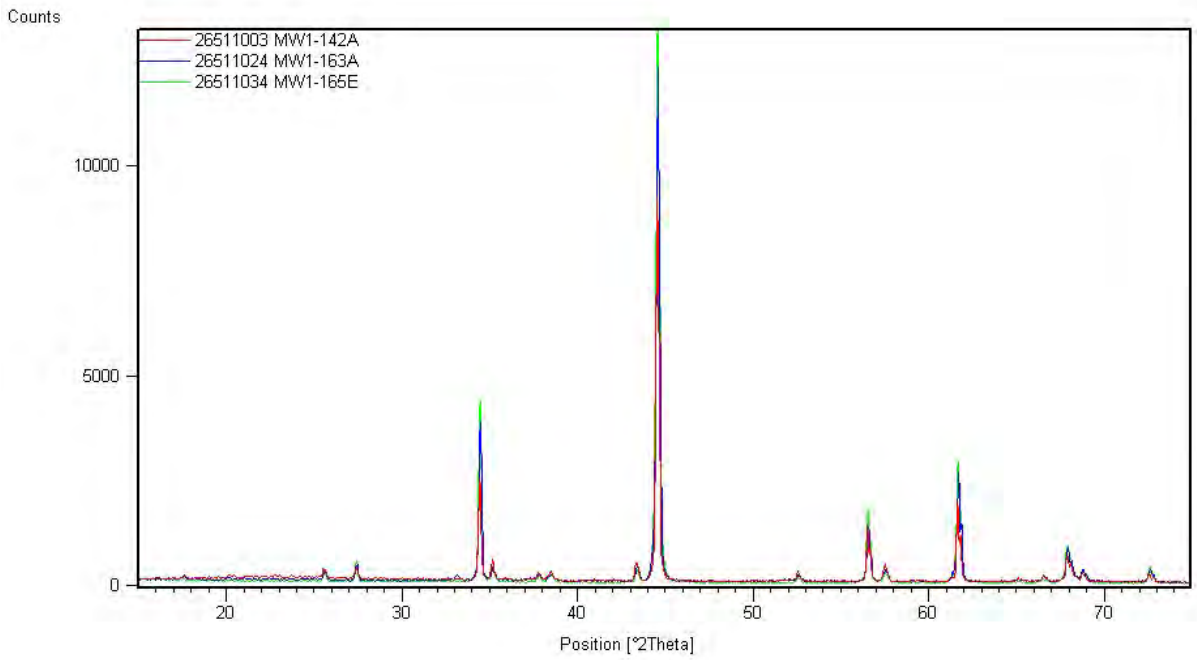

Figure 33. XRD patterns for 142A (red), 163A (blue) and 165E (green). All patterns have minimal amounts of aluminum but slightly increased aluminum oxide.

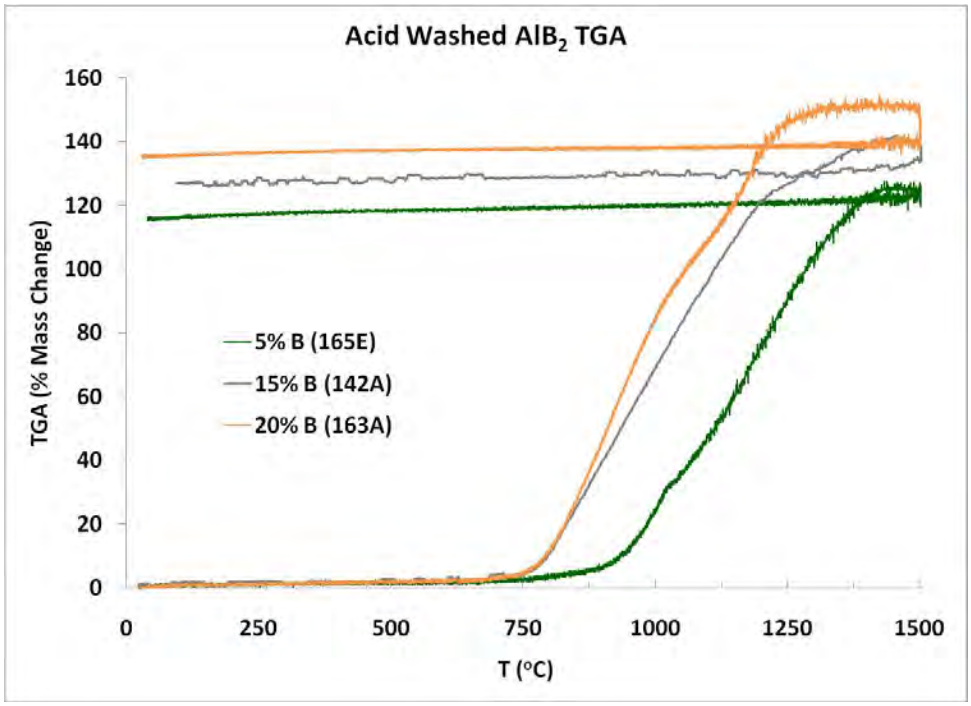

Figure 34. TGA of acid-washed "AlB_2" powders containing different amounts of free B (Green = 5 %, blue = 15 %, and orange = 20 %). Powders (heated in air at 10°C/min) were held at 1500°C.

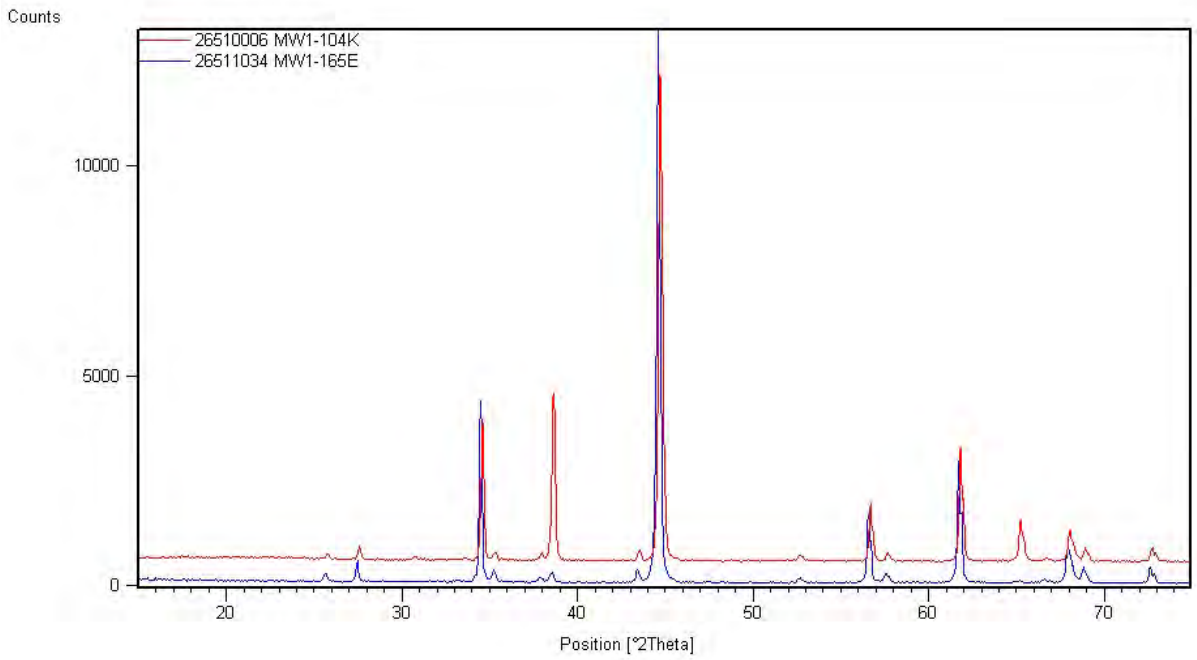

Figure 35. Comparison of initial material delivered (104K (red)) and recently synthesized material (165E (green)). Note that the aluminum (38° and 65° 2θ) has been nearly eliminated.

eliminated, as seen from XRD pattern in Figure 35. The weight percent of AlB_2 in these powders is above 90% by unadjusted Rietveld (see Table 12). It would be worthwhile testing these high-purity powders in explosive formulations to see if they offer any advantage over the previously prepared materials.

A much better alternative to acid-washing, which is expensive and time consuming, is to reduce the amount of free Al and B by improved processing. To date, the best results have brought the value of aluminum down from about 20 % to about 8 wt. %, which is a substantial improvement. Testing in explosive formulations should be used to see if differences can be observed.

Table 12
Phase Comparison of AlB_2 Powders

	Rietveld Analysis (Weight %)				Adjusted Rietveld* (Weight %)				
Sample	AlB_2	Al	Al_2O_3	Al_3BC	AlB_2	Al	B	Al_2O_3	Al_3BC
104K	76.0	19.1	3.8	1.1	64.8	16.3	14.7	3.2	0.9
165E	93.1	1.0	5.8	0.0			NA		

* Rietveld analysis adjusted for undetectable free boron.

Conclusions

- A nearly single phase material has been synthesized with only minor impurities. The Al_2O_3 in the final powder is mainly from oxygen in the starting powders.
- Free boron and free aluminum change the oxidation characteristics of AlB_2 in air at atmospheric pressure.
- An increasing amount of free boron decreases the initiation temperature of AlB_2 (towards the initiation temperature of pure boron) but increases the extent of oxidation.
- An increasing amount of free aluminum slows down oxidation at high temperatures but does not have much impact on initiation temperature.
- The surface area of these powders may be, and probably is, different between powders. These measurements should be made to assess the differences seen between these powders.
- Oxidation in air at atmospheric pressure is likely a poor indicator of what one can expect in an explosive mixture. Initial combustion calorimetry data from ARDEC suggest that AlB_2 (104K) had a higher extent of oxidation than Al + 2B, which is opposite of oxidation kinetics in flowing air.

VI. Surface Treatments of AlB_2 to Limit Degradation in Moist Environments

Background

Metal fuel additives are used for explosive formulations to increase the energy density of an energetic mixture. These additives are often small diameter powders with large surface area-to-volume ratios that are added to organic-based energetic systems. While the high surface area gives the powders favorable energetic characteristics upon ignition, it also leaves them vulnerable to oxidation during handling, transportation and storage. Metal powders, such as Mg and Al, are oxidized by atmospheric water vapor through the formation of surface hydroxides and oxides. It is expected that high humidity and/or high temperature conditions will accelerate the oxidation process. This oxidation process is undesirable, as a powder with a higher mass fraction of surface oxide will have a lower energy density and the oxide will change the ignition reaction kinetics at the organic-particle interface in situ.

Boron is relatively resistant to reaction with water at storage temperatures[114], but boric acid, a water soluble compound, has a substantial vapor pressure at low temperatures[115]. When Al and B are mechanically mixed together one would expect the Al to hydrolyze readily and the boron to be resistant to oxidation under ambient storage conditions.

Aluminum/boron physical mixtures[116] as well as diboride (AlB_2) have been investigated as an alternative fuel additive due to their increased energy density compared to conventional additives[12]. Results are unclear at the present time since Mitani and Izumikawa found that Al increased the kinetics of ignition but that only the B burned, while recent testing by ARDEC suggests that Al and B mixtures only resulted in aluminum combustion. ARDEC found that AlB_2 was more energetic than the Al + 2B mixture.

AlB_2 was hypothesized to have lower sensitivity to water than conventional metal additives due to the formation of more favorable aluminum and boron chemical bonds. AlB_2 was compared to boron, aluminum, and a physical mixture in the ratio one mole of Al to two moles of B. Al has a known sensitivity to hydration and requires passivation to prevent hydrolysis. Removal of free aluminum from AlB_2 by an acid wash was expected to improve resistance to degradation. An electroless tin coating was applied to AlB_2 in order to limit oxidation. Alternatively, silane coatings were applied to make the materials hydrophobic, even though these coatings are permeable to water vapor. Muller et al.[117] suggested that amines offer better protection from moisture absorption for nanoscaled TiN than organic polymers

containing oxygen so a commercially available amine coating was also investigated. The purpose of this milestone was to find ways to protect AlB_2, if not already moisture resistant, under ordinary storage conditions.

Experimental Procedures

AlB_2 powder was synthesized from a stoichiometric ratio of the elements. The reaction of aluminum and boron does not proceed completely, leaving some unreacted starting material. Compositions of the tested powers are reported in Table 13. The aluminum, boron, and, by extension, Al + 2B, compositions are reported as they were given by the manufacturer. The composition of AlB_2, was measured by XRD and corrected for free boron, which is not easily detected.

It is interesting to note that a commercially (H. C. Starck through ABCR) supplied AlB_2 powder, which was almost identical to our synthesized powder by XRD (see Figure 36), claimed to have a composition of over 95% AlB_2 by chemical analysis. Starck measured an O content of 1.9 %. It is clear that their analysis made no determination of separate aluminum-boron phases, which may have an impact on both moisture sensitivity and overall energetic performance. The discrepancy also suggests that the Rietveld fitting of XRD scans overestimates the oxygen content (via Al_2O_3) of the powder.

Samples of the Ceramatec control AlB_2 powder were treated with six different surface modifications. These included silane, fluorosilane, amine, and tin coatings, as well as an acid treatment to remove the free Al. The different surface treatments were given a code, as shown in Table 14. The silane treatments were prepared by making a solution of 95 vol. % methanol-5 vol. % distilled water, adjusting the pH to 4.5-5.5 with acetic acid, adding 35 grams of AlB_2 powder to 100 cc of solution while stirring, and finally adding 2 grams of the silane solution while stirring. The powders in solution were stirred for 30 minutes at 500 rpm, filtered, washed with methanol, rinsed with acetone, and dried at 110°C for 15 minutes. The amine solution was made by adding 2.15 grams of octadecylamine (Aldrich 305391) to 500 cc of hexane and heating to get into solution. The AlB_2 powder (35 grams) was stirred for two hours and then filtered, rinsed with hexane, and dried at 110°C for 15 minutes.

An electroless Tin was applied to 35 grams of AlB_2 powder by adding the powder, while stirring, to 475 ml of the electroless Tin solution. The powder was then washed with water, acetone, and dried at 110°C for 15 minutes.

The acid wash was accomplished by adding 50 grams of AlB_2 powder to 700 ml of water and slowly adding dilute HCl to the powder until the reaction stopped. The solution was filtered, rinsed with water and acetone, and dried at 110°C overnight. The powder stuck to the filter paper. The powder was pulverized in a mortar and pestle and screened -325 mesh to remove the filter paper. However, some of the filter paper remained in this powder.

Table 13
Compositions of Starting Powders

	Particle	Surface	Composition (Weight %)					
Sample	Size (μm)	Area (m^2/g)	Al	B	Al_2O_3	B_2O_3	AlB_2	Other
Al	3.4	1.4	99.4	0.0	0.6	0.0	0.0	0.0
B	1.2	10.9	0.0	97.6	0.0	2.0	0.0	0.4
Al + 2B	2.8	6.2	55.2	43.2	0.3	0.9	0.0	0.2
AlB_2	8.5	2.0	10.6	10.2	3.4	0.0	74.7	1.0

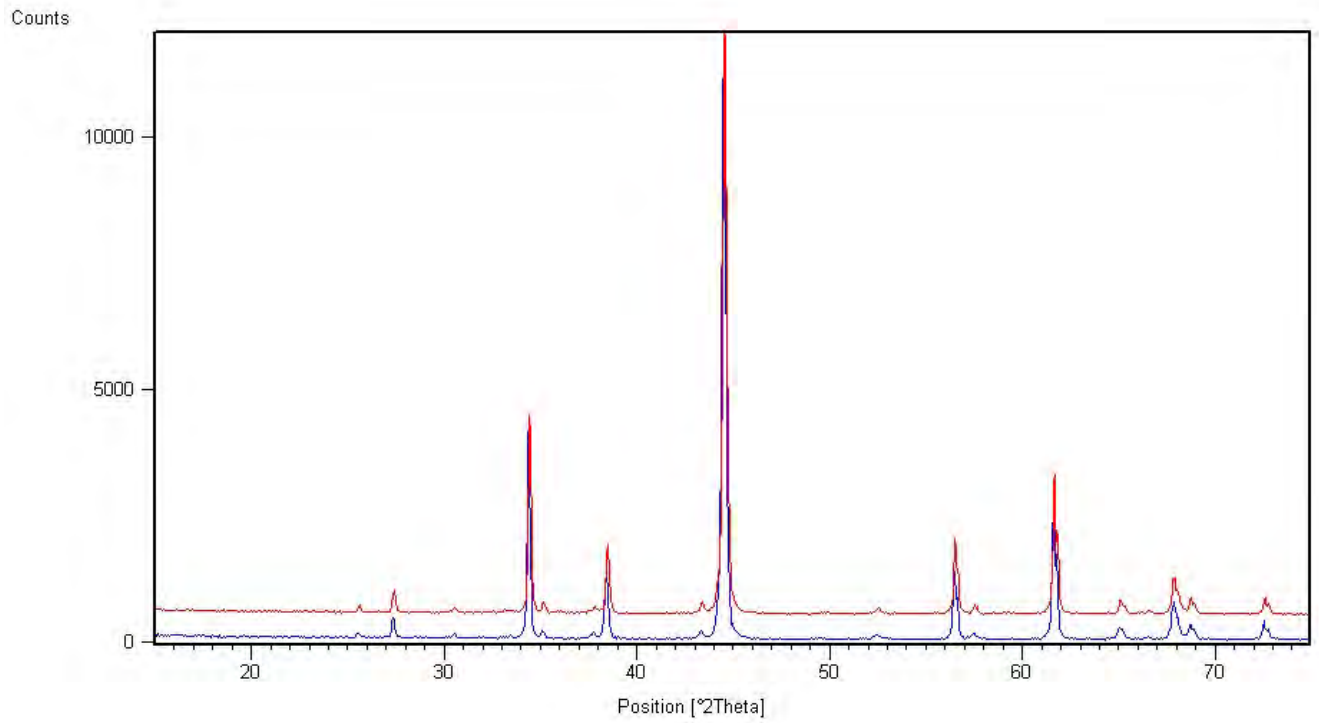

Figure 36. XRD comparison of H. C. Starck AlB_2 (red) and material manufactured in-house (blue). The patterns are nearly identical, despite discrepancies in reported compositions.

Salt solutions were made for different relative humidities[118]. A relative humidity chamber at ≈10% was made by adding KOH (Alfa Aesar 13451) to deionized water to form a saturated solution in the bottom of a bell jar. Relative humidity chambers at 75% and 90 % were

Table 14
AlB_2 Surface Treatments

Treatment	Code	Approach
Silane	S	n-octadecyltrimethoxysilane[a]
Fluorosilane	FS	Tridecafluoro-1,1,2,2-tetrahydrooctyl triethoxysilane[b]
Amine	A	Octadecylamine[c]
Silane (Shin-Etsu)	SE	3,3,3 Trifluoropropyl trimethoxysilane[d]
Tin Coating	Sn	Electroless Sn solution[e]
HCl Wash	HCl	HCl washed, water/acetone rinsed. and dried at 110°C

a. Gelest SI06645.
b. Gelest SI TB175.0
c. Aldrich 305391.
d. Shin Etsu KBM-7103
e. Liquid Tin (MG Chemicals No. 421).

prepared using NaCl (Sigma Adrich S9886) and KNO_3 (Spectrum P1345), respectively. The bell jars were equilibrated at temperature inside convection ovens (Yamato DKN 400). Powders were weighed (Shimadzu AUW 2200) before starting the tests and at periodic intervals during the test. X-ray diffraction (Phillips X'Pert) and scanning electron microscopy (Joel 5900 LV) were used to characterize powders.

Tests at 100 % relative humidity were made inside a constant temperature water bath (Polyscience model 2L) by placing ≈one gram of powder in a test tube filled with 15 cc of deionized water and heating at 80°C for 135 hours. The powders were dried for 24 hours, crushed, and x-rayed.

Results and Discussion

Figures 37 and 38 show results from the first set of tests which did not include B, Al, or Al-B mixtures. These tests, conducted over a month time period show that octadecylamine and silane (n-octadecyltrimethoxysilane[a]) coatings provide significant protection compared to the uncoated control powder, even at high humidity levels. It is very clear, however, that storage of powders in low-temperature, low-humidity environments will allow AlB_2 to avoid oxidation.

Two of the treatments (HCl wash and Sn coating) were much worse than the control. While XRD showed Sn present after the electroless deposition (see Figure 39), SEM images showed that the Sn did not coat the particles evenly, but was poorly distributed and agglomerated (see Figure 40). These results do not preclude that a well-deposited (uniform and dense) electroless coating could provide protection. The rapid oxidation of the HCl washed powder was surprising and may be the result of chlorine remaining after the treatment, as evidenced by EDS. In any regard, removal of Al by an HCl wash is tedious and results in poor yields. Further testing therefore concentrated on the silane or amine-coated materials.

Based on Figure 37(e) it appeared that the n-octadecyltrimethoxysilane (S), due to its low moisture pick-up, or the octadecylamine (A), due to its low slope after initial exposure to moisture, were the most promising coatings. SEM evaluation could not detect the coatings, in accord with expectation that the coatings were very thin. It should be noted that an XRD of the control sample after exposure to 90% relative humidity for 4 weeks at 40°C showed that the material was unchanged (see Figure 41). This suggests that simply storing the powder in closed, well-packaged containers will result in adequate lifetimes for AlB_2 powder.

Accelerated tests for the top candidate materials in comparison to B, Al, and Al-B mixtures are shown in Figure 43. All powders were dried at 110°C for 24 hours prior to taking initial weights. The weight gain for Al is consistent with $Al(OH)_3$ formation, which was confirmed by x-ray diffraction. The AlB_2 powder is much more resistant to degradation than fine Al powder, in accord with expectation. At 60°C and 75 % relative humidity, the silane (S) coating provided the best protection with the amine (A) coating a distant second (see Figure 42(a)). The boron lost weight, presumably due to the formation of boric acid, which is soluble in water and has a high vapor pressure[115]. What was surprising, however, was the excellent performance of the intimately mixed Al+2B powder, which did not follow Vegard's law (rule of mixtures) with regard to Al oxidation. It is suspected that the milling step provided additional passivation of Al , indicating that Al/B mixtures are candidates for energetic applications and should continue to be compared to their boride counterparts.

Increased temperature accelerated the aluminum hydration and caused all coatings to show weight gain (see Figure 42(b)). It is very apparent that none of these coatings are

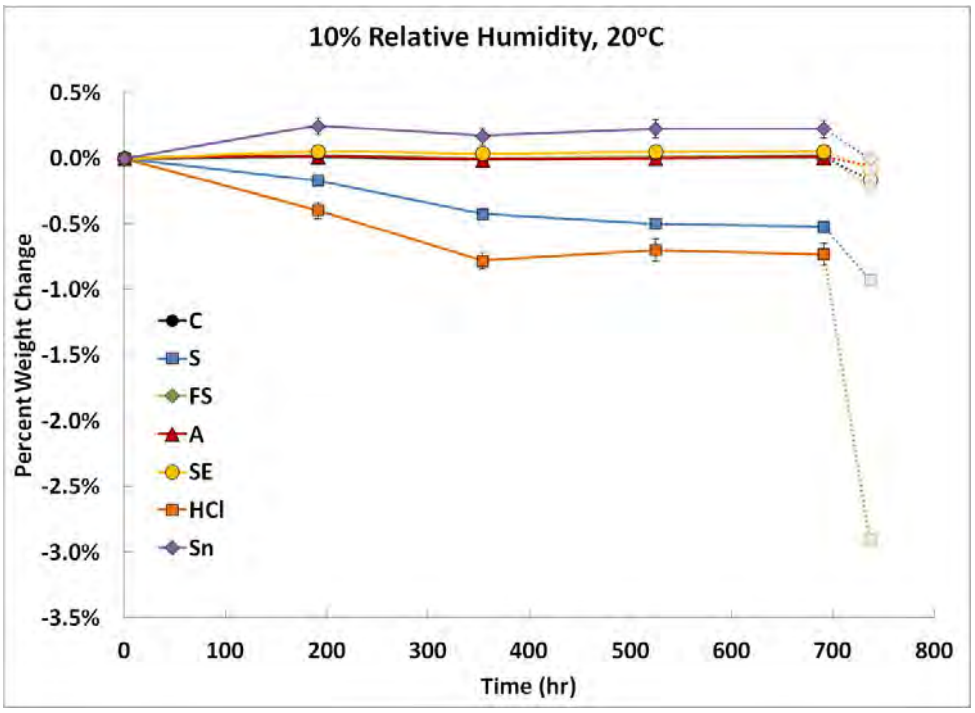

(a)

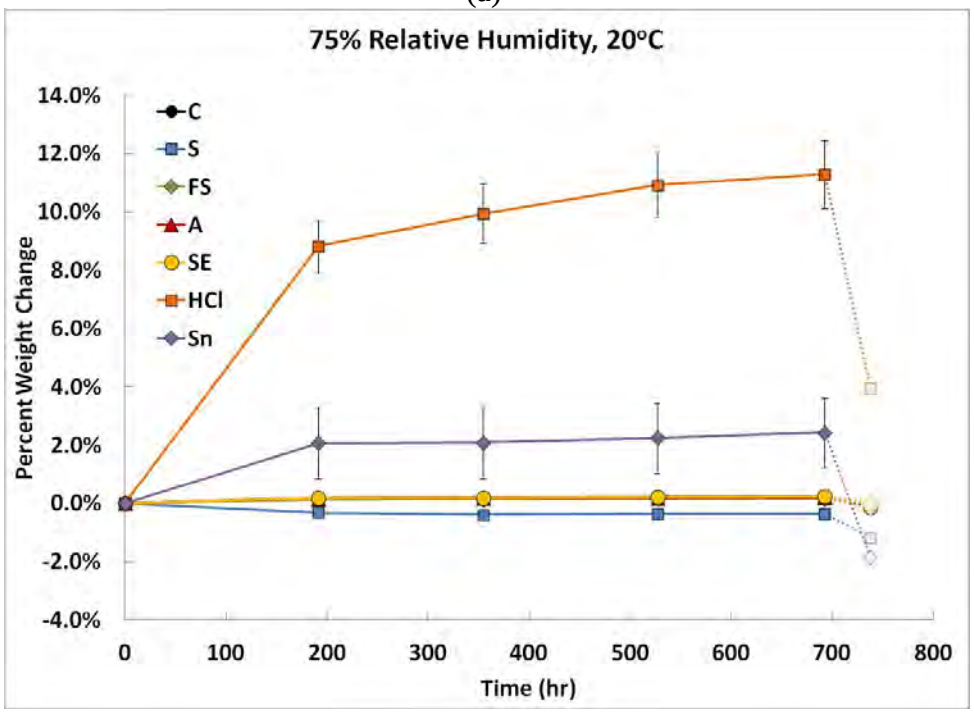

(b)

Figure 37. Weight change of AlB_2 samples in either 10 or 75 % relative humidity (RH) at room temperature (RT) compared to the same samples in either 75% or 90% RH at 40°C. The open symbols at 738 hours represent the sample weight after heating to 110°C overnight to dry the powders. (a) 10 % RH at RT, (b) 75 % RH at RT. All of the AlB_2 powders, with the exception of the acid-washed and Sn coated samples, show little change in mass at room temperature.

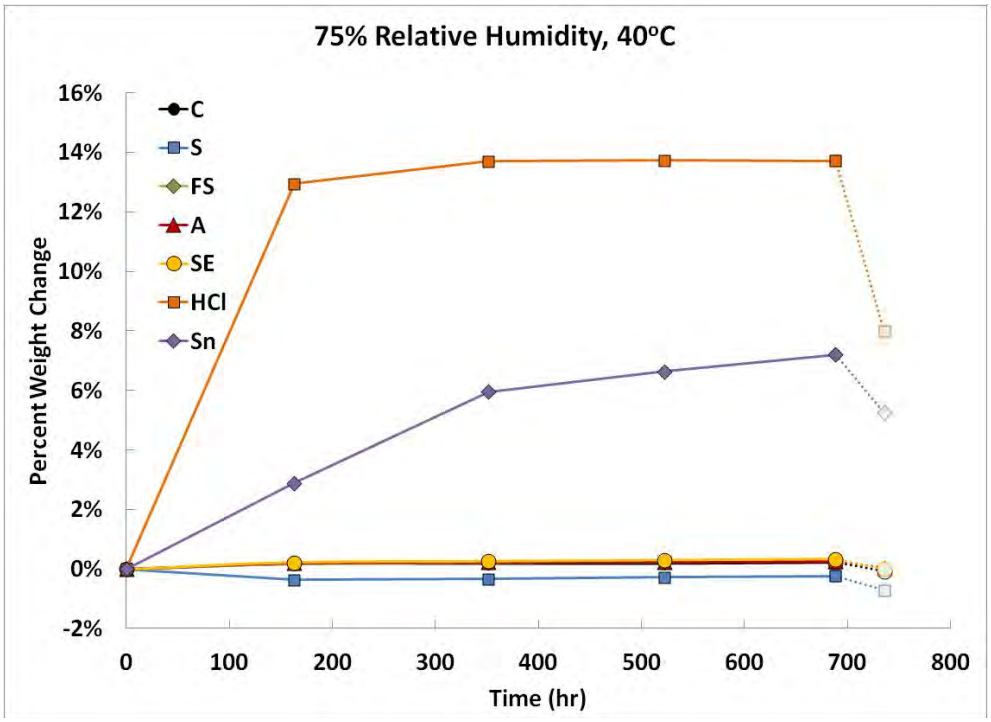

(c)

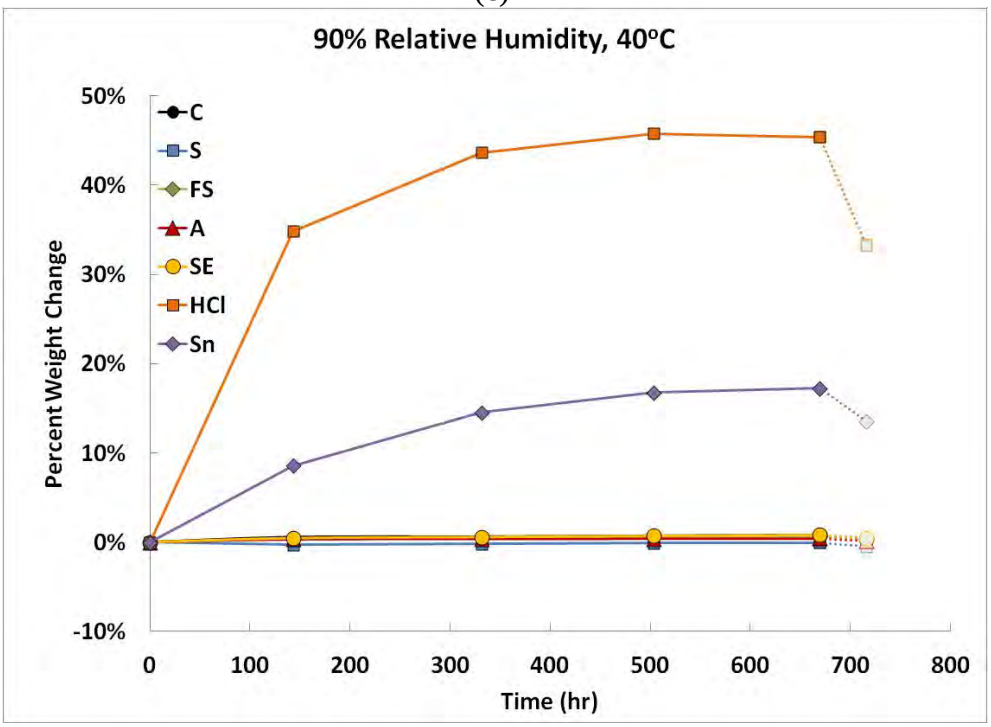

(d)

Figure 37 (continued). Moisture sensitivity at 40°C. (c) 75 % RH and (d) 90 % RH. It is apparent that weight change is dependent on both temperature and relative humidity.

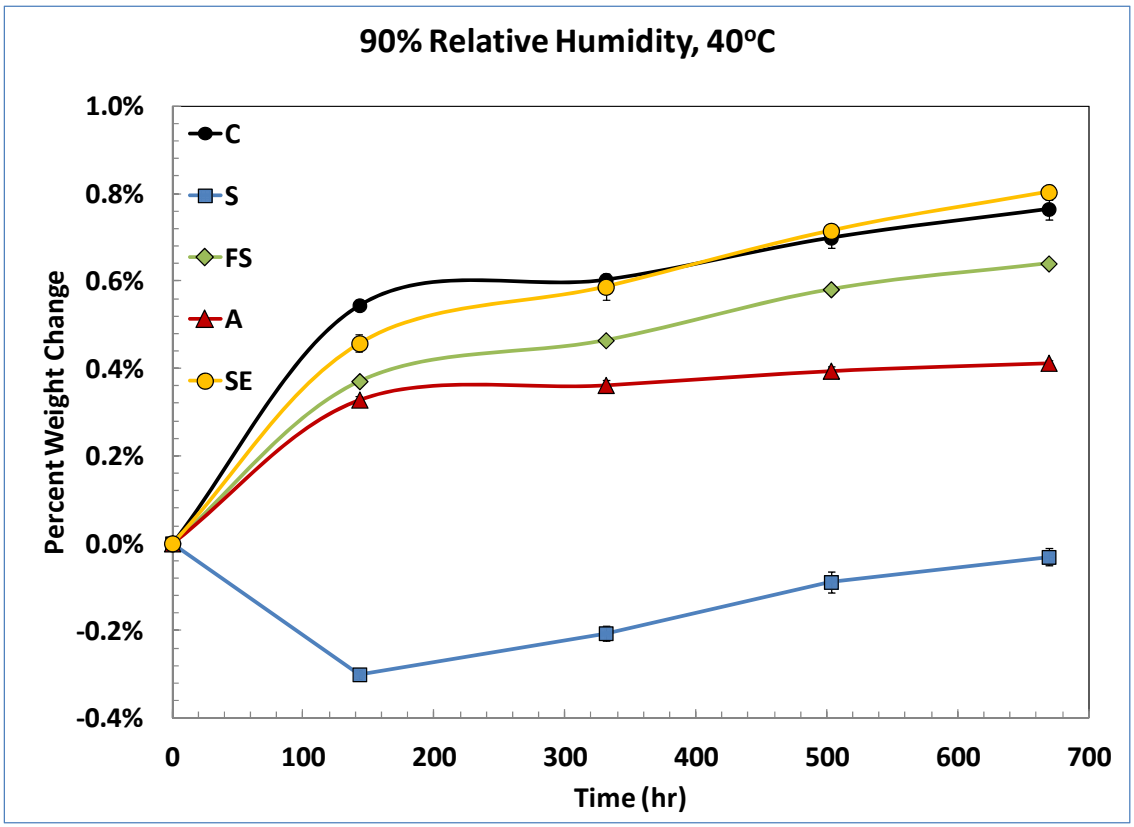

(e)

Figure 37 (continued). Comparison of control with silane-coated or amine-coated powders under the most aggressive condition (90 % RH/40°C) of first set of tests. Octadecylamine (A) is attractive because it shows little change as a function of time. The n-octadecyltrimethoxysilane (S) sample is of interest due to its low weight gain.

impervious to moisture absorption, which is clearly activated by temperature. Short-term exposure to boiling water caused no problem for the aluminum boride powder, but longer term (135 hours) exposure to 100 % relative humidity (samples encapsulated in water) at 80°C caused severe degradation for all materials. The Al powder turned white due to hydroxide formation and gained 162 % of its initial mass. The control powder agglomerated (see Figure 43), turned gray, was primarily amorphous (see gray scan in Figure 44), and gained 130% of its initial mass. The silane (S) coated powder also turned gray, did not coarsen (see Figure 45), still showed some crystallinity (see Figure 46), but gained 109% of its initial mass. Thus it is apparent that high humidity combined with high temperature is detrimental to silane-coated powders. The fluorosilane fared slightly better, gaining 73% of its initial mass.

One of the main advantages of forming the borides is seen by examining the Al+2B powder, which looked identical in color after the same exposure treatment. However, SEM &EDS (Figure 47), and XRD (Figure 48) clearly show how the Al hydrolyzed to $Al(OH)_3$, which is not apparent in the AlB_2 samples. The weight gain for this material was 79 %, but clearly was aided by some dissolution of boron as boric acid.

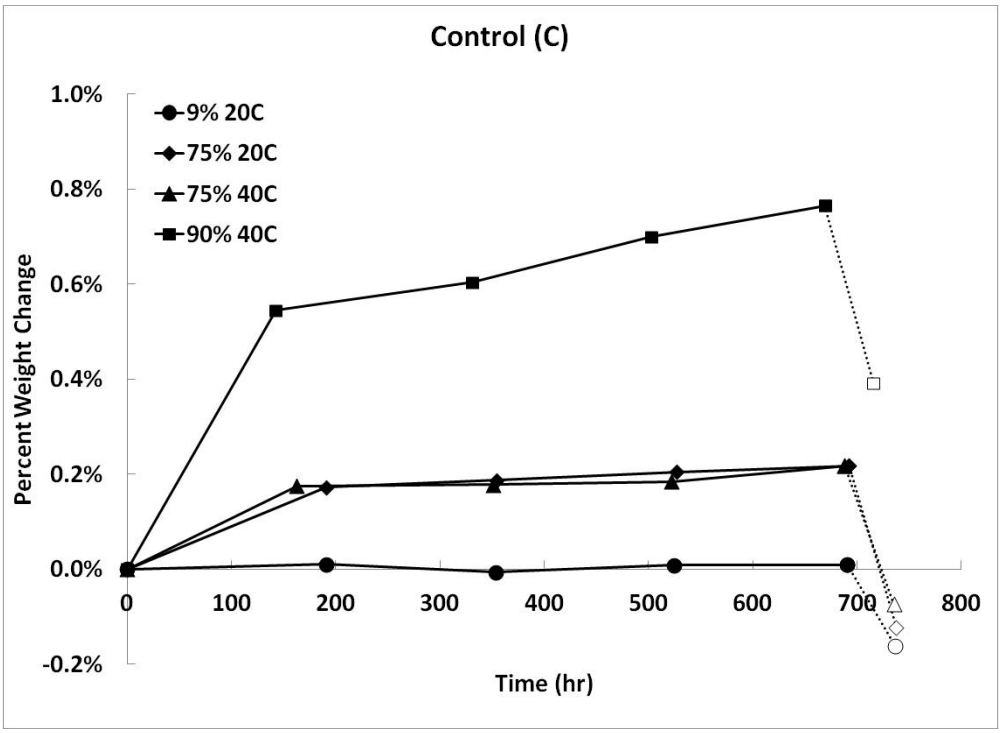

(a)

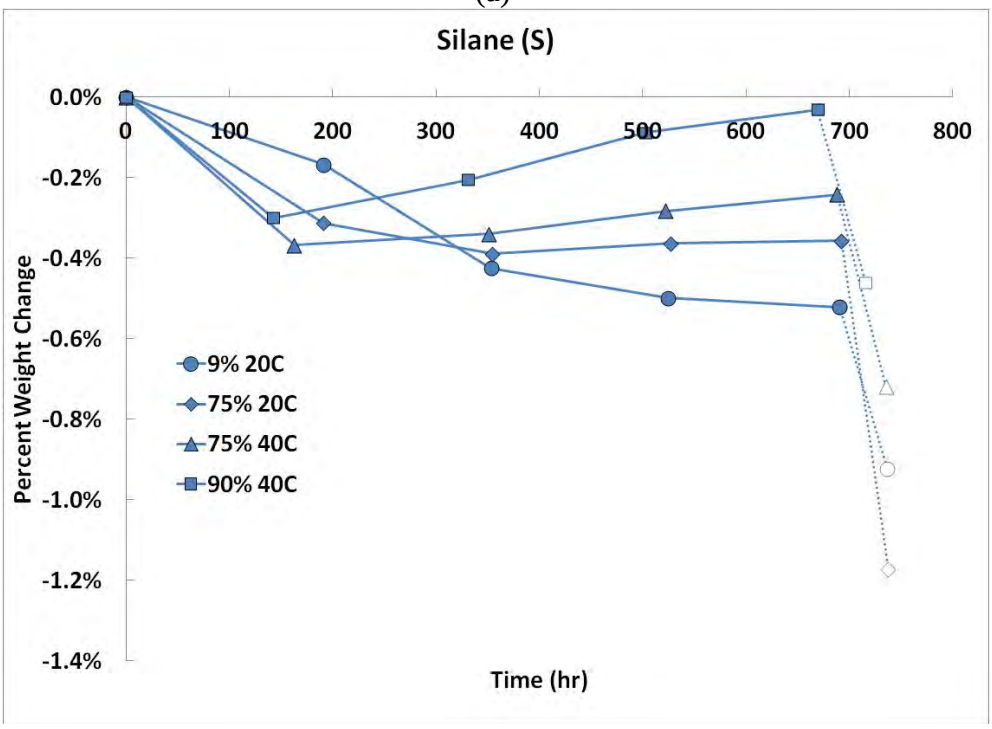

(b)

Figure 38. Comparison of powders under different conditions of relative humidity and temperature. These are the same data as shown in Figure 37. (a) AlB_2 control (C) showing insensitivity to temperature at 75 % RH, (b) silane (n-octadecyltrimethoxysilane) powder (S) suggesting that there was still moisture trapped within the agglomerated powder.

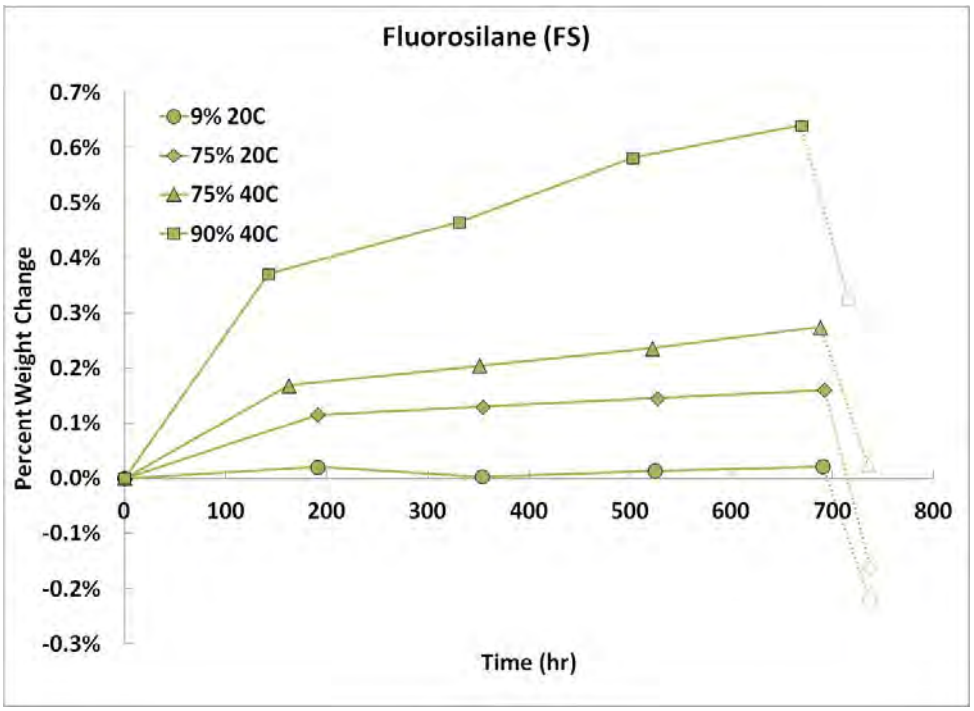

(c)

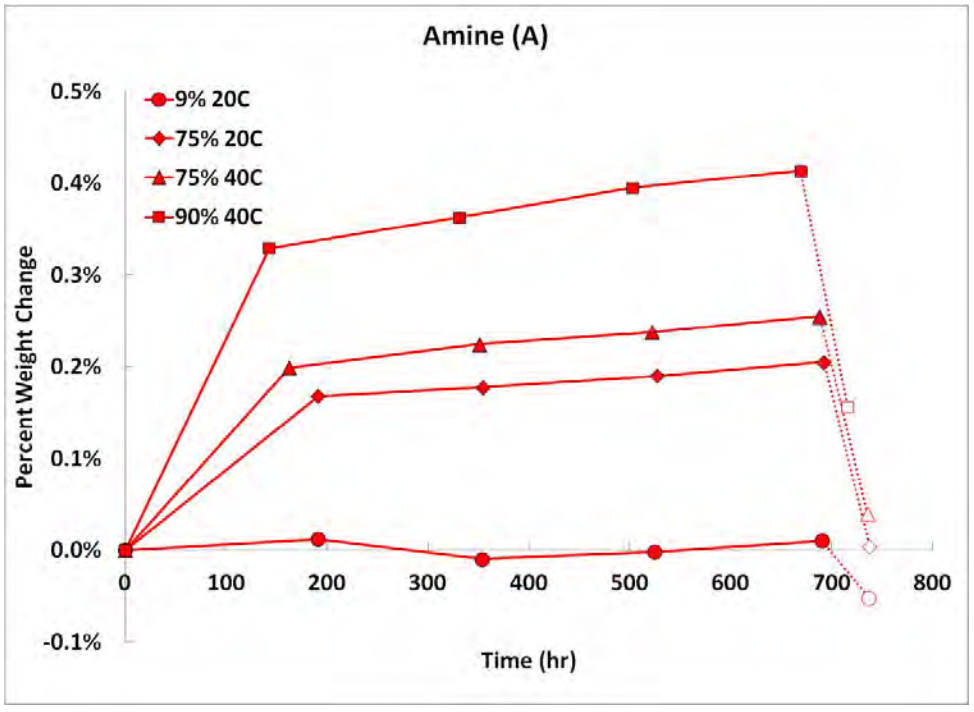

(d)

Figure 38 (continued). (c) Tridecafluoro-1,1,2,2-tetrahydrooctyl triethoxysilane (FS), (d) octadecylamine (A).

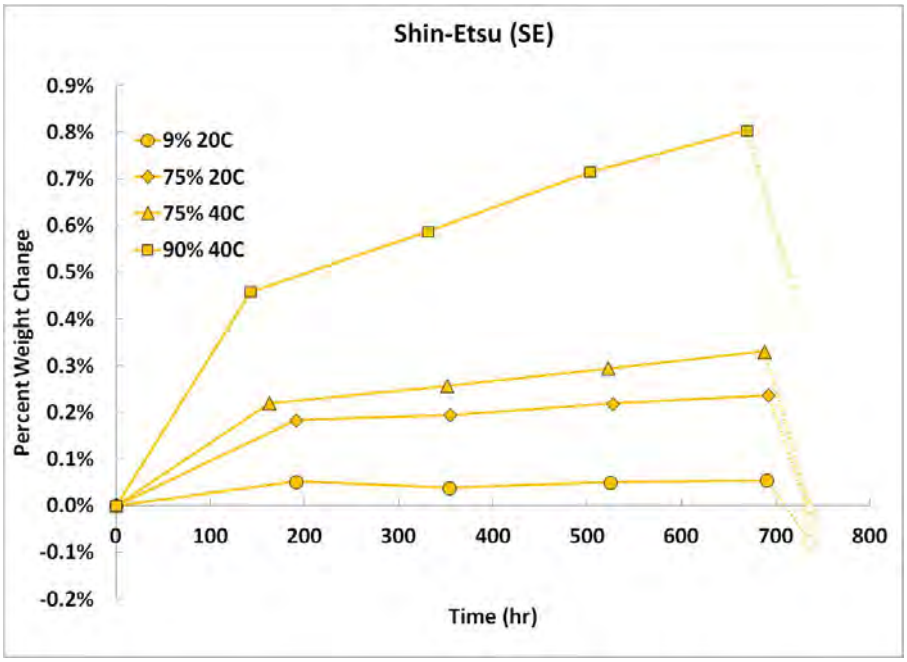

(e)

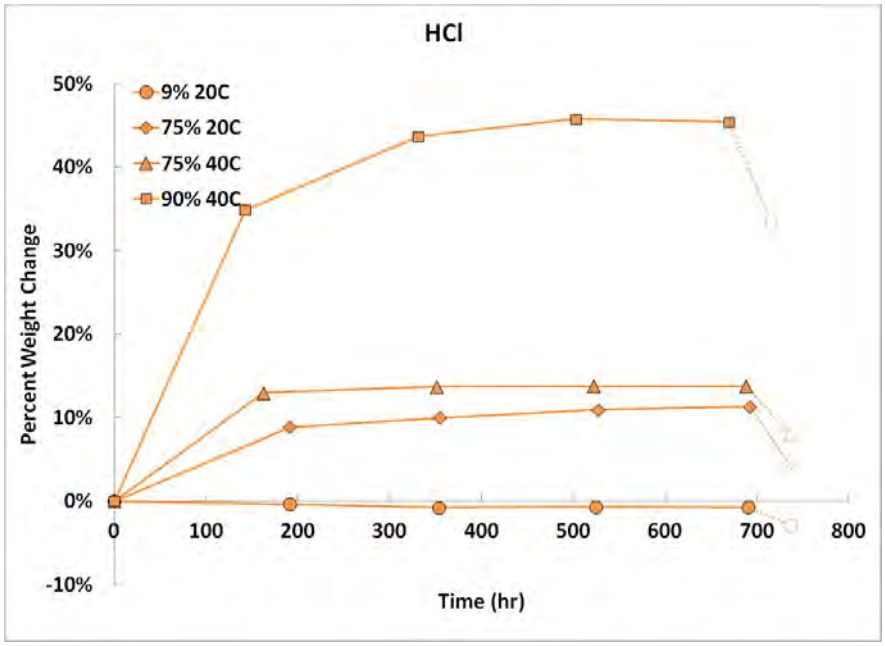

(f)

Figure 38 (continued). (e) 3,3,3 trifluoropropyl trimethoxysilane (FS), (f) acid-wash sample (HCl). This sample gained the most weight of any sample under all conditions. Though XRD showed the presence of some cellulose from the filter paper used, the weight upon drying suggests that the weight gain was due to more than H_2O absorption by cellulose.

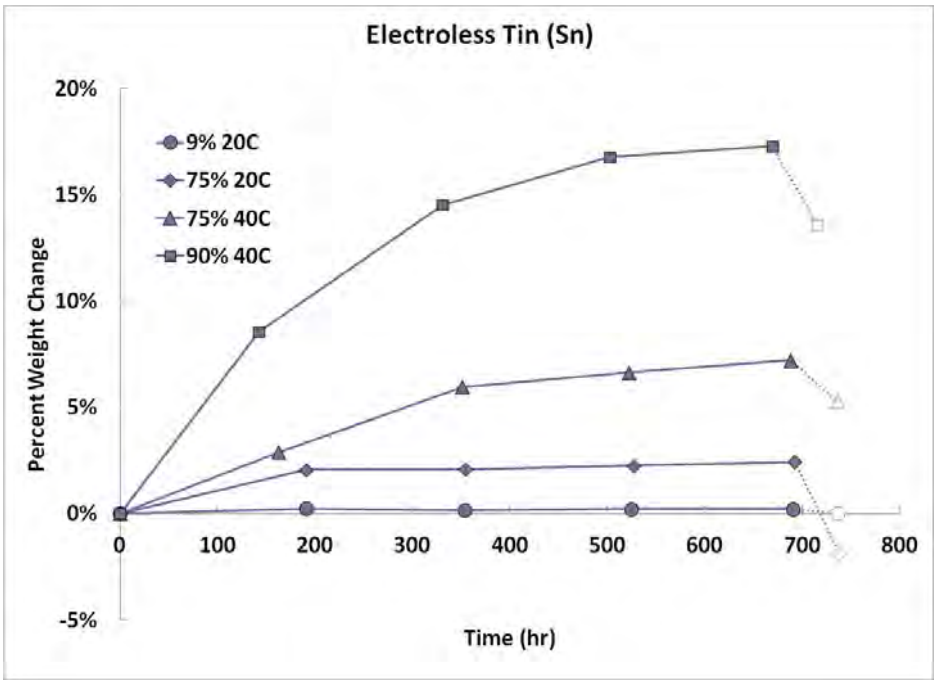

(g)

Figure 38 (continued). (g) Electroless Sn-coated powder.

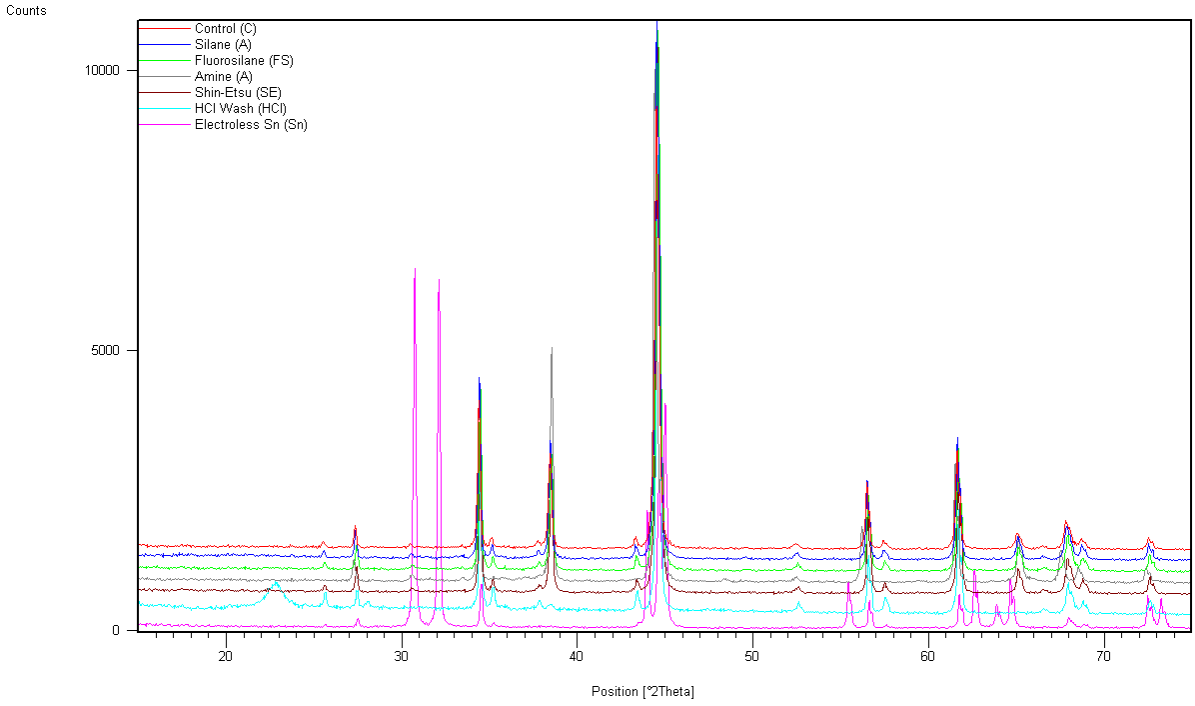

Figure 39. X-ray diffraction patterns of samples prior to moisture study showing no change between control and silane or amine-coated powders. HCl washed shows absence of Al with evidence of cellulose contamination from filter paper. Electroless Sn clearly shows tin peaks.

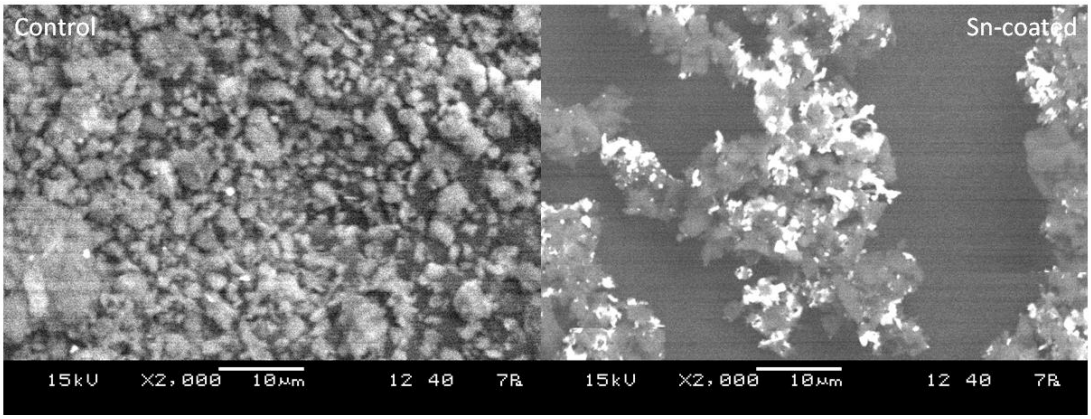

(a)

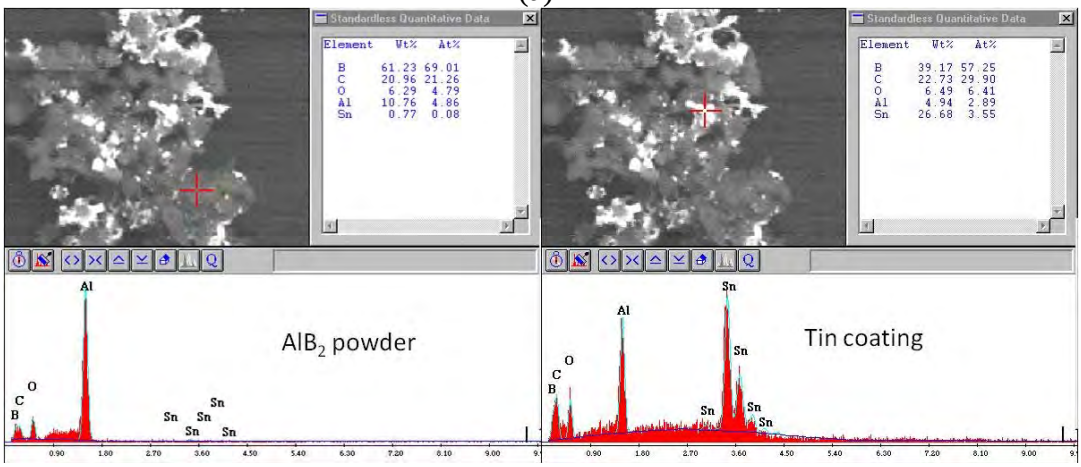

(b)

Figure 40. SEM backscattered images of (a) control on left and electroless Sn-coated powder on right, and (b) EDS spectra showing that bright phase is tin coating, which is poorly distributed on the surfaces of the AlB_2 powder.

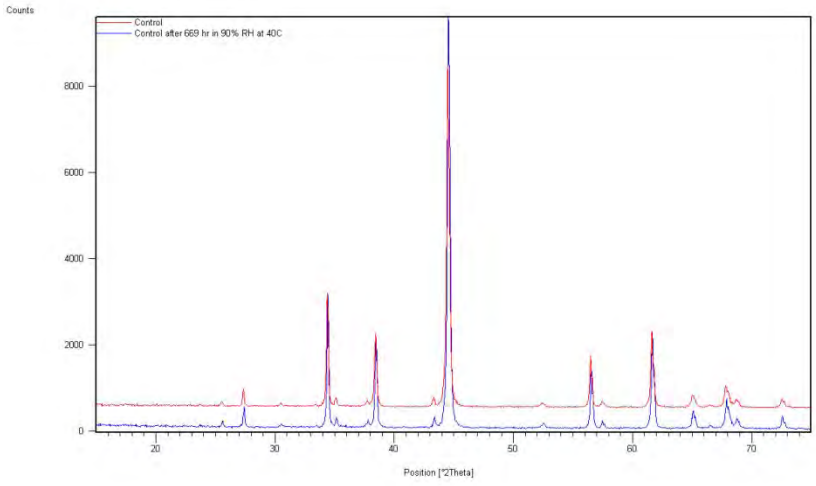

Figure 41. XRD patterns of control powder before (red) and after (blue) exposure to 90% RH for 669 hours at 40°C. Note that phases in AlB_2 powder have not changed due to moisture exposure.

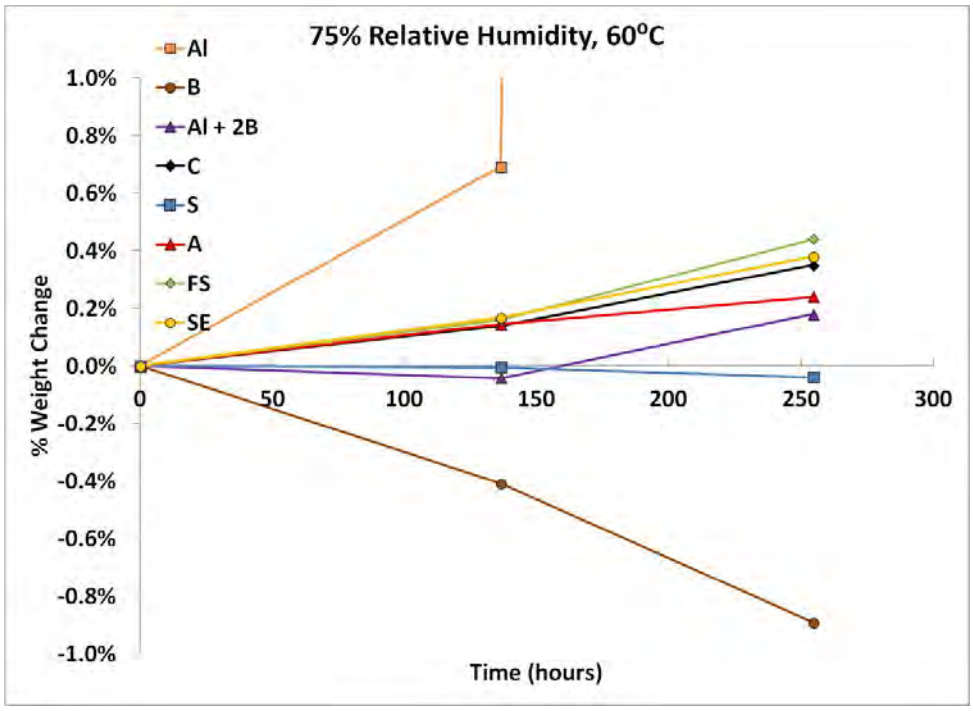

(a)

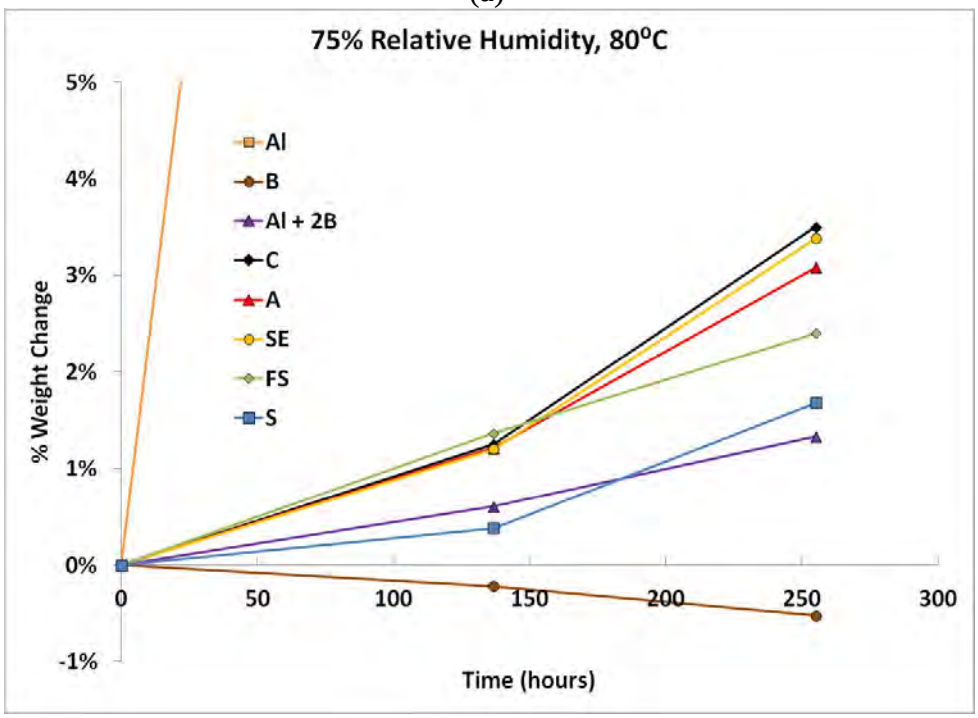

(b)

Figure 42. Weight change of the top performing coatings (S, A, FS, SE) and the starting powders for AlB_2 (Al, B, Al + 2B) versus the control (C). (a) 60°C and 75 % RH. The chamber had a leak during the first 142 hours and eventually dried out, but was refilled for all measurements afterward. Al (orange) reached 66% mass gain, over two orders of magnitude more than any other. (b) 75% RH and 80°C. Al reached 71% weight gain. Boron (B) is believed to lose weight due to the formation of volatile boric acid, which is dissolved in the salt solution.

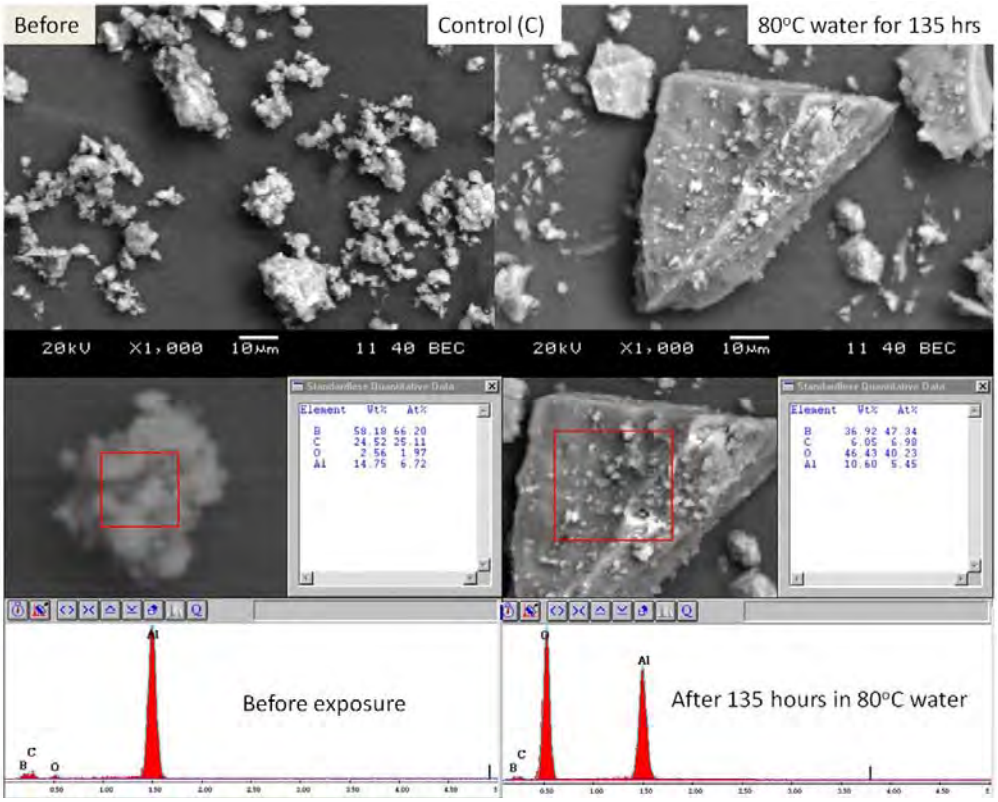

Figure 43. SEM backscattered images (top) and EDS spectra (bottom) of control powder before and after exposure to water at 80°C for 135 hours. Oxidation is easily evident due to enhanced oxygen peak in EDS spectra.

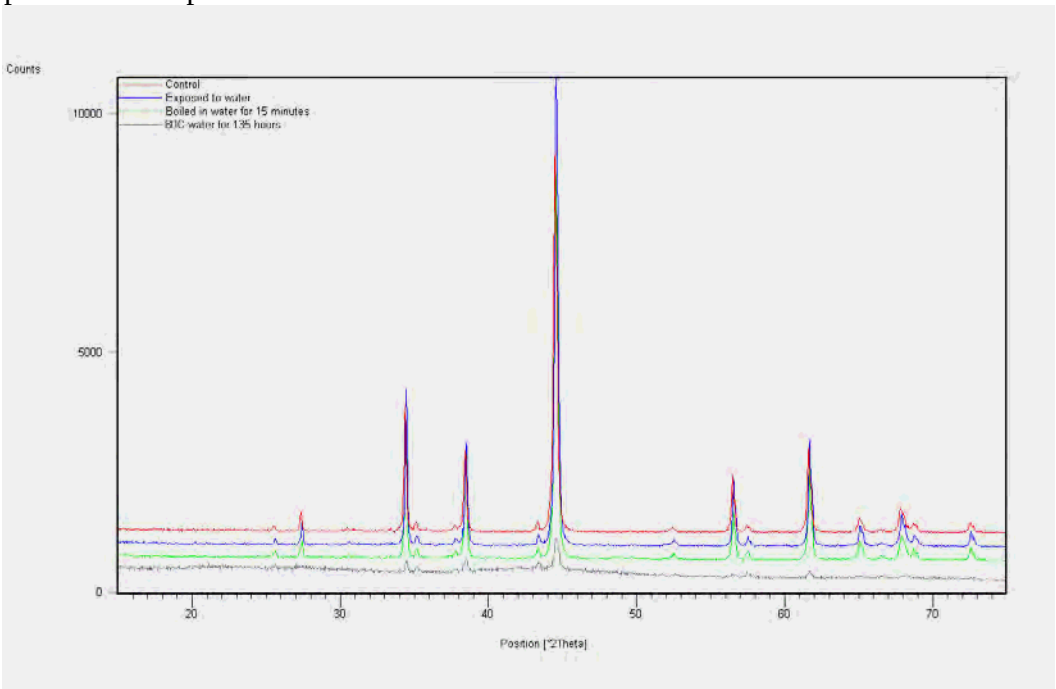

Figure 44. X-ray diffraction scans of control powder (red) exposed to water at room temperature (blue), boiled in water for 15 minutes (green), and heated at 80°C in water for 135 hours. Only long-term exposure to water changed the XRD pattern.

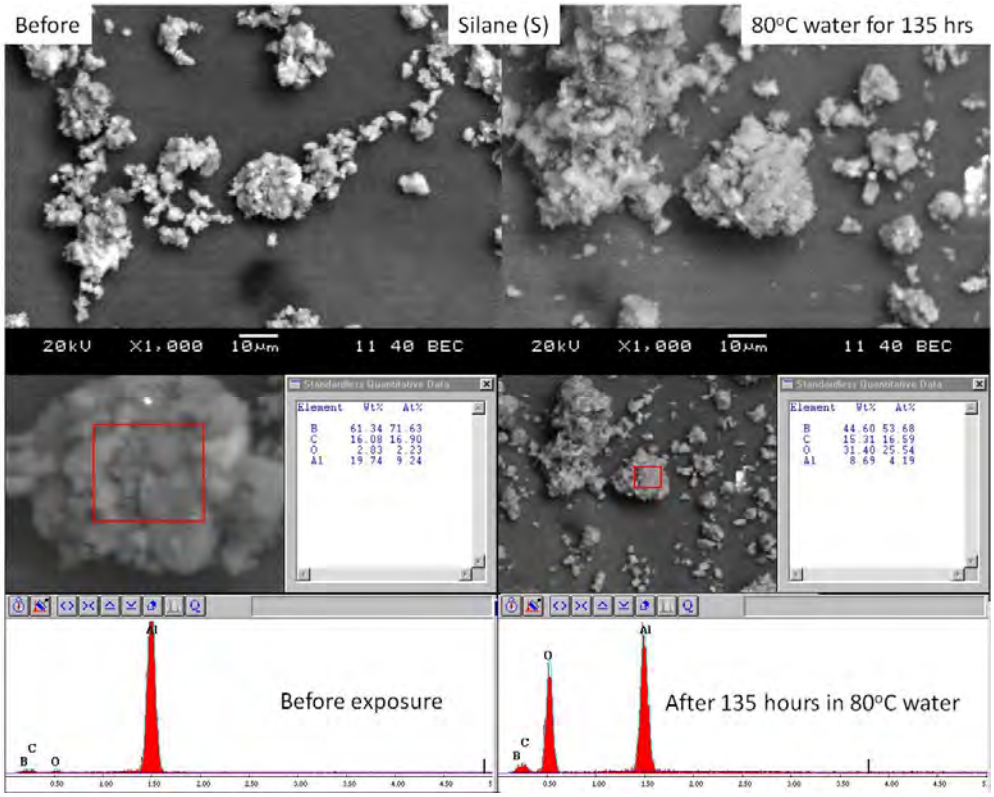

Figure 45. SEM backscattered images (top) and EDS spectra (bottom) of silane-coated (S) powder before and after exposure to water at 80°C for 135 hours. Compare with Figure 43.

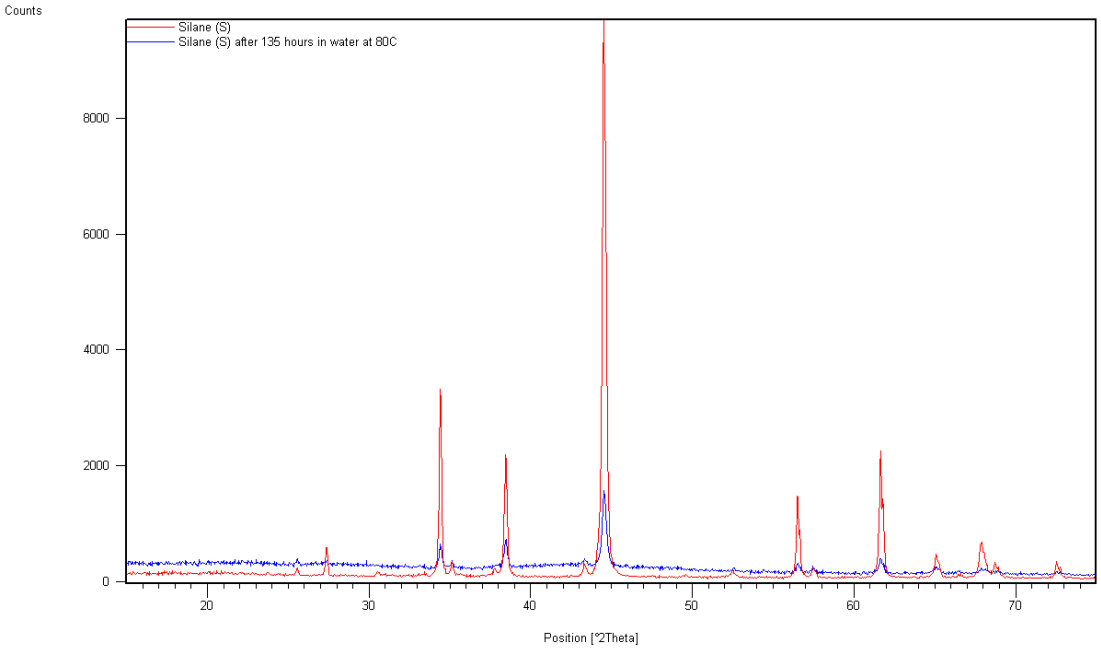

Figure 46. X-ray diffraction patterns of silane-coated (S) powder (red) and same powder exposed to water at 80°C for 135 hours (blue) showing peak broadening and lower intensities. Compare to Figure 44.

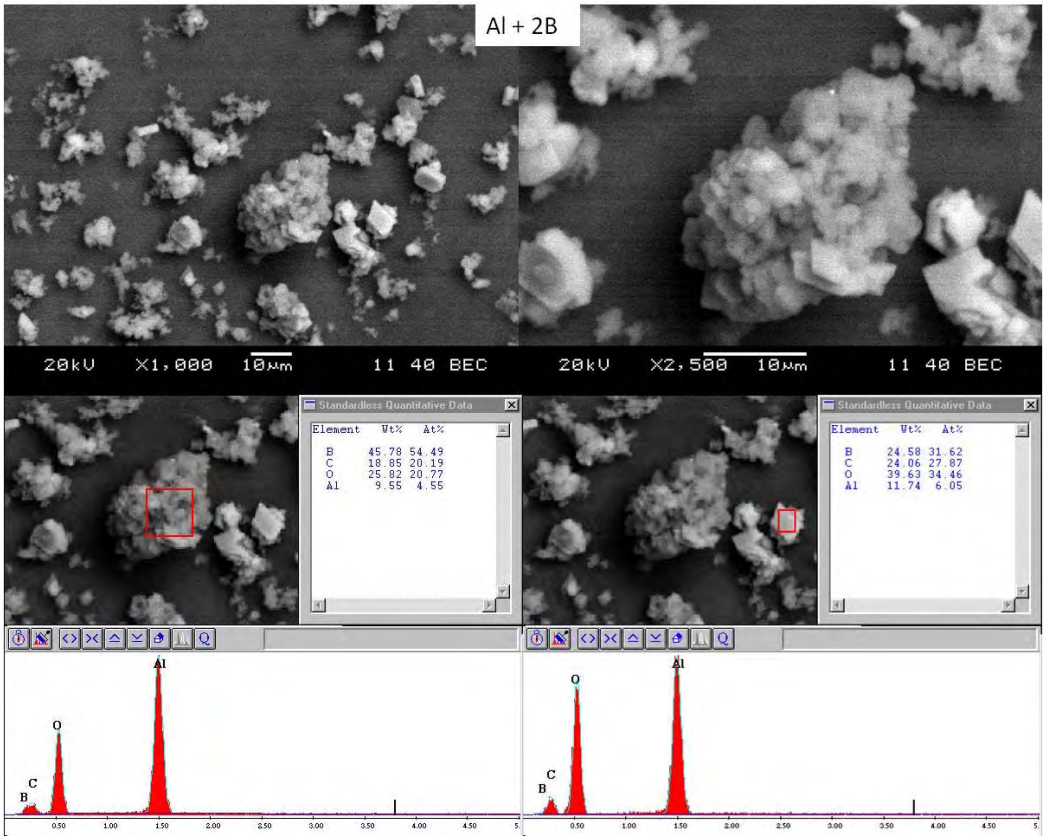

Figure 47. SEM and EDS of Al + 2B after exposure to water at 80°C for 135 hours. Plate-shaped $Al(OH)_3$ is evident throughout the microstructure.

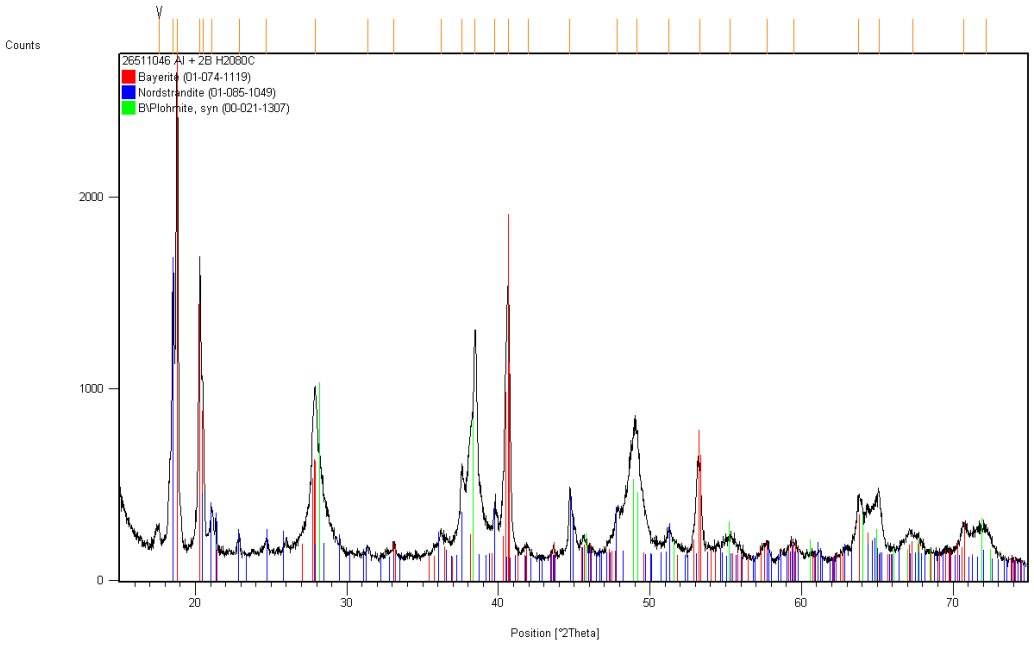

Figure 48. XRD pattern of Al+2B after exposure to water at 80°C for 135 hours. Aluminum hydroxide (Bayerite and Nordstradite) is prevalent in the material as the Al was attacked. The boron does not show up due to its low atomic number, but it is still present.

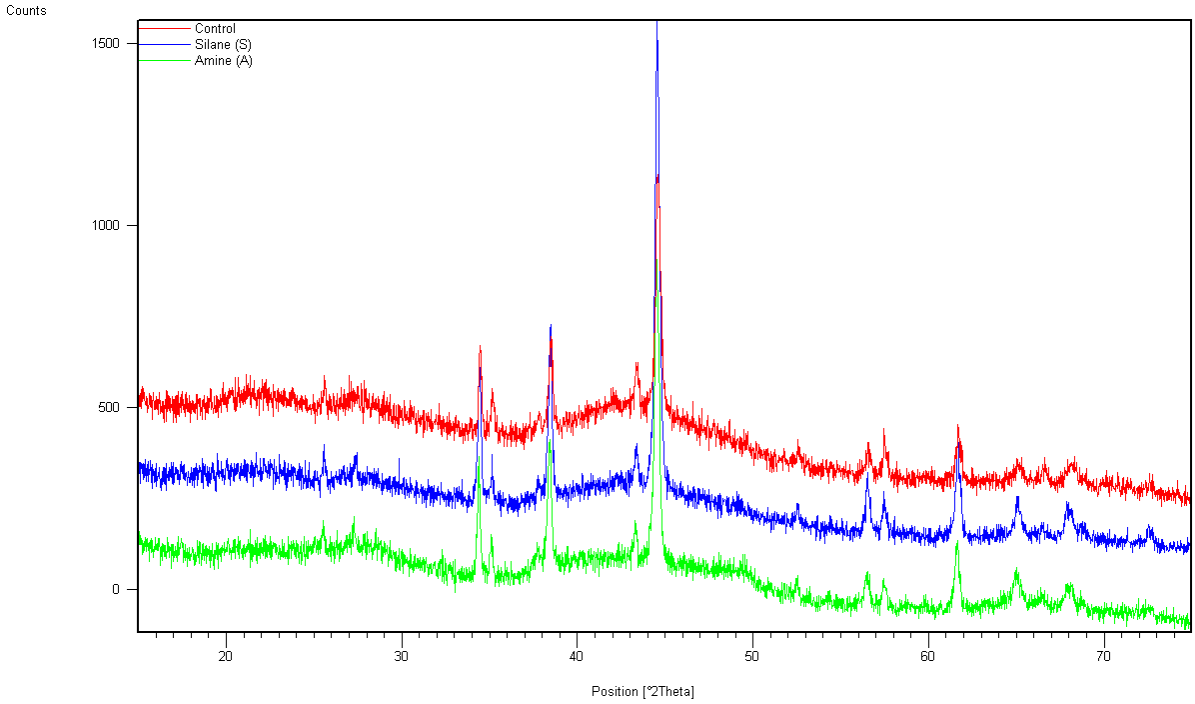

Figure 49. XRD patterns of powders heated at 80°C for 135 hours in water. The red pattern is the control, while the blue is silane (S) and the green is the amine (A). There is not a dramatic difference in XRD patterns, although the intensity scales inversely with the degree of oxidation.

The amine and Shin-Etsu fluorosilane both gained 112 %. When compared to the control powder, the silane (S) and amine (A) powders show only slightly stronger AlB_2 peaks (see Figure 49). None of the coatings protected the AlB_2 powder under these aggressive conditions.

An interesting question is whether the powders would have been protected better by a polymeric coating, which is what happens when the powders are mixed in energetic formulations. A polymeric, hydrophobic polymer will likely give much better protection than any of the coatings investigated. It is likely that one is only concerned with storage prior to mixing into energetic formulations. It is very easy to control storage conditions, by sealing in vacuum-packed bags under an Ar cover gas, such that these powders can be stored for years.

Conclusions

- Fine Al is susceptible to oxidation, forming $Al(OH)_3$ in moist environments. Boron is only affected by the formation of boric acid, which is water soluble. When intimately mixed Al and B powders were made, they showed good stability at 60°C in 75% relative humidity.
- The formation of AlB_2 gives improved stability over Al+2B mixtures, as expected. It is very likely that there is no issue with storing AlB_2 powders for long periods of time if stored under low-humidity condition. Once energetic formulations are prepared, it is

believed that the binder will protect them from exposure to moisture making short-term storage of these mixes possible.

- An n-octadecyltrimethoxysilane provided excellent protection at temperatures up to 60°C under high humidity conditions. It was slightly better than the fluorosilanes and amine investigated. Even at higher temperatures, under moderate humidity conditions, the silane provided significant protection. The weight gain, for example, at 80°C and 75 % relative humidity for a silane-coated powder was about one-third that of the control powder.
- None of the powder was able to withstand exposure to water for an extended period of time (135 hours) at 80°C even though short (15 minute) exposure to boiling water did not cause significant problems. The way the silane coatings were prepared, although hydrophobic, still allowed degradation of the powders when stored in hot water.
- Studies using thin hydrophobic polymeric coatings should be conducted.

VII. Characterization of Three Kilogram Sample Delivered to ARDEC

Background

AlB_2 was picked as the material to supply a three kilogram sample due to its performance based on combustion calorimetry testing at Nammo (Mesa, AZ). The AlB_2 indicated complete combustion in detonation calorimetry while the Al + 2B had a heat output that suggested that only 68 % efficiency was achieved. The difference in heat output, between the two samples was significant, as evidenced by an increase of 609 J/g when the diboride mixture was tested compared to the intimately mixed elements.

AlB_2 has been synthesized from a direct reaction of the elements[119-121], mechanical alloying[122], peritectic decomposition[123,124], single crystal growth from the melt[125], reacting Al with borax or boron oxide[126], reacting KBF_4 with Al[84], and filtration of AlB_2 from molten metals[127]. The low peritectic decomposition temperature, which is generally considered to be between 950 and 975°C, and slow kinetics for formation of AlB_2 from Al and AlB_{12}, make it difficult to get phase-pure AlB_2. Phase-pure AlB_2, based on XRD, has been achieved by removal of secondary phases after synthesis[128].

Ceramatec previously supplied powders to ARDEC (see Figures 50 and 51) which were made by the direct reaction of Al and B. The surface area of the powders ranged between 1.6 and 2 m^2/g. Surface area can be used to estimate the mean particle size assuming that all of the particles are monosized spheres, as given in Equation (2). Using this approach the ultimate particle size was in the one micrometer range, suggesting that the particles are agglomerated, a fact supported by microscopy. The 500 g sample supplied to ARDEC was tested using combustion calorimetry and did very well in comparison to a mixture of the Al and B, prepared from the same starting powders, as discussed above.

Experimental Procedures

AlB_2 powder was synthesized from a stoichiometric ratio of the elements. This material was given the Ceramatec code MW1-172I, which can be taken as the lot number. While the powder was scaled up, processing changes were also made. The powder processing details are proprietary to Ceramatec. Three kilograms of material were shipped to ARDEC on 11-29-11. The reaction of aluminum and boron does not proceed completely, leaving some unreacted

starting material. A commercially (H. C. Starck through ABCR) supplied AlB_2 powder, was used for comparison to the material we synthesized. A smaller sample (100 grams) of this material was also shipped on the same date.

Results and Discussion

The XRD patterns for the 3 kg sample and the Stark material are shown in Figure 3. Table 15 compares the Rietveld analysis for the two materials delivered previously (lots MW1-104K and MW1-113I) to the new lot of powder and the Starck control. The control powder claimed to have a composition of over 95% AlB_2 by chemical analysis. Starck measured an O content of 1.9 %. It is clear that their analysis did not account for all phases present. The discrepancy also suggests that the Rietveld fitting of XRD scans overestimates the oxygen content (via Al_2O_3) of the powder. Despite these issues, the Starck AlB_2 powder is still a very good material and likely acceptable as an energetic material.

One reason for the higher Al_2O_3 content in the 3 kg Ceramatec sample is the finer particle size of the AlB_2 (see Table 16 and Figure 53). It is likely to have more energetic capacity than the two previously supplied materials due to its finer particle size. SEM images of the powder compared to the Starck material are shown in Figure 54. Due to the finer particle size, the Milestone #9 sample begins to oxidize earlier in air, but reaches the same extent of reaction as the Starck material (see Figure 55).

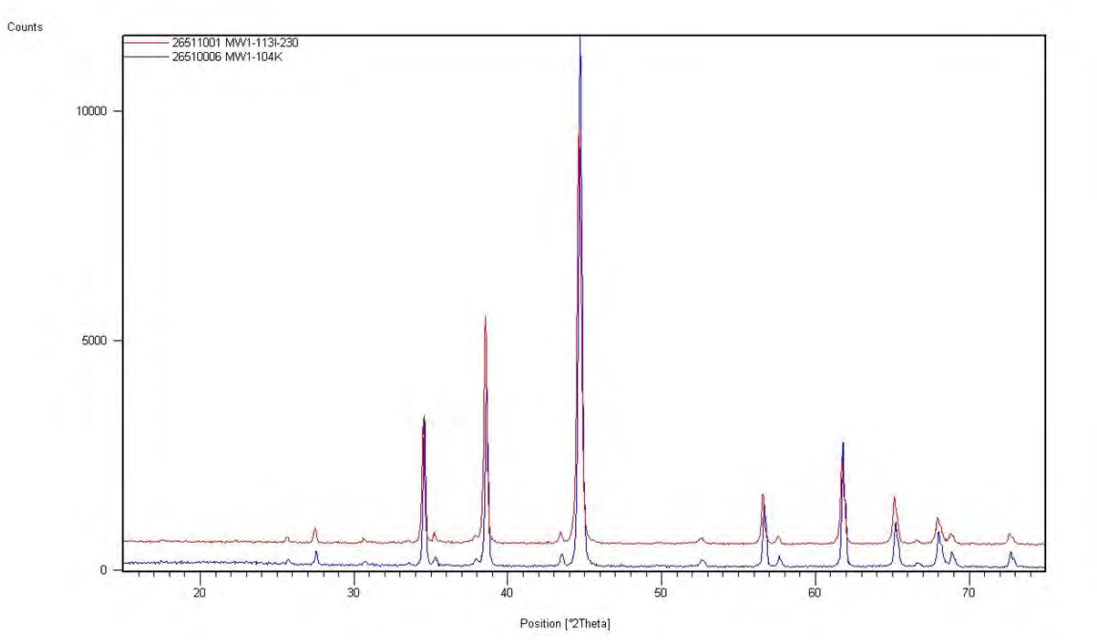

Figure 50. X-ray diffraction patterns comparing 500 g MW1-131I (red) compared to 50 g MW1-104K (blue) showing similar phases in both powders.

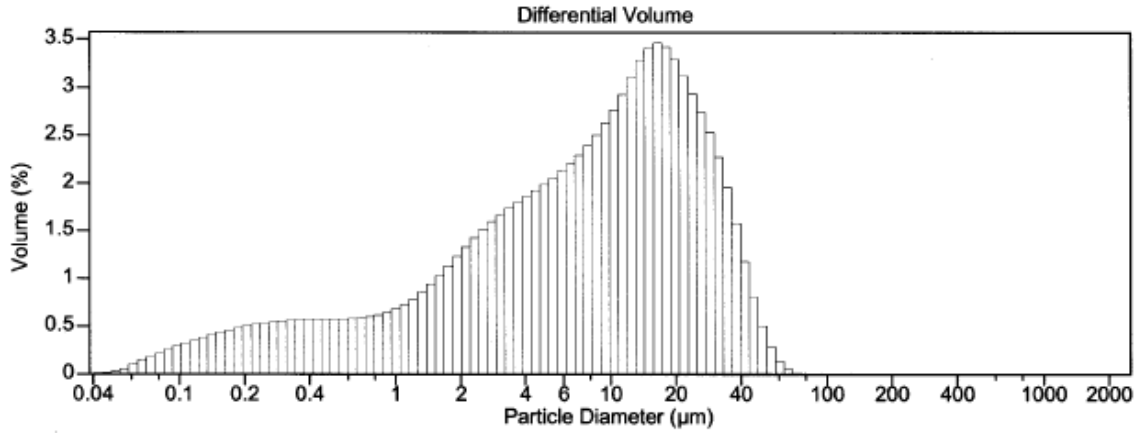

Volume Statistics (Arithmetic)			10023.$02
Calculations from 0.040 µm to 2,000 µm			
Volume	100.0%		
Mean:	11.92 µm	S.D.:	11.56 µm
Median:	8.437 µm	C.V.:	97.0%
D(3,2):	1.310 µm		
Mode:	16.40 µm		

% <	10	25	50	75	90
Size µm	0.528	2.590	8.437	18.08	28.78

(a)

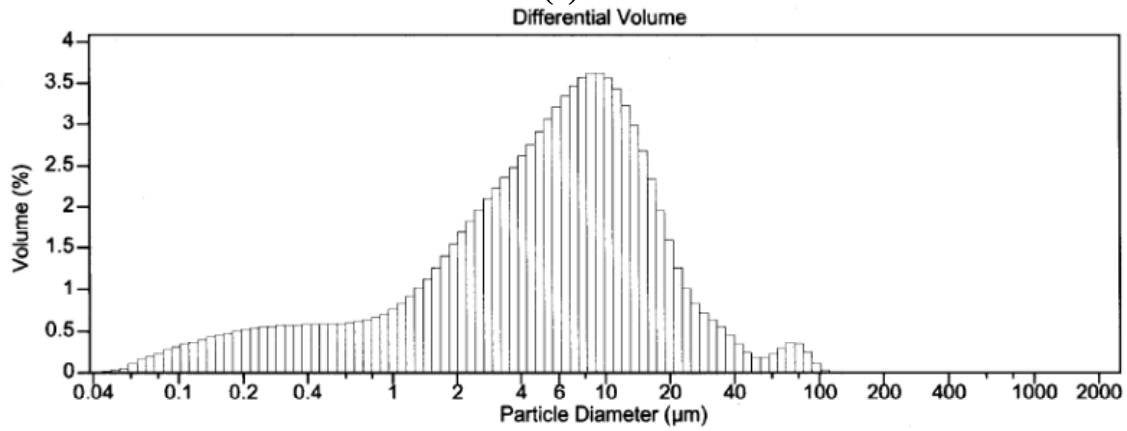

Volume Statistics (Arithmetic)			11002.$05
Calculations from 0.040 µm to 2,000 µm			
Volume	100.0%		
Mean:	8.914 µm	S.D.:	11.80 µm
Median:	5.725 µm	C.V.:	132%
D(3,2):	1.213 µm		
Mode:	9.371 µm		

% <	10	25	50	75	90
Size µm	0.497	2.206	5.725	11.17	18.56

(b)

Figure 51. Particle size distributions (measured in isopropanol) of previously supplied -230 mesh AlB_2. (a) 50 g (MW1-104K) and (b) 500 g (MW1-113I).

Table 15
Rietveld Analysis of Powders Synthesized at Ceramatec Compared to Starck AlB_2

	Rietveld Analysis* (Weight %)				
Code	AlB_2	Al	B	Al_2O_3	Al_3BC
AlB_2 -230 (MW1-104K (50 g))	76.0 [64.8]	19.1 [16.3]	[14.7]	3.8 [3.2]	1.1 [0.9]
AlB_2 -230 (MW1-113I (500 g))	68.7 [57.7]	26.1 [21.9]	[16.1]	3.9 [3.3]	1.2 [1.0]
AlB_2 -230 (MW1-172I (3 kg))	83.8 [75.4]	11.7 [10.5]	[10.0]	3.1 [2.8]	1.3 [1.2]
Starck AlB_2 (lot 31102/06)	88.5 [82.4]	6.2 [7.5]	[6.9]	3.4 [3.2]	1.4 [1.3]

* Rietveld analysis adjusted for free boron in parentheses.

All of the powders have the same phases present, but the amounts differ as shown in Table 15. At present, due to the paucity of test data, it is unclear if these four powders would differ in performance in an energetic application.

The low peritectic temperature makes it problematic to make a phase pure material, without post-processing purification. The 3 kg sample received no such treatment and it is hypothesized that this is also true of the Starck material.

As to the question as what is the cost to produce 5 kg. ABCR sells small quantities of AlB_2 made by Starck. The cost for one and five kg quantities of Starck powder was $1,540 and $6,075, respectively, when quoted in August of this year. A recent quote for their remaining supply (14 kg) was $14,840 (or $1,060/kg). Since ABCR adds a fee, it is expected that the price for 5 kg of AlB_2 would be considerably less expensive than $1,060/kg if produced in large quantities. Robert Jensen of Starck was contacted in order to get pricing information on the Starck powder, since it was suspected that this would be the best way to judge costs as volumes increase. He says that Starck no longer makes this material, but would be willing to do so if the volumes were attractive. The pricing for the AlB_2, at least initially, would be ≈$500/kg for 100 kg. There is a significant cost to start this production, which has to be taken into account when pricing small quantities of this material.

Starck said that they are running into the small volume vs. market volume argument. If the quantities stay small, and Starck continues to use small scale equipment, the costs will stay in the

Table 16
Surface Area and Particle Size Comparison

	Surface Area	Particle Size (μm)			Calculated
Code	(m^2/g)	d_{10}	d_{50}	d_{90}	Mean	Average (μm)
AlB_2 -230 (MW1-104K (50 g))	1.64	0.5	8.4	28.8	11.9	1.2
AlB_2 -230 (MW1-113I (500 g))	1.96	0.5	5.7	18.6	8.9	1.0
AlB_2 -230 (MW1-172I (3 kg))	3.81	0.3	3.4	9.1	4.1	0.5
Starck AlB_2 (lot 31102/06)	2.07	0.6	6.7	23.2	10.0	0.6

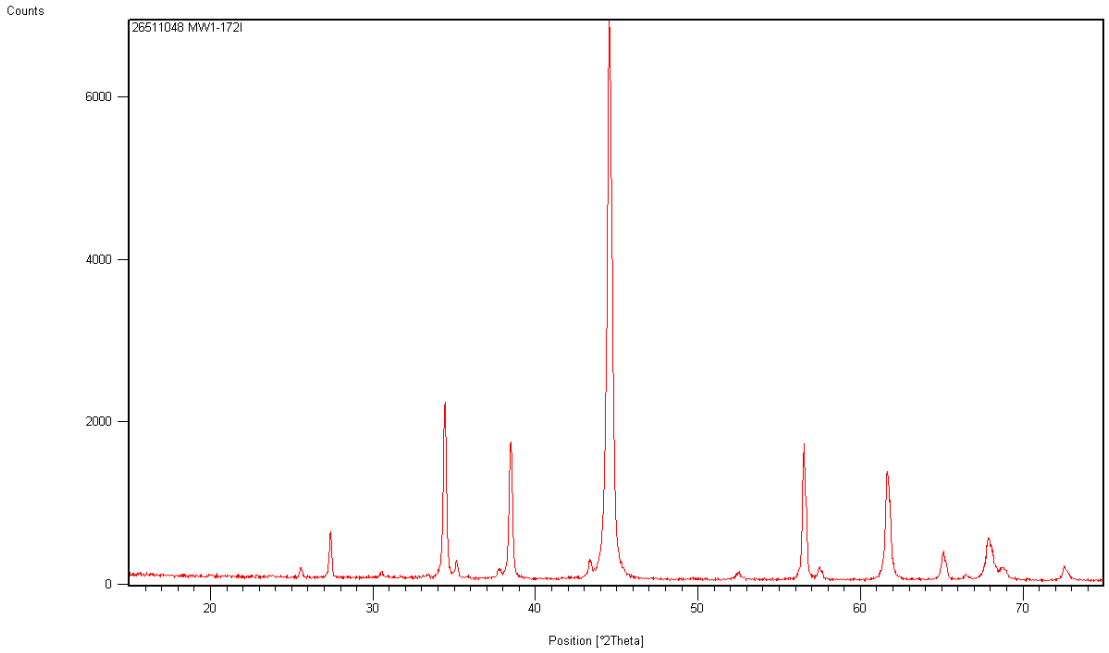

(a)

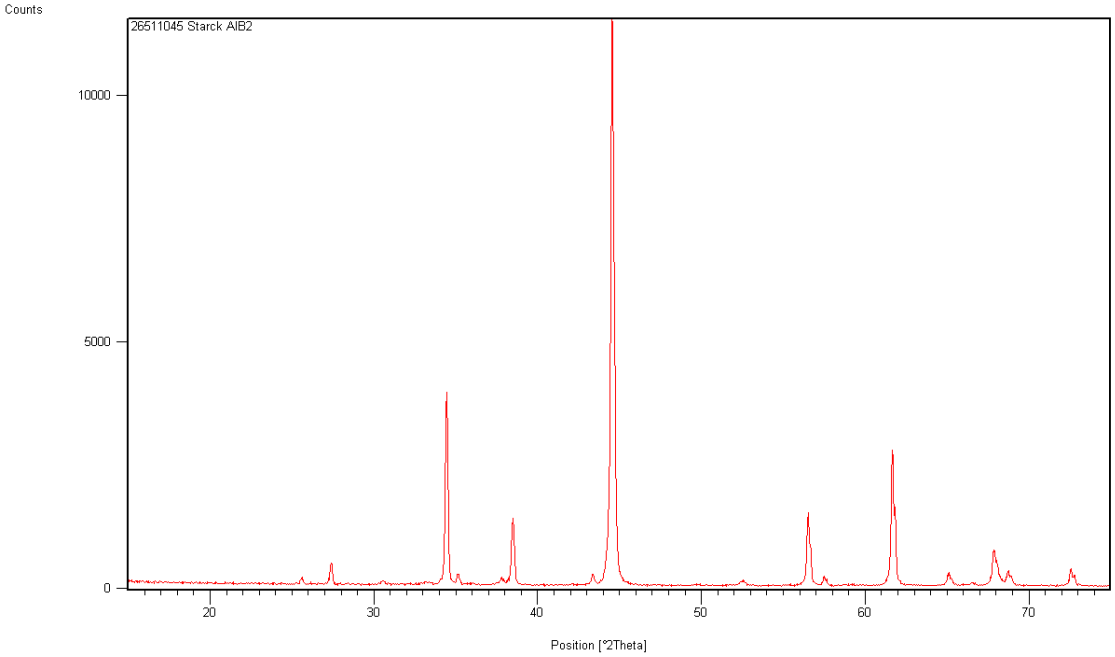

(b)

Figure 52. XRD patterns for (a) MW1-172I and (b) Starck powder. Both powders contain similar phases to those produced previously (compare to Figure 50).

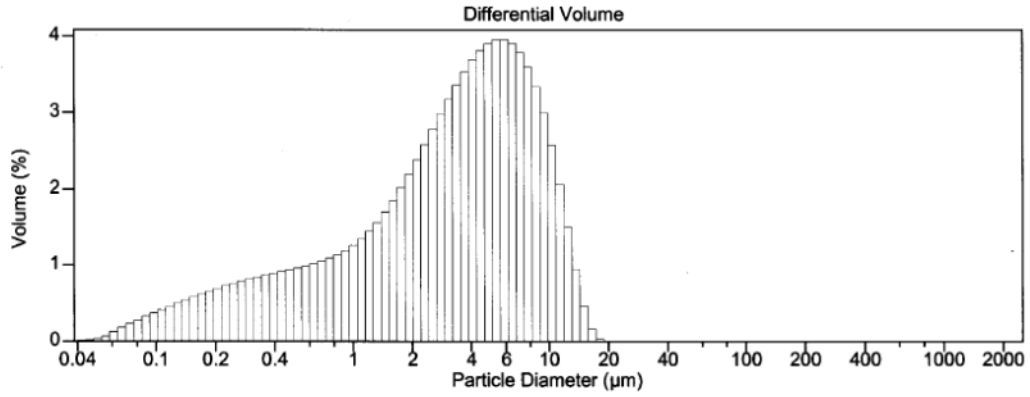

Volume Statistics (Arithmetic) 11005.$01

Calculations from 0.040 µm to 2,000 µm

Volume	100.0%		
Mean:	4.124 µm	S.D.:	3.422 µm
Median:	3.355 µm	C.V.:	83.0%
D(3,2):	0.916 µm		
Mode:	5.878 µm		

% <	10	25	50	75	90
Size µm	0.340	1.250	3.355	6.218	9.162

(a)

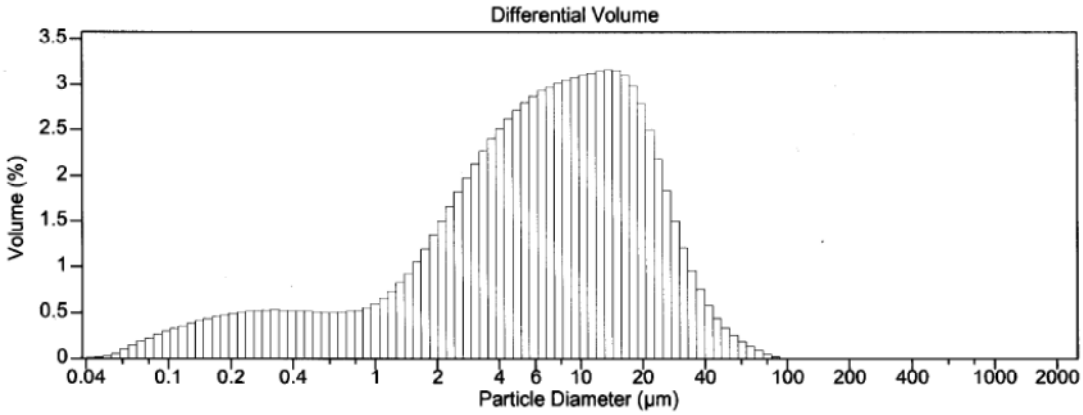

Volume Statistics (Arithmetic) 11006.$01

Calculations from 0.040 µm to 2,000 µm

Volume	100.0%		
Mean:	9.993 µm	S.D.:	10.42 µm
Median:	6.684 µm	C.V.:	104%
D(3,2):	1.309 µm		
Mode:	13.61 µm		

% <	10	25	50	75	90
Size µm	0.562	2.632	6.684	14.26	23.23

(b)

Figure 53. Particle size distributions (measured in isopropanol) of AlB_2 powders. (a) MW1-172I and (b) Starck powder. Compare to Figure 51.

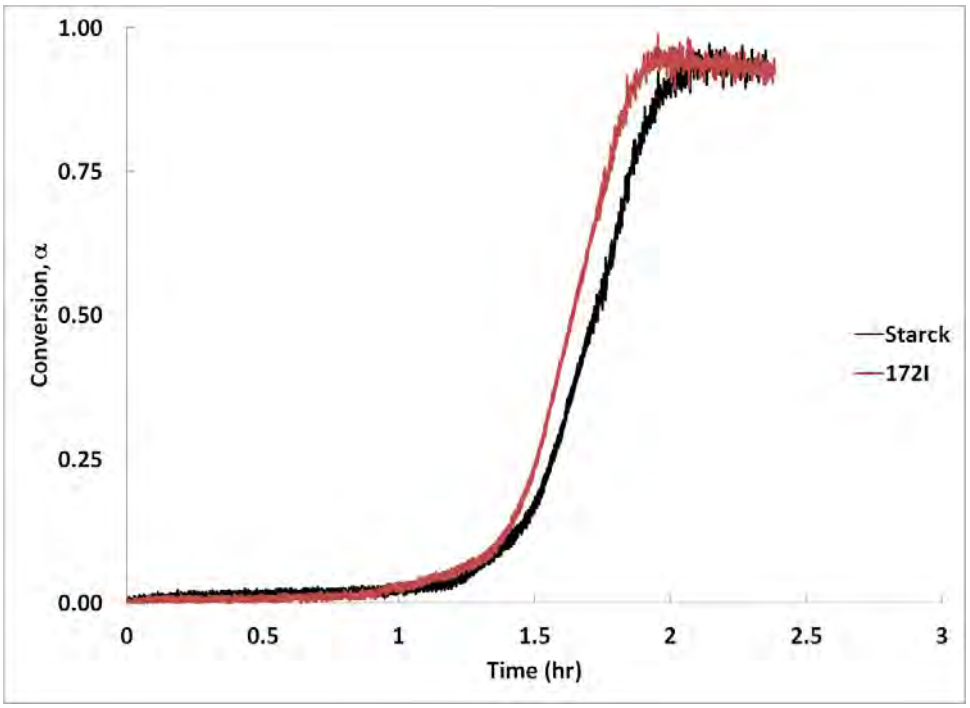

(a)

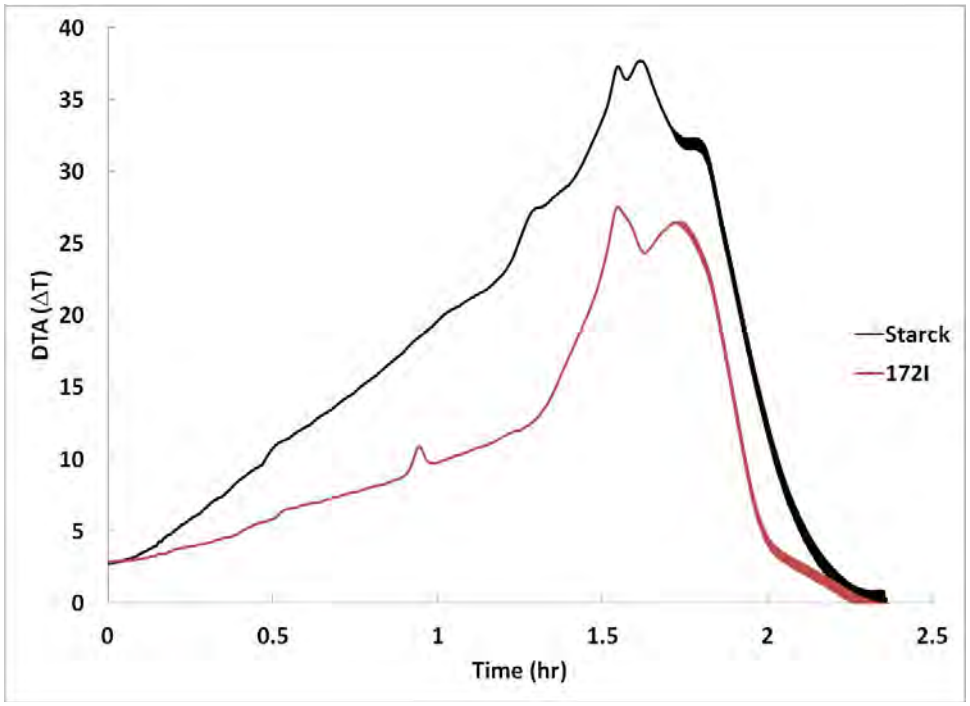

(b)

Figure 54. TGA (a) and DTA (b) of Starck and MW1-172I powders.

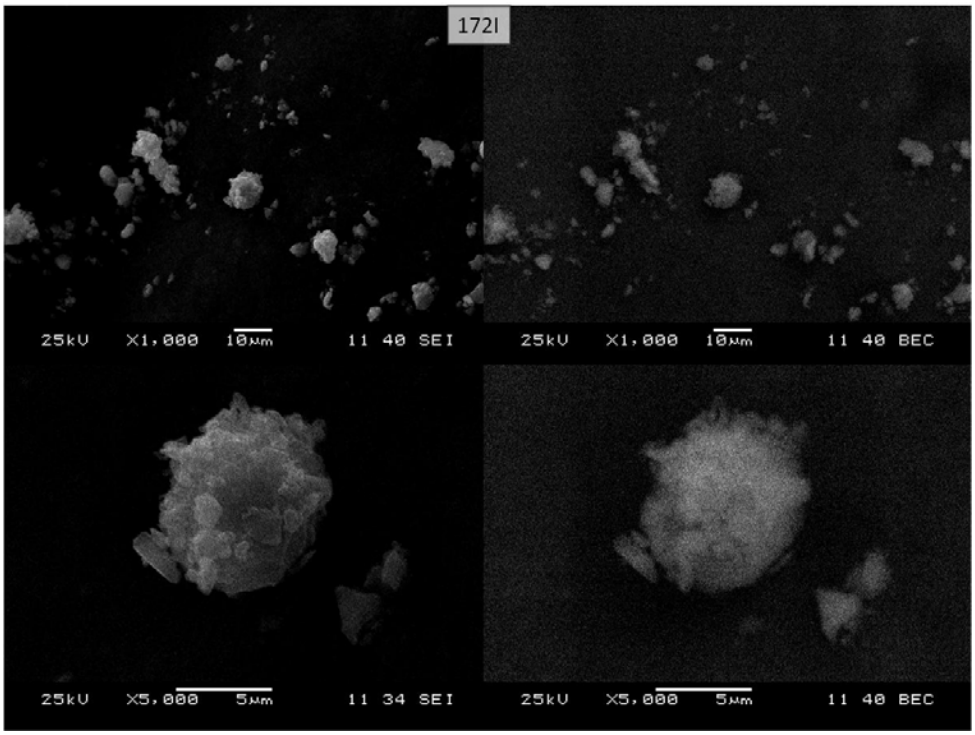

(a)

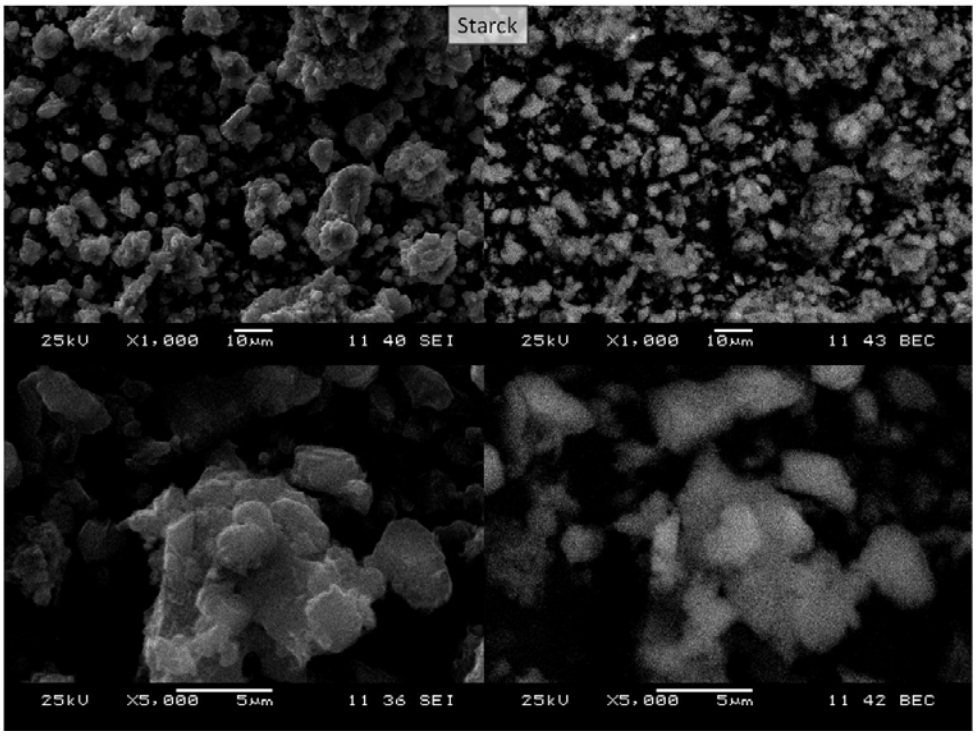

(b)

Figure 55. SEM images of (a) MW1-172I and (b) Starck AlB_2, secondary on left and backscattered on right.

same range. However if there is truly a market for this material, and demand can go up to larger quantities (i.e. tons/year), Starck said that they can use more efficient production techniques and decrease pricing (estimated to possibly go down towards $200/kg). Starck was clear that the costs can be improved if there is a large enough application/market for the AlB_2. It is clear that AlB_2 is an expensive material at the present time.

Conclusions

- Three kilograms of AlB_2 powder, made by reacting high-purity B with fine Al using proprietary conditions at Ceramatec, were supplied to ARDEC to complete Milestone #9. The powder has a surface area of 3.8 m^2/g, a d_{50} of 3.4 μm, and an overall AlB_2 content of 83.8 wt. % as judged by Rietveld analysis while compensating for free boron which is not identified by XRD.
- A commercial source of AlB_2 was found through H. C. Starck, a well-known German supplier. This powder, which is sold at $1,215/kg (in 5 kg quantities) through a distributor (ABCR), was compared to the powder produced at Ceramatec. The Starck powder has a surface area of 2.1 m^2/g, a d_{50} of 6.7 μm, and an overall AlB_2 content of 88.5 wt. % based on Rietveld analysis. One hundred grams of this powder was supplied to ARDEC for comparative testing. The Starck powder is of high quality and is useful as a source of AlB_2 for further testing by the Army. Fourteen kilograms of this material is currently available at a cost of $1,060/kg.
- The question as to the cost of 5 kg of AlB_2, when produced in large quantities, was addressed by contacting H. C. Starck. The cost for 100 kg of AlB_2 would be ≈$500/kg but pricing could drop to $200/kg at the tonnage level.

VIII. Conclusions

1. A literature survey identified a wide variety of materials with high specific heats of combustion. MgB_2, $Mg_{0.5}Al_{0.5}B_2$, and AlB_2 are all attractive due to their small endotherms due to decomposition in comparison to their large exotherms due to oxidation. These hexagonal borides have weak bonding between planes in contrast to the strong covalent bonding in all three dimensions typical of most borides, including AlB_2 and $MgAlB_{14}$.

2. A large number of samples were supplied to ARDEC. Only three have been tested to date, which include $MgAlB_{14}$, AlB_2, and Al+2B. Based on combustion calorimetry of mixes prepared by ARDEC, the AlB_2 appears to be the best candidate of these three materials. Further testing is needed to guide the development of lightweight fuels.

3. Static oxidation in flowing air to 1500°C showed that fine boron readily reacts at ≈500°C, but Al and AlB_2 are more insensitive to oxidation. Both Al and AlB_2 oxidize to greater than 95% of their theoretical values, as compared to only 70% for B. Reacting AlB_2, as compared to Al+2B, results in greater insensitivity but more complete oxidation in air. More testing at ARDEC is needed to determine if the static oxidation tests have any merit in predicting sensitivity or extent of reaction in explosive mixes.

4. The moisture resistance of AlB_2 can be improved by coating with n-octadecyl trimethoxysilane, which provided excellent protection at temperatures up to 60°C under high humidity conditions. It was slightly better than the fluorosilanes and amine investigated. Even at higher temperatures, under moderate humidity conditions, the silane provided significant protection. The weight gain, for example, at 80°C and 75 % relative humidity for a silane-coated powder was about one-third that of the control powder. Coating boride powders with hydrophobic binders is worthy of investigation.

5. All of the objectives of this program were met, including providing ARDEC with over 20 different powders for screening, two powders (AlB2 and Al+2B) in 500 gram quantities, and scale up to a 3 kg quantity of AlB_2. AlB_2 is not made commercially in large quantities and is therefore at least ten times more expensive than Al. Because B_4C is made in large quantities, it is equivalent in price to Al. Further work should focus on making energetic fuels by using B_4C and Al mixtures, or by reacting these inexpensive materials to make compounds such as Al_3BC. While niche markets certainly will exist for materials like AlB_2, lightweight fuels will only find widespread use if they are cost competitive with existing Al and Mg fuels.

References

1. R. A. Cutler, "Engineering Properties of Borides," Engineered Materials Handbook, Ceramics and Glasses, Vol. 4 (ASM, Metals Park, PA. 1991).
2. G. V. Samsonov and I. M. Vinitskii, Handbook of Refractory Compounds (Plenum Press, 1980).
3. T. Lundstrom, "Transition Metal Borides," pp. 351-376 in Boron and Refractory Borides (Springer-Verlag, Berlin, 1977).
4. H. Nowotny and P. Rogl, "Ternary Metal Borides," pp. 413-448 in Boron and Refractory Borides (Springer-Verlag, Berlin, 1977).
5. W. S. Williams, "Transition Metal Carbides, Nitrides, and Borides for Electronic Applications," *J. Met*., **49**[3] 38-42 (1997).
6. Carbide, Nitride, and Boride Materials Synthesis and Processing, ed. by A. W. Weimer (Chapman and Hall 1997).
7. L. Rangaraj, C. Divakar, and V. Jayaram, "Processing of Refractory Metal Borides, Carbides, and Nitrides," *Key Eng. Mater*., **395** 69-88 (2009).
8. K. Iizumi and K. Kudaka, "Crystal Structures and Synthesis of the Borides of Transition Metal Elements," *Academic Reports, Tokyo Institute of Polytehnics*, **21** 1-8 (1998).
9. C. Mitterer, "Borides in Thin Film Technology," *J. Sol. St. Chem*., **133**[1] 279-291 (1997).
10. T. Lundstrom, "Preparation and Crystal Growth of Non-Oxidic Refractories from Molten Metallic Solutions," *J. Less-Common Met*., **100** 215-228 (1984).
11. B. J. Avlett, "Production of Thin Films of Metals, Metal Silicides, and Metal Borides by Chemical Vapour Deposition Using Single Organometallic Precursors," Trans. Inst. Met. Finishing, 72, 127-129 (1994).
12. H. T.-S. Hsia, "Air_Augmented Combustion of Boron and Boron-Metal Alloys," AFRTL-TR-71-80 (June 1971).
13. M. J. van Setten and M. Fichtner, "On the Enthalpy of Formation of Aluminum Diboride, AlB_2," *J. Alloys Comp*. **477** L11-L12 (2009).

14. C. L. Yeh and K. K. Kuo, "Ignition and Combustion of Boron Particles," *Prog. Energy Comb. Sci.*, **22**[6] 511-41 (1996).
15. Phase Diagrams for Ceramists, Vol. 10, edited by A. E. McHale (American Ceramic Society, Westerville, OH, 1994).
16. O. N. Carlson, *Bull. Alloys Phase Diagrams*, **11**[6] 560-66 (1990).
17. P. Rogl and J. C. Schuster: Phase Diagrams of Ternary Boron Nitride and Silicon Nitride Systems. Monograph Series on Alloy Phase Diagrams, pp. 3-5 (ASM International, Materials Park, OH, 1992).
18. B. Hussman and M. Pfitzner, "Extended Combustion Model for Single Boron Particles Part I: Theory" *Combust. and Flame* **157** 803-821 (2010); B. Hussman and M. Pfitzner, "Extended Combustion Model for Single Boron Particles Part 2: Validation" *Combust. and Flame* **157** 822-833 (2010).
19. A. Macek J. M. Semple, "Combustion of Boron Particles," *Combust. Sci. Tech*. **1**, 181-191 (1969).
20. S. Li, *Combust. Sci. Tech*. **77**, 149-169 (1991).
21. N. Kubota, Propellants and Explosives, (Wiley-VCH, Weinheim 2007).
22. B. M. Rice, "Applications of Theoretical Chemistry in Assessing Energetic Materials for Performance or Sensitivity," pp. 335-367 in Overviews of Recent Research on Energetic Materials, Ed. by R. W. Shaw, T. B. Brill and D. L. Thompson (World Scientific, New Jersey, 2005).
23. C. M. Faeth, Proc. 21st. *JANNAF Combust. Meet., CPIA Publication* **412**[2] 15-29 (1984).
24. S. N. Schmotolocha and R. B. Edelman, AFOSR-TR-73-1082 (1972).
25. T. Letsoalo and J. E. Lowther, "Systematic Trends in Boron Icosahedral Structured Materials," *Physica B: Cond. Matt*.,**403**[17] 2760-67 (2008).
26. G. Alecu, "Crystal Structure of Some High-Temperature Superconductors," *Rom. Report Phys.* **56**[3] 404-412 (2004).
27. Z. Li, Q. Z. Qu, B. Huang, and Z. Li, "Crystal Structure and Morphology of a New Compound, LiB," *J. Alloys Comp*. **311** 256-264 (2000).
28. A. N. Kolmogorov and S. Curtarolo, "Prediction of Different Crystal Structure Phases in Metal Borides: A Lithium Analog to MgB_2," *Phys. Rev. B*, **73**[18] 180501-4 (2006).
29. Handbook of Chemistry and Physics, 63rd Edition (CRC Press, Boca Raton, 1982).
30. R. Naslain, J. Etourneau, and P. Hagenmuller, "Alkali Metal Boride," pp. 262-292 in Boron and Refractory Borides (Springer-Verlag, Berlin, 1977).
31. F. Wang, M. Mitchell, R. Sutula, and J. Holden, *J. Less-Common Met.*, **61** 237 (1978).
32. G. Mair, R. Nesper, and H. G. von Schnering, *J. Solid State Chem.*, **75** 30 (1988).
33. M. Kobayashi, I. Higashi, H. Matsuda, and K. Kimura, K., *J. Alloys Compds.*, **221** 120 (1995).
34. I. Highasi and Y. Takahasi, "Boron-Rich Phases Grown from Al-M-B Melts (M=Li, Ti, V, Cr, Mn, Fe, Co, Ni, Cu)," *J. Less Common Metals*, **81**[1] 135-142 (1981).
35. T. Ito and I. Higashi, *Acta Crystallogr., Sec. B: Structural Science*, **39** 239 (1983).
36. F. S. Maron and M. S. Germaidze, "New Method for Preparation of Lithium Boride," *J. Appl. Chem. USSR*, **43**[8] 1837-8 (1970).
37. S. Okada, et al., "Crystal Growth of $MgAlB_{14}$-Type Compounds Using Molten Salts and Some Properties," *J. Alloys Comp*., **458**[1-2] 297-301 (2008).
38. I. Barin, Thermochemical Data of Pure Substances, (VCH, New York, 1993).
39. ASM Handbook, Volume 3, Alloy Phase Diagrams (1992).

40. M. M. Korsukova, et al., "The Crystal Structure of Defective $YAlB_{14}$ and $ErAlB_{14}$," *J. Alloys Comp*., **187**[1] 39-48 (1992).
41. I. Higashi and Y. Takahasi, "A Ternary Boron-Rich Phase $Al_{1.00}Cu_{0.79}B_{25}$ Grown from a Molten Al-Cu-B Mixture," *J. Less Common Metals*, **108**[1] 177-88 (1985).
42. E. G. Domalski and G. T. Armstrong, "Heats of Formation of Metallic Borides by Fluorine Bomb Calorimetry," TR-65-110 (AFAPLTR65110 (October 1965).
43. V. A. Neronov, "Aluminum Borides," Report FTD-HT-23-1214-68 (May 1969).
44. L. G. Fasolino, "Thermochemistry of Selected Compounds," Final Report on Contract Nonr-360800 (December 1968).
45. T. I. Serbryakova, "Production Methods, Physicochemical Properties and Use of Borides and Boride-Based Alloys," *Poroshkovaya Metallurgiya*, **9-10** 125-126 (1994).
46. K. A. Nguyen, G. N. Srinvas, T. P. Hamilton, and K. Lammertsma, "Stability of Hyperlithiated Borides," *J. Phys. Chem. A*, **103**[6] 710-715 (1999).
47. Y. Imai, M. Mukaida, M. Ueda, and A. Watanabe, "Screening of the Possible Boron-Based n-Type Thermoelectric Conversion Materials on the Basis of the Calculated Densities of States of Metal Borides and Doped β-Boron," *Intermetallics*, **9**[8] 721-734 (2001).
48. A. Passerone, M. L. Muolo, and D. Passerone, "Wetting of Group IV Diborides by Liquid Metals," *J. Mater. Sci*., **41**[16] 5088-5098 (2006).
49. D. B. Wilson and J. M. Stoltzfus, "Metals Flammability: Review and Model Analysis," *ASTM Special Technical Publication 1395* 469-496 (2001).
50. R. R. Dirks and K. E. Spear, "Optimization of Thermodynamic Data for Silicon Borides," *Calphad: Computer Coupling of Phase Diagrams and Thermochemistry*, **11**[2] 167-175 (1987).
51. R. Tremblay and R. Angers, "Preparation of High-Purity SiB4 by Solid-State Reaction Between Si and B," *Ceram. Int*. **15**[2] 73-78 (1989).
52. L. Chen, T. Goto, M. Mukaida, M. Niino, and T. Hirai, "Phase Diagram and Thermoelectric Property of Si-B System Ceramics," *J. Japan Soc. Pow. and Pow. Met*., **41**[11] 1299-1303 (1994).
53. H. Nakamura, K. Murata, T. Anan, and Y. Hara, "Oxidation of Zirconium Borides," *J. Japan Explosives Society*, **55**[4] 142-146 (1994).
54. M. Woerle, R.Nesper, G. Mair, M. Schwarz, and H. G. von Schnering, "JCPDS Pattern 85-2010 for Lithium Boron Carbide (LiBC)," *Z. Anorg. Allg. Chem.* **621** 1153, (1995).
55. W. Jung, "JCPDS Pattern 83-2010 for $B_2Li_{1.2}Ni_{2.5}$ and Pattern 31-730 for $B_6Li_{3.59}Ni_{7.52}$"*Z. Naturf., B: Anorg. Chem., Org. Chem., Bioc., Biop., Bio.*, **32**, 1371, (1977).
56. A. Guette, M. Barrett, R. Naslain, and P. Hagenmuller, "Crystal Structure of Magnesium Heptaboride, Mg_2B_{14}," *J. Less-Common Met*., **82** 325-334 (1981).
57. I. Higashi, "Crystal Chemistry of α-AlB_{12} and γ-AlB_{12}," *J. Sol. St. Chem.*, **154** 168-176 (2000).
58. E. L. Davidchuk, V. I. Dimitrov, M. L. Rafalovich, Y. I. Tulupov and N. A. Salavinskaya, "Kinetics of Boron Combustion in Dry Air," *Combustion, Explosion and Shock Waves*, **27**[1] 40-47 (1991).
59. P. P. Elischer, G. Cleal and M. Wilson, "The Development of a Boron and Iron Oxide Delay System," Australian Defense Report MRL-R-994 (April 1996).
60. R. O. Foelsche, R. L. Burton, and H. Krier, "Boron Particle Ignition and Combustion at 30-150 Atm.," *Combustion and Flame*, **117** 32-58 (1999).

61. Y. S. Kwon, A. A. Gromov, A. P. Ilyin, E. M. Popenko, and G. H. Rim, "The Mechanism of Combustion of Superfine Aluminum Powders, *Combustion and Flame*, **133** 385-391 (2003).
62. X. Xiaojing, D. Bohua, Q. Zuanhui, and L. Yuanhui, "Preparation and Synthesis Mechanism of Li-B Alloy," Rare Metal Materials and Eng., 38[1] 172-175 (2009).
63. J. M. Mota, J. Abernojar, M. A. Martinez, F. Velasco, and A. J. Criado, "Borides and Vitreous Compounds Sintered as High-Energy Fuels," *J. Sol. St. Chem*, **177** 619-627 (2004).
64. P. Plitzer, P. Lane, and M. C. Concha, "Computational Determination of the Energetics of Boron Ignition/Combustion Reactions," *J. Phys. Chem., A*, **103** 1419-1425 (1999).
65. S. M. Pourmortazavi, S. S. Hajimirsadeghi, I. Kohsari, M. Fathollahi, and S. G. Hosseini, "Thermal Decomposition of Pyrotechnic Mixtures Containing Either Aluminum or Magnesium Powder as Fuel," *Fuel*, **87** 244-251 (2008).
66. A. Ulas, K. K. Kuo, and C. Gotzmer, "Ignition and Combustion of Boron Particles in Fluorine-Containing Environments," *Combustion and Flame*, **127** 1935-1957 (2001).
67. E. L. Dreizin, D. G. Keil, W. Felder, and E. P. Vicenzi, "Phase Changes in Boron Ignition and Combustion," *Combustion and Flame*, **119** 272-290 (1999).
68. K. Wang, Z. Y. Fu, W. M. Wang, Y. C. Wang, H. Wang, J. Y. Zhang, and Q. J. Zhang, "Study of the Thermodynamics and Kinetics in the Combustion Reaction Between Titanium and Boron Powders," *Key Eng. Mater*. **351** 189-194 (2007).
69. G. Young, K. Sullivan, M. R. Zachariah, and K. Yu, "Combustion Characteristics of Boron Nanoparticles," *Combustion and Flame*, **156** 322-333 (2009).
70. W. Zhou, R. A. Yetter, F. L. Dryer, H. Rabitz, R. C. Brown, and C. E. Kolb, "Effect of Fluorine on the Combustion of "Clean" Surface Boron Particles," *Combustion and Flame*, **112** 507-521 (1998).
71. W. Zhou, R. A. Yetter, F. L. Dryer, H. Rabitz, R. C. Brown, and C. E. Kolb, "A Comprehensive Physical and Numerical Model of Boron Particle Ignition," 26th Int. Symposium on Combustion, The Combustion Institute, 1909-1917 (1996).
72. H. W. Li, K. Miwa, N. Ohba, T. Fujita, T. Sato, Y. Yan, S. Towata, M. W. Chen, and S. Orimo, "Formation of an Intermediate Compound with a $B_{12}H_{12}$ Cluster: Experimental and Theoretical Studies on Magnesium Borohydride ($Mg(BH_4)_2$," *Nanotechnology* **20** 1-7 (2009).
73. L. Meda, G. Marra, L. Galfetti, F. Severini, and L. De Luca, "Nano-Aluminum as Energetic Material for Rocket Propellants," *Mater. Sci. Eng. C* **27** 1393-1396 (2007).
74. A. Rai, D. Lee, K. Park, and M. R. Zachariah, "Importance of Phase Change of Aluminum in Oxidation of Aluminum Nanoparticles," *J. Phys. Chem. B* **108** 14793-14795 (2004).
75. G. Severa, W. Ronnebro, and C. M. Jensen, "Direct Hydrogenation of Magnesium Boride to Magnesium Borohydride: Demonstration of > 11 Weight Percent Reversible Hydrogen Storage," *Chem. Commun*., **46** 421-423 (2010).
76. M. A. Trunov, S. M. Umbrajkar, M. Schoenitz, J. T. Mang, and E. L. Dreizin, "Oxidation and Melting of Aluminum Nanoparticles," *J. Phys. Chem. B* **110** 13094-13099 (2006).
77. M. Worle, R. Nesper, G. Mair, and H. G. von Schnering, "$Li_6B_{18}(Li_2O)_x$-A Boride with a Porous Framework of B6 Octahedra," *Sol. St. Sci*. **9** 459-464 (2007).
78. T. G. Abzianidze, A. M. Eristavi, and S. O. Shalamberidze, "Strength and Creep in Boron Carbide (B4C) and Aluminum Dodecaboride (α-AlB12)," *J. Solid State Chemistry* **154** 191-193 (2003).

79. J. Fjellstedt, A.E.W. Jarfors, L. Svendsen, “Experimental Analysis of the Intermediary Phases AlB_2, AlB_{12} and TiB_2 in the Al–B and Al–Ti–B systems,” *J. Alloys and Compounds* **283** 192–197 (1999).
80. S.V. Meschel, O.J. Kleppa, “Standard Enthalpies of Formation of $A1B_{12}$ and $A1_4C_3$ by High Temperature Direct Synthesis Calorimetry,” *J. of Alloys and Compounds* **227** 93-96 (1995).
81. Y.S. Kwon, A. A. Gromov, A. P. Ilyin, “Reactivity of Superfine Aluminum Powders Stabilized by Aluminum Diboride,” Combustion and Flame **131** 349–352 (2002).
82. D. Mirkovi´c, J. Gröbner, R. Schmid-Fetzer, Olga Fabrichnaya, Hans Leo Lukas, “Experimental Study and Thermodynamic Re-Assessment of the Al–B System,” *J. of Alloys and Compounds* **384** 168–174 (2004).
83. M.J. van Setten, M. Fichtner, “On the Enthalpy of Formation of Aluminum Diboride, AlB_2,” *J. of Alloys and Compounds* **477** L11–L12 (2009)
84. X. Wang, “The Formation of AlB_2 in an Al–B Master Alloy” *J. of Alloys and Compounds* **403** 283–287 (2005).
85. V. L. Solozhenko, E. G. Solozhenko, C. Lathe, “Equation of State and Thermal Stability of Al_3BC,” *Solid State Comm.* **137** 533–535 (2006).
86. J.C. Viala, J. Bouix, G. Gonsales, C. Esnouf, “Chemical Reactivity of Aluminum with Boron Carbide” *J. of Materials Science* **32**[17], 4559-4573 (1997).
87. D. A. Andersson, L. Casillas, M. I. Baskes, J. S. Lezama, S. D. Conradson, “Modeling of the Phase Evolution in $Mg_{1-x}Al_xB_2$ ($0 < x < 0.5$) and Its Experimental Signatures” *J. Phys. Chem. B* **113** 11965–11976 (2009).
88. B. A. Cook, J. L. Harringa, T. L. Lewis, and A. M. Russell, “A New Class of Ultra-Hard Materials Based on $AlMgB_{14}$,” *Scripta Mater* **42**[6] 592-602 (2000)
89. H.E. Calderóna, R.G.I. Hidalgo, Z.H. Melgarejoc, O.M. Suárez, “Effect of AlB_2–Mg Interaction on the Mechanical Properties of Al-Based Composites,” *Materials Science and Engineering A* **527** 2258–2264 (2010).
90. S. Margadonna, K. Prassides, I. Arvanitidis, M. Pissas, G. Papavassiliou, A.N. Fitch, “Crystal Structure of the $Mg_{1-x}Al_xB2$ Superconductors near x=0.5,” *Physical Review B* **66**, 014518 (2002).
91. S. Okadaa, T. Tanakab, A. Satoc, T Shishidod, K. Kudoue, K. Nakajimad, T. Lundstrom, “Crystal Growth and Structure Refinement of a New Higher Boride $NaAlB_{14}$,” *J. of Alloys and Compounds* **395** 231–235 (2005).
92. M.Kh. Shorshorov, V.I. Potapov, V.I. Anipov, V.V. Trutnev, L.A. Akinfieva, T.K. Potapova, “Interaction Between Boron and an Alloy of the Mg-Al System,” *Fizika I Khimiya Obrabotki Materialov* **17**[3] 142-143 (1983)
93. J.S. Slusky, N. Rogado, K.A. Regan, M.A. Hayward, P. Khalifah, T. He, K. Inumaru, S.M. Loureiro, M.K. Haas, H.W. Zandburgen, R.J. Cava, “Loss of Superconductivity with the Addition of Al to MgB_2 and a Structural Transition in $Mg_{1-x}Al_xB_2$,” *Nature* **410** 343-345 (2001).
94. T. I. Serebryakova, V. I. Lyashenko and V. D. Levandovskii, “Interaction in the System Li-B and Some Properties of Lithium Boride Phases,” *Poroshkovaya Metallurgiya*, **1–2**, 54–58 (1994).
95. N. Vojteer, M. Schroeder, C. Rçhr, and H. Hillebrecht, “Li2B12Si2: The First Ternary Compound in the System Li/B/Si: Synthesis, Crystal Structure, Hardness, Spectroscopic Investigations, and Electronic Structure,” *Chem. Eur. J.* **14** 7331–7342 (2008).

96. V. Adasch, K.U. Hessb, T. Ludwig, N. Vojteer, H. Hillebrecht, “Synthesis and Crystal Structure of MgB_{12},” *J. of Solid State Chemistry* **179** 2916–2926 (2006).
97. R.A. Fisher, Guangtao Li, J.C. Lashley, F. Bouquet, N.E. Phillips, D.G. Hinks, J.D. Jorgensen, G.W. Crabtree, “Specific heat of $Mg^{11}B_2$,” *Physica C* **385** 180–191 (2003).
98. E. Bauer, Ch. Paul, St. Berge, S. Majumdar, H. Michor, M. Giovannini, A. Saccone, A. Bianconi, “Thermal Conductivity of Superconducting MgB_2,” *J. Phys.: Condens. Matter* **13** L487–L493 (2001).
99. A. Bharathi, S.J. Balaselvi, S. Kalavathi, G.L.N. Reddy,V.S. Sastry, Y. Hariharan, T.S. Radhakrishnan, “Carbon Solubility and Superconductivity in MgB_2,” *Physica C* **370** 211–218 (2002).
100. S.L. Bud’ko, P.C. Canfield, V.G. Kogan, “Magnesium Diboride: Basic Physical Properties and High Upper Critical Field Anisotropy,” *Physica C* **382** 85–92 (2002).
101. G. Giunchi, L. Malpezzi, N. Masciocchi, “A New Crystalline Phase of the Boron-Rich Metal-Boride Family: the Mg_2B_{25} Species,” *Solid State Sciences* **8** 1202–1208 (2006).
102. D.G. Hinks, J.D. Jorgensen, H. Zheng, S. Short, “Synthesis and Stoichiometry of MgB_2,” *Physica C* **382** 166–176 (2002).
103. Zi-Kui Liu,D. G. Schlom, Q. Li, X. X. Xi, “Thermodynamics of the Mg–B System: Implications for the Deposition of MgB_2 Thin Films,” *Appl. Phys. Lett*. **78**[23] 4 (2001).
104. I. Maurin, S. Margadonna, K. Prassides, T. Takenobu, Y. Iwasa, A. N. Fitch, “Carbon Miscibility in the Boron Layers of the MgB_2 Superconductor,” *Chem. Mater*. **14** 3894-3897 (2002).
105. M. Pranthaman, J.R. Thompson, D.K. Christen, “Effect of Carbon-Doping on Bulk Superconducting MgB_2 Samples,” *Physica C* **335** 1-5 (2001)
106. J. Shimoyama, K. Hanafusa, A. Yamamoto, Y. Katsura, S. Horii, K. Kishio, H. Kumakura, “Dramatic Effects of Ag Addition on Low Temperature Synthesis of MgB_2,” *Journal of Physics: Conference Series* **97** 012255 (2008).
107. M.R. Cimberle, M. Novak, P. Manfrinetti, A. Palenzona, “Magnetic Characterization of Sintered MgB_2 Samples: Effect of Substitution or ‘Doping’ with Li, Al and Si,” *Supercond. Sci. Technol*. **15** 43–47 (2002).
108. M. Walle, J. Koch, D. Tabersky, K. Hametner, N. D. Zhigadlo, S. Katrych,b J. Karpinskib, D. Gunther, “Analyses of Lithium-Doped and Pure Magnesium Diboride using Ultraviolet Nano- and Femtosecond Laser Ablation Inductively Coupled Plasma Mass Spectrometry,” *J. Anal. At. Spectrum*. **25** 193–195 2010.
109. S.K. Dutta, G.E. Gazza, “Properties of Hot Pressed SiB_6,” *Ceramic Bulletin*, **52**[7] 552-554 (1973).
110. S.P. Luh, H.C. Perng, T.K. Liu, H.S. Chu, “Influence of Boron Coating on its Fuel-Rich Solid Propellant,” *Xiyou Jinshu Cailiao Yu Gongcheng* **38**[1] 172-175 (2010).
111. A. Jillavenkatesa, S. J. Dapkunas, and L-S H. Lum, “Particle Size Characterization,” NIST Special Publication 960-1 (July 2001).
112. M. Schoenitz and E. L. Dreizin, “Constant Volume Explosions of Aerosols of Metallic Alloys and Powder Blends,” *J. Prop. Pow*., **19**[3] 405-412 (2003).
113. R. L. Mazzi and B. E.Warren, “The Structure of Vitreous Boron Oxide” *J. App Crystallography* **3**[4] 251-257 (1970).
114. T. Abu-Hamed, J. Karni, and M. Epstein, “The Use of Boron for Thermochemical Storage and Distribution of Solar Energy,” *Solar Energy*, **81**[1] 93-101 (2007).

115. R. Pankajavalli, S. Anthonysamy, K. Anathasivan, P. R. Vasudeva Rao, “Vapour Pressure and Standard Enthalpy of Sublimation of H_3BO_3,” J. Nuclear Materials, 362 128-31 (2007).
116. T. Mitani and M. Izumikawa, “Combustion Efficiencies of Aluminum and Boron in Solid Propellants,” J. Spacecraft, 28[1] 79-84 (1991).
117. R. Muller, M. Knapp, K. Heckmann, M. von Ruthendorf, and G. Boden, “Protecting Nanoscaled Non-Oxidic Particles from Oxygen Uptake by Coating with Nitrogen-Containing Surfactants, *Langmuir*, **20** 2598-2606 (2004).
118. L. Greenspan, “Humidity Fixed Points of Binary Saturated Aqueous Solutions,” *J. Res. NBS-A, Phys. Chem*., **81A**[1] 89-96 (1977).
119. H. Funk, Z. Anorg. Allgem. Chem., **142**, 269 (1925).
120. E. J. Felten “The Preparation of Aluminum Diboride, AlB_2”, *J. Am. Chem. Soc*., **78**[23], 5977–5978 (1956).
121. H. Zhu, S. Wang, Z. Li, X. Liu, and L. Jiang, “Effect of Sintering Temperature and Holding Time on Synthesis of AlB_2,” *Chinese Journal of Rare Metals*, **34**[5] (2010).
122. D. Agaogullari, H. Gokce, I. Duman, and M. L. Ovecoglu, “Aluminum Diboride Synthesis from Elemental Powders by Mechanical Alloying,” *J. Europ. Ceram. Soc*., **32**[3] (2012).
123. V. I. Matkovich, J. Economy, and R. F. Giese, Jr., “Presence of Carbon in Aluminum Borides,” *J. Am. Chem. Soc*., **86**, 2337-40 (1964).
124. A. C. Hall and J. Economy, “The role of Al-B Peritectic Transformation in the Formation of High Aspect Ratio AlB_2,” *J. Phase Equilibria*, **21**[1] 63-69 (1999).
125. J. Economy, “Synthesis and Properties of New Reinforcing Agents and Superconducting Filaments, *Appl. Polymer Syn*., **31** 23-35 (1977).
126. A. C. Hall and J. Economy, “Preparing High- and Low-Aspect Ratio AlB_2 Flakes from Borax or Boron Oxide, *JOM*, **52**[2] 42-44 (2000).
127. M. Reeve, “Method of Producing an Aluminum Borides,” European Patent Application 130,016 (October 14, 1987).
128. D. Mirkovic, J. Grobner, R. Schmid-Fetzer, O. Fabrichnaya, and H. L. Lukas, “Experimental Study and Thermodynamic Re-Assessment of the Al-B System,” *J. Alloy Comp*., **384**[1-2] 168-174 (2004).

Appendix A
Particle Size Distributions Measured in Isopropanol

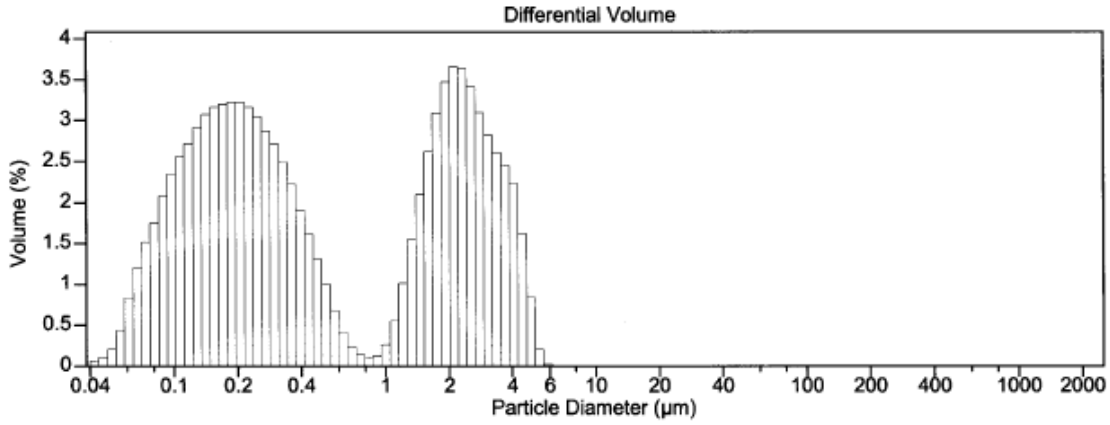

Volume Statistics (Arithmetic) 10039.$02

Calculations from 0.040 µm to 2,000 µm

Volume	100.0%		
Mean:	1.178 µm	S.D.:	1.303 µm
Median:	0.358 µm	C.V.:	111%
D(3,2):	0.252 µm		
Mode:	2.106 µm		

% <	10	25	50	75	90
Size µm	0.0996	0.162	0.358	2.097	3.205

Figure A1. Starck amorphous B.

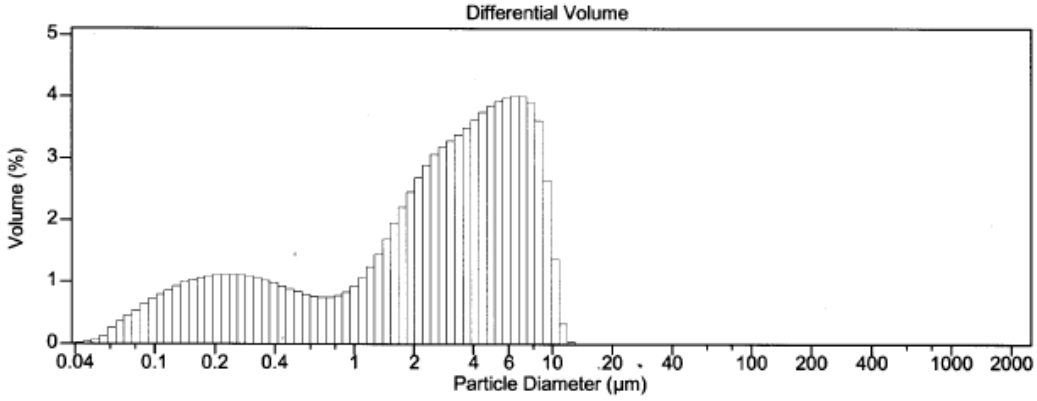

Volume Statistics (Arithmetic) 10040.$01

Calculations from 0.040 µm to 2,000 µm

Volume	100.0%		
Mean:	3.441 µm	S.D.:	2.835 µm
Median:	2.852 µm	C.V.:	82.4%
D(3,2):	0.635 µm		
Mode:	6.452 µm		

% <	10	25	50	75	90
Size µm	0.195	0.851	2.852	5.466	7.770

Figure A2. Valimet H3 Al.

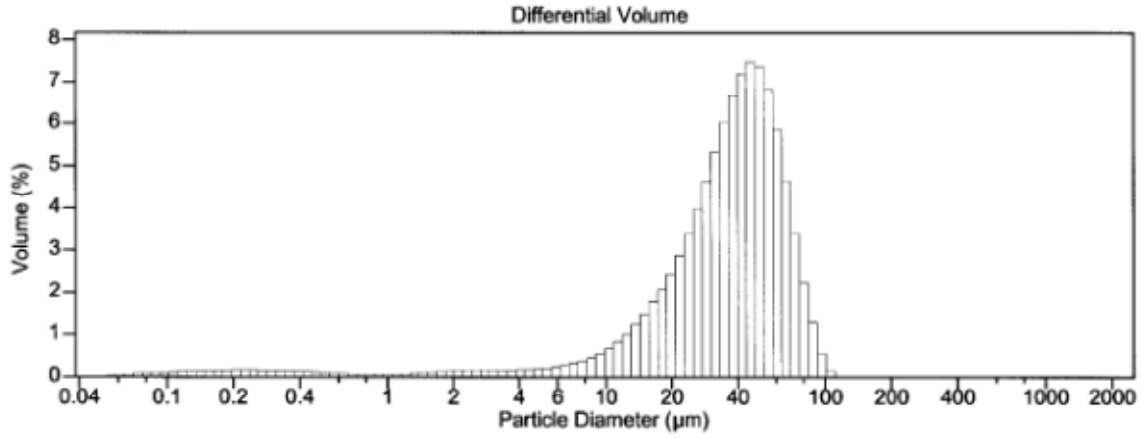

Volume Statistics (Arithmetic) 10044.$02

Calculations from 0.040 µm to 2,000 µm

Volume	100.0%		
Mean:	38.86 µm	S.D.:	20.75 µm
Median:	38.21 µm	C.V.:	53.4%
D(3,2):	4.137 µm		
Mode:	45.75 µm		

% <	10	25	50	75	90
Size µm	11.91	24.14	38.21	52.63	66.48

Figure A3. Atlantic Equipment Engineer's Mg.

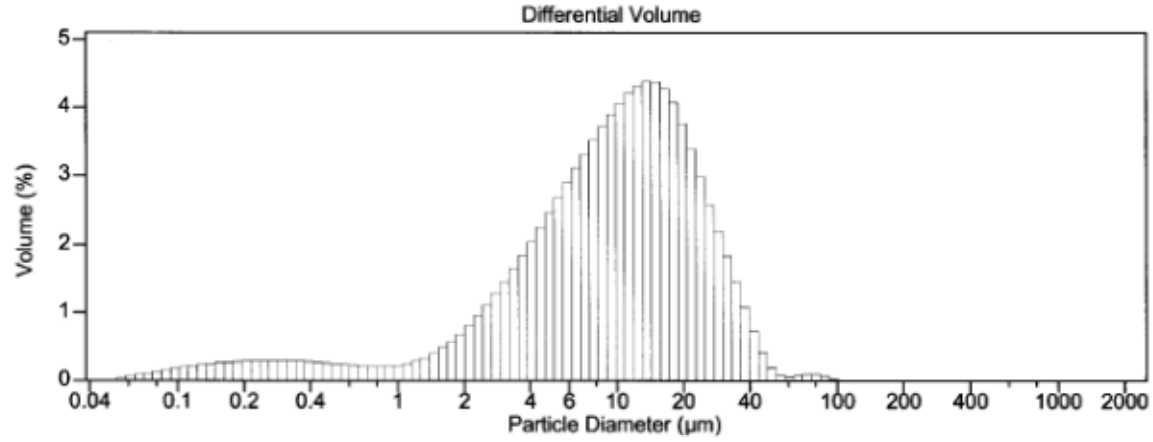

Volume Statistics (Arithmetic) 10022.$04

Calculations from 0.040 µm to 2,000 µm

Volume	100.0%		
Mean:	12.41 µm	S.D.:	10.38 µm
Median:	10.02 µm	C.V.:	83.7%
D(3,2):	2.120 µm		
Mode:	13.61 µm		

% <	10	25	50	75	90
Size µm	1.986	4.928	10.02	17.27	25.88

Figure A4. Valimet MgAl.

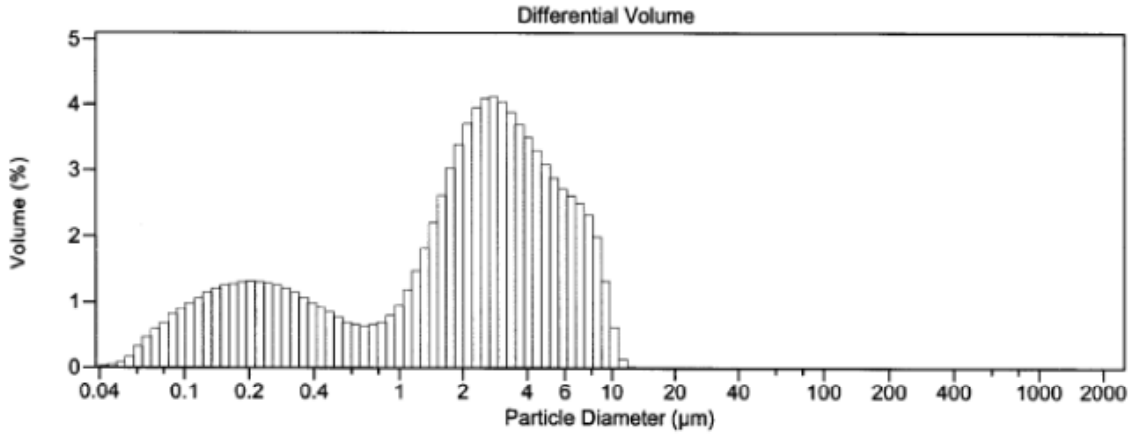

Volume Statistics (Arithmetic) 10015.$02

Calculations from 0.040 µm to 2,000 µm

Volume	100.0%		
Mean:	2.782 µm	S.D.:	2.444 µm
Median:	2.256 µm	C.V.:	87.8%
D(3,2):	0.542 µm		
Mode:	2.787 µm		

% <	10	25	50	75	90
Size µm	0.165	0.583	2.256	4.089	6.522

Figure A5. Al + 2B (MW1-90A).

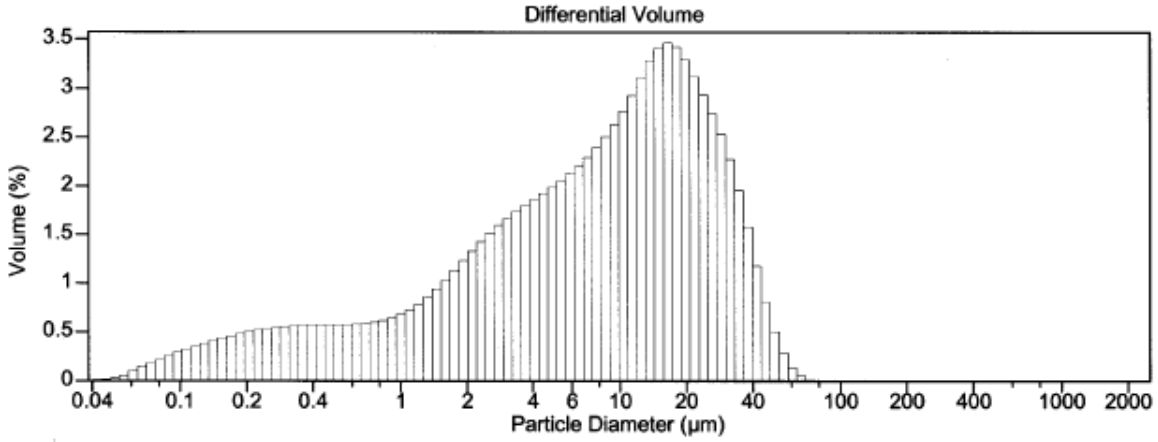

Volume Statistics (Arithmetic) 10023.$02

Calculations from 0.040 µm to 2,000 µm

Volume	100.0%		
Mean:	11.92 µm	S.D.:	11.56 µm
Median:	8.437 µm	C.V.:	97.0%
D(3,2):	1.310 µm		
Mode:	16.40 µm		

% <	10	25	50	75	90
Size µm	0.528	2.590	8.437	18.08	28.78

Figure A6. -230 mesh AlB_2 (MW1-104K).

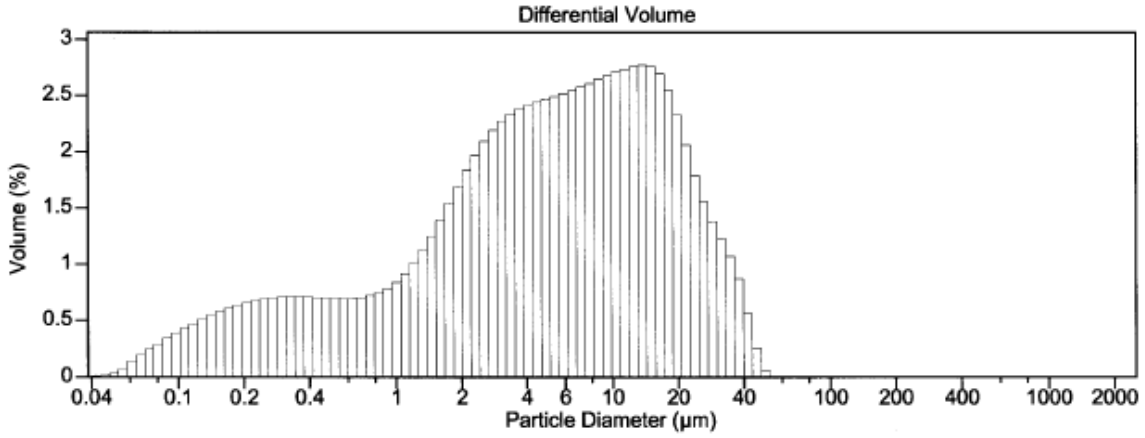

Volume Statistics (Arithmetic) 10018.$02

Calculations from 0.040 µm to 2,000 µm

Volume	100.0%		
Mean:	8.512 µm	S.D.:	9.118 µm
Median:	5.159 µm	C.V.:	107%
D(3,2):	1.016 µm		
Mode:	13.61 µm		

% <	10	25	50	75	90
Size µm	0.356	1.762	5.159	12.55	21.53

Figure A7. -325 mesh AlB_2 (MW1-104K).

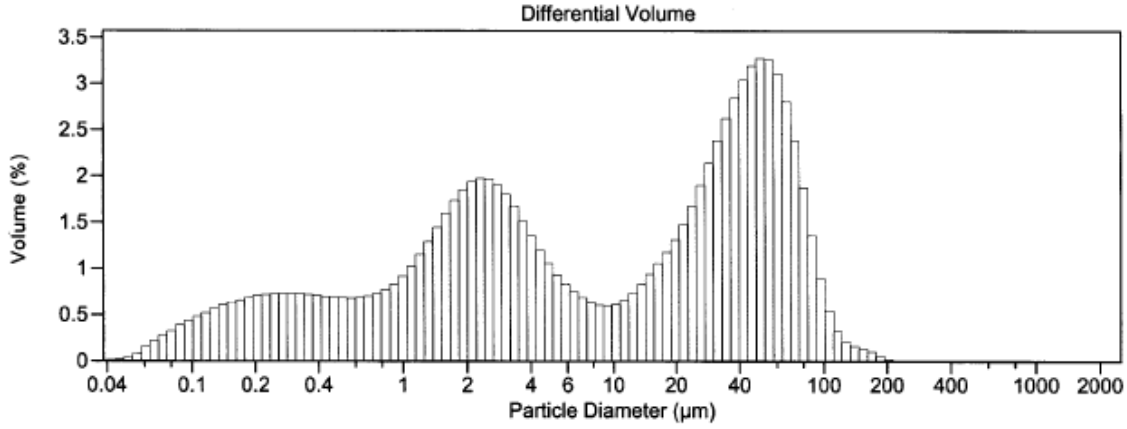

Volume Statistics (Arithmetic) 10011.$01

Calculations from 0.040 µm to 2,000 µm

Volume	100.0%		
Mean:	24.00 µm	S.D.:	28.74 µm
Median:	8.612 µm	C.V.:	120%
D(3,2):	0.982 µm		
Mode:	50.23 µm		

% <	10	25	50	75	90
Size µm	0.322	1.593	8.612	42.02	65.36

Figure A8. Mg + 2B (RC15-148C).

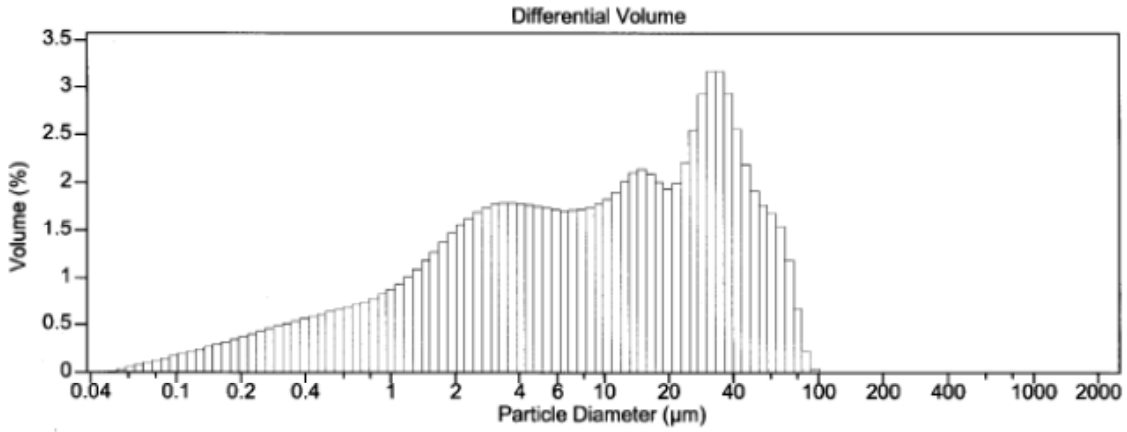

Volume Statistics (Arithmetic) 10037.$02

Calculations from 0.040 µm to 2,000 µm

Volume	100.0%		
Mean:	17.34 µm	S.D.:	19.18 µm
Median:	9.189 µm	C.V.:	111%
D(3,2):	1.620 µm		
Mode:	34.58 µm		

% <	10	25	50	75	90
Size µm	0.696	2.418	9.189	28.27	46.04

Figure A9. -230 mesh MgB_2 (MW1-116A).

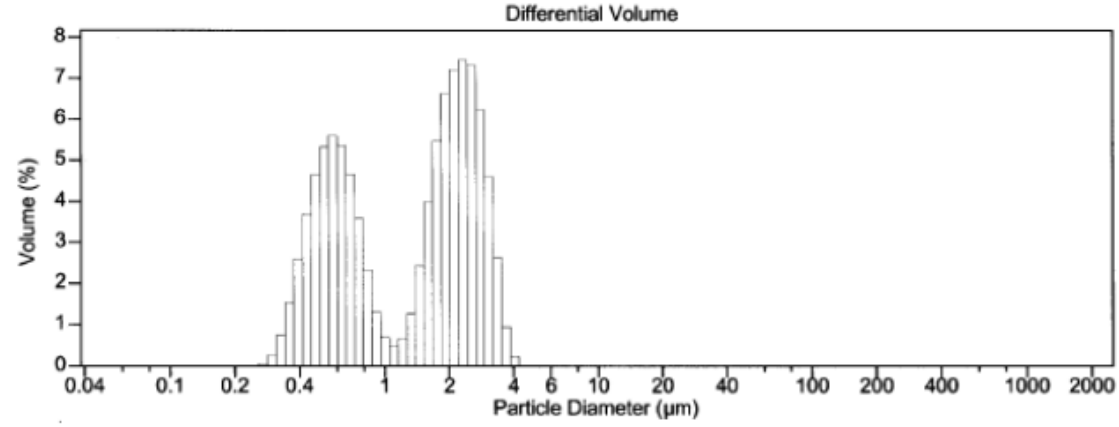

Volume Statistics (Arithmetic) 10036.$02

Calculations from 0.040 µm to 2,000 µm

Volume	100.0%		
Mean:	1.557 µm	S.D.:	0.950 µm
Median:	1.622 µm	C.V.:	61.0%
D(3,2):	0.953 µm		
Mode:	2.312 µm		

% <	10	25	50	75	90
Size µm	0.462	0.604	1.622	2.335	2.854

Figure A10. -325 mesh MgB_2 (MW1-116A).

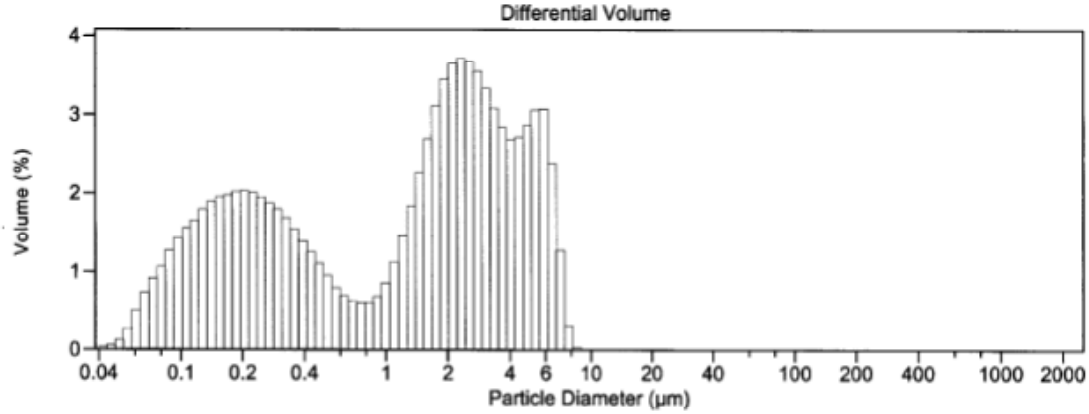

Volume Statistics (Arithmetic) 10013.$02

Calculations from 0.040 µm to 2,000 µm

Volume	100.0%		
Mean:	2.019 µm	S.D.:	1.936 µm
Median:	1.605 µm	C.V.:	95.8%
D(3,2):	0.378 µm		
Mode:	2.312 µm		

% <	10	25	50	75	90
Size µm	0.125	0.255	1.605	3.150	5.134

Figure A11. 0.5MgAl + 2B (MW1-61A).

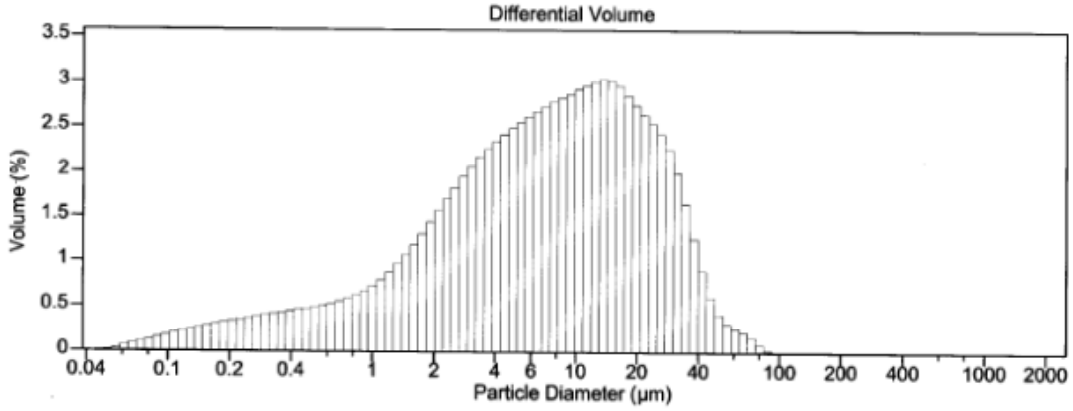

Volume Statistics (Arithmetic) 10035.$02

Calculations from 0.040 µm to 2,000 µm

Volume	100.0%		
Mean:	11.35 µm	S.D.:	11.79 µm
Median:	7.347 µm	C.V.:	104%
D(3,2):	1.696 µm		
Mode:	13.61 µm		

% <	10	25	50	75	90
Size µm	0.878	2.788	7.347	16.31	27.53

Figure A12. -230 mesh $Mg_{0.5}Al_{0.5}B_2$ (MW1-114A).

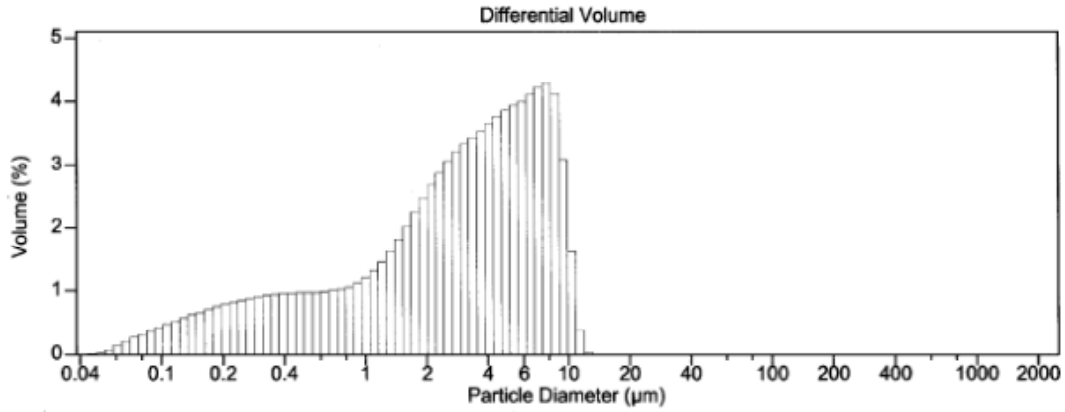

Volume Statistics (Arithmetic)			10034.$02
Calculations from 0.040 µm to 2,000 µm			
Volume	100.0%		
Mean:	3.646 µm	S.D.:	2.864 µm
Median:	3.045 µm	C.V.:	78.5%
D(3,2):	0.834 µm		
Mode:	7.776 µm		

% <	10	25	50	75	90
Size µm	0.295	1.146	3.045	5.737	8.026

Figure A13. -325 mesh $Mg_{0.5}Al_{0.5}B_2$ (MW1-114A).

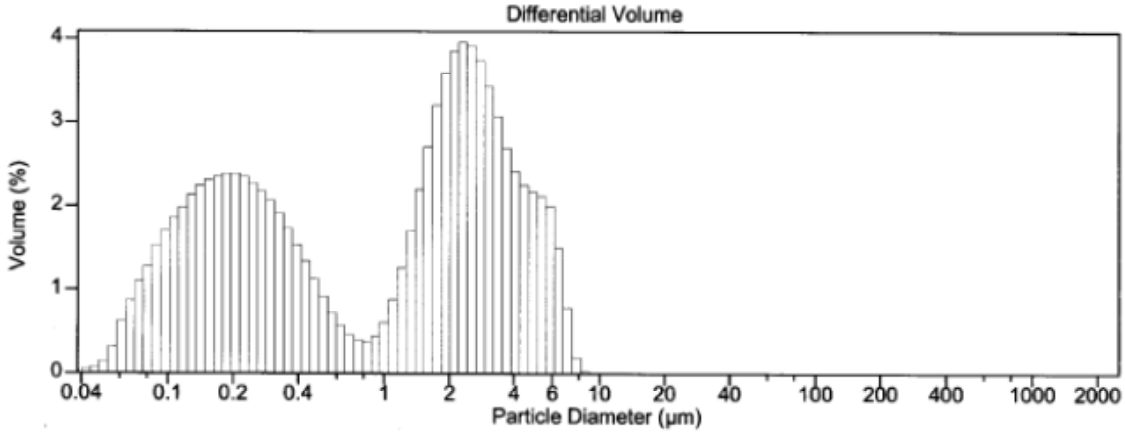

Volume Statistics (Arithmetic)			10042.$02
Calculations from 0.040 µm to 2,000 µm			
Volume	100.0%		
Mean:	1.753 µm	S.D.:	1.772 µm
Median:	1.374 µm	C.V.:	101%
D(3,2):	0.329 µm		
Mode:	2.312 µm		

% <	10	25	50	75	90
Size µm	0.114	0.212	1.374	2.757	4.431

Figure A14. Mg + Al + 14B (BI1-12D).

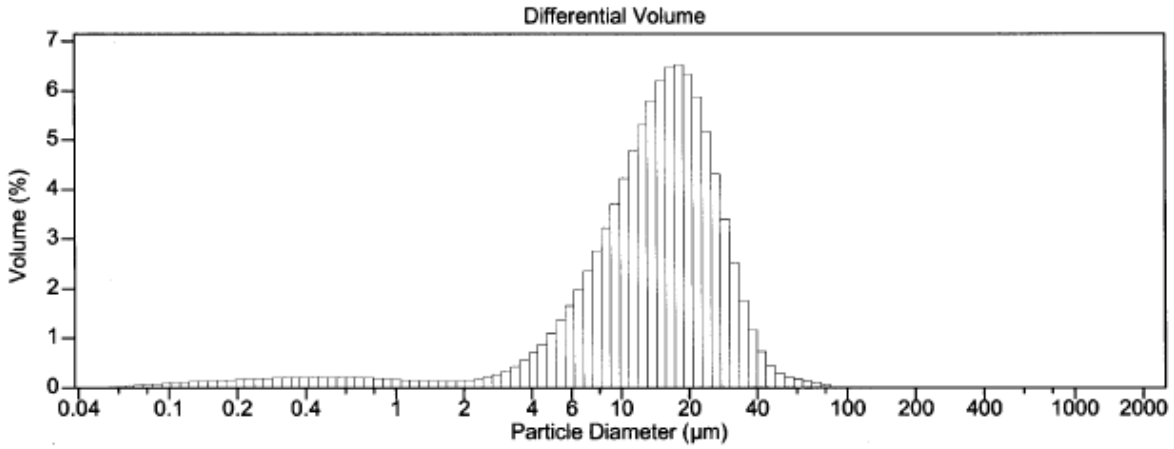

Volume Statistics (Arithmetic)			10033.$02
Calculations from 0.040 µm to 2,000 µm			
Volume	100.0%		
Mean:	15.95 µm	S.D.:	10.04 µm
Median:	14.70 µm	C.V.:	63.0%
D(3,2):	3.395 µm		
Mode:	18.00 µm		

% <	10	25	50	75	90
Size µm	4.756	9.132	14.70	21.19	28.22

Figure A15. -230 mesh $MgAlB_{14}$ (MW1-95B).

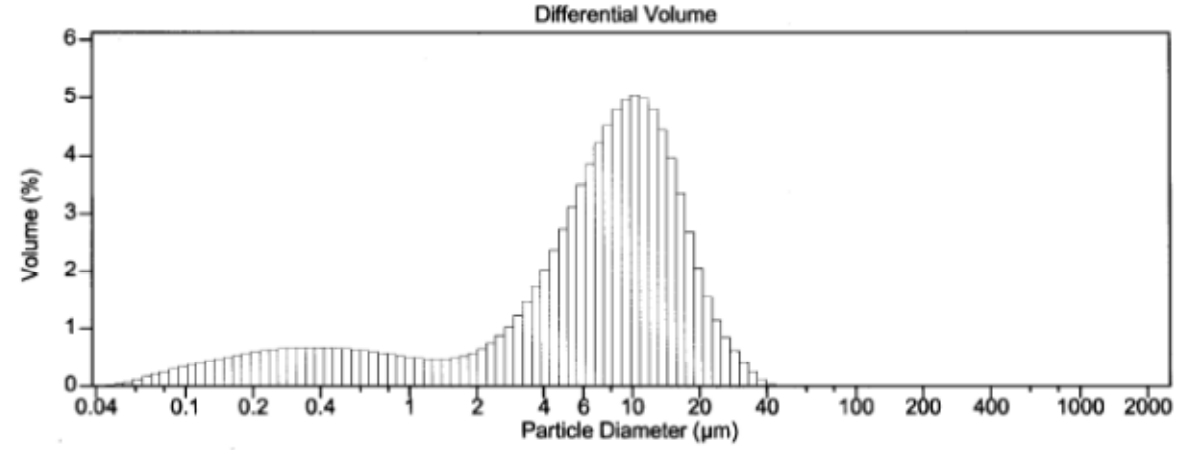

Volume Statistics (Arithmetic)			10032.$02
Calculations from 0.040 µm to 2,000 µm			
Volume	100.0%		
Mean:	8.430 µm	S.D.:	6.620 µm
Median:	7.528 µm	C.V.:	78.5%
D(3,2):	1.183 µm		
Mode:	10.29 µm		

% <	10	25	50	75	90
Size µm	0.410	3.372	7.528	12.16	17.08

Figure A16. -325 mesh $MgAlB_{14}$ (MW1-95B).

Appendix B
Particle Size Distributions for Alternative Borides (Measured in Isopropanol)

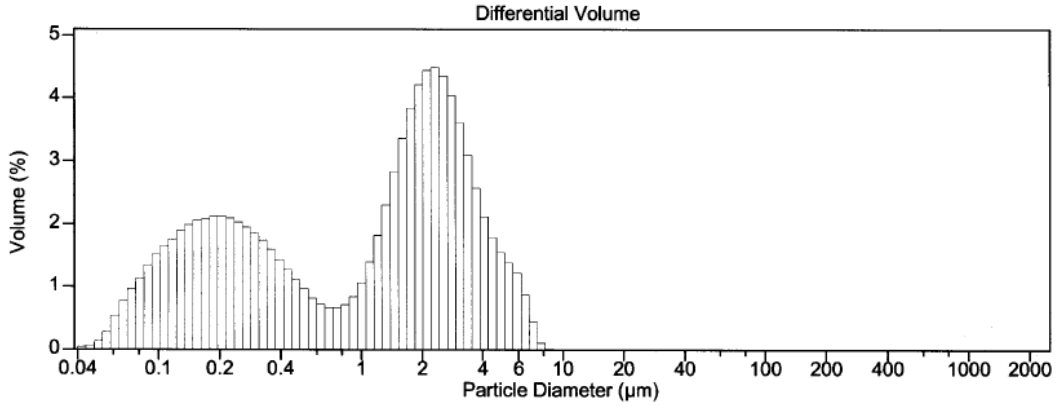

Volume Statistics (Arithmetic) 10043.$02

Calculations from 0.040 µm to 2,000 µm

Volume	100.0%		
Mean:	1.652 µm	S.D.:	1.567 µm
Median:	1.404 µm	C.V.:	94.8%
D(3,2):	0.358 µm		
Mode:	2.312 µm		

% <	10	25	50	75	90
Size µm	0.121	0.240	1.404	2.542	3.797

Figure B1. B_4C powder.

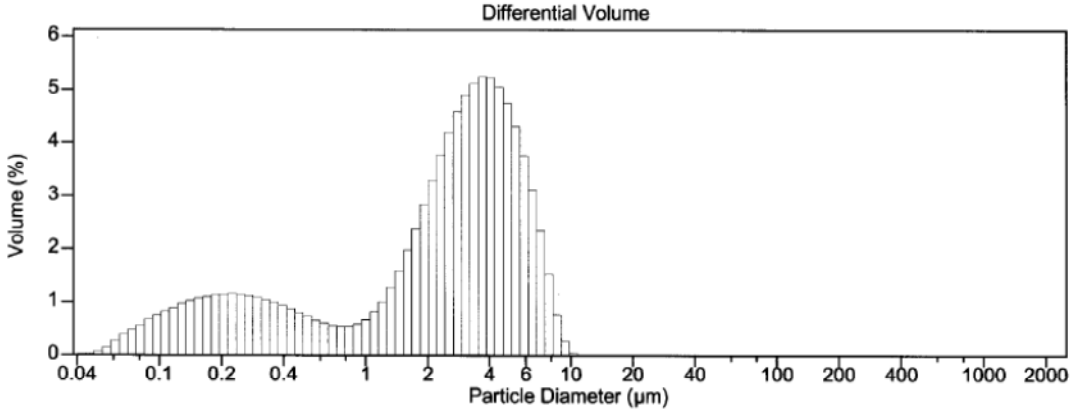

Volume Statistics (Arithmetic) 10041.$02

Calculations from 0.040 µm to 2,000 µm

Volume	100.0%		
Mean:	2.883 µm	S.D.:	2.135 µm
Median:	2.721 µm	C.V.:	74.0%
D(3,2):	0.620 µm		
Mode:	3.687 µm		

% <	10	25	50	75	90
Size µm	0.189	0.949	2.721	4.324	5.885

Figure B2. Si powder.

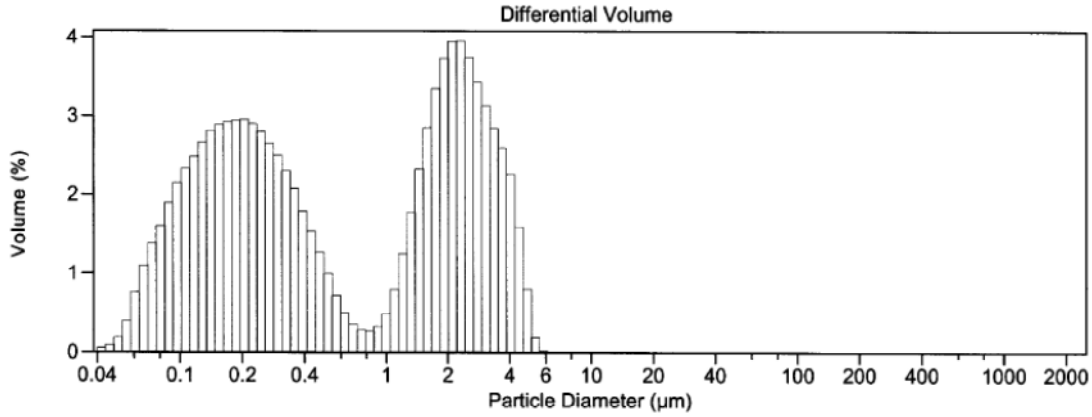

Volume Statistics (Arithmetic)			10014.$02
Calculations from 0.040 µm to 2,000 µm			
Volume	100.0%		
Mean:	1.253 µm	S.D.:	1.302 µm
Median:	0.447 µm	C.V.:	104%
D(3,2):	0.272 µm		
Mode:	2.312 µm		

% <	10	25	50	75	90
Size µm	0.103	0.174	0.447	2.186	3.239

Figure B3. Al + 12B (MW1-91A).

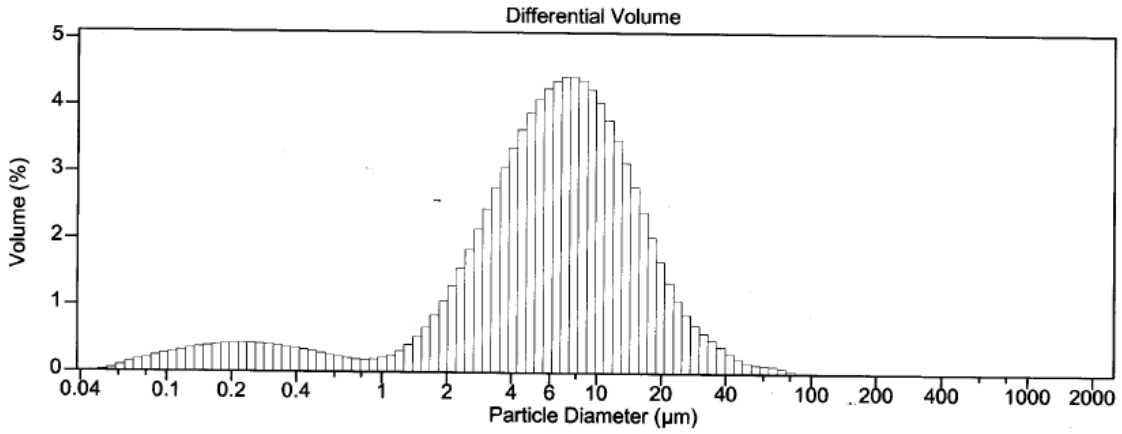

Volume Statistics (Arithmetic)			10047.$02
Calculations from 0.040 µm to 2,000 µm			
Volume	100.0%		
Mean:	8.560 µm	S.D.:	8.361 µm
Median:	6.432 µm	C.V.:	97.7%
D(3,2):	1.502 µm		
Mode:	7.776 µm		

% <	10	25	50	75	90
Size µm	1.255	3.445	6.432	11.06	17.52

Figure B4. -230 mesh AlB_{12} (MW1-91C).

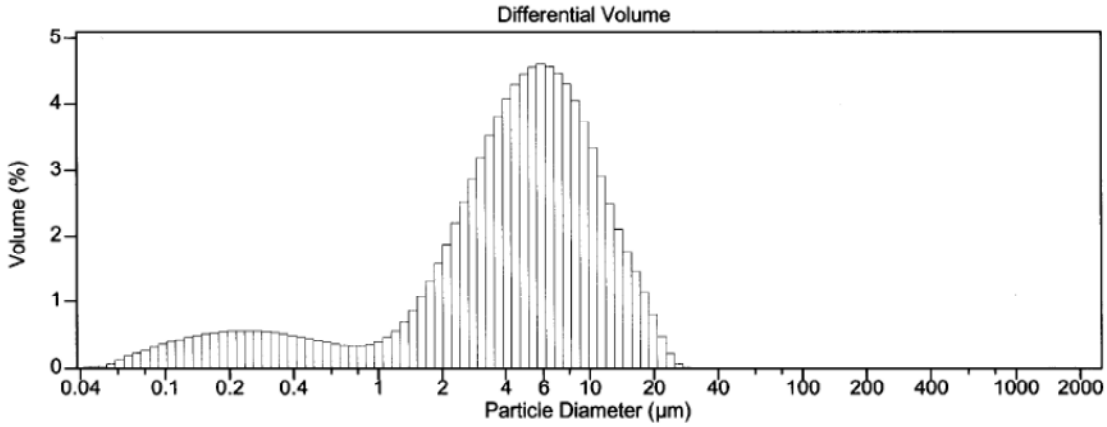

Volume Statistics (Arithmetic) 10022.$02

Calculations from 0.040 µm to 2,000 µm

Volume	100.0%		
Mean:	5.797 µm	S.D.:	4.555 µm
Median:	4.828 µm	C.V.:	78.6%
D(3,2):	1.143 µm		
Mode:	5.878 µm		

% <	10	25	50	75	90
Size µm	0.459	2.518	4.828	8.087	12.10

Figure B5. -325 mesh AlB_{12} (MW1-91C).

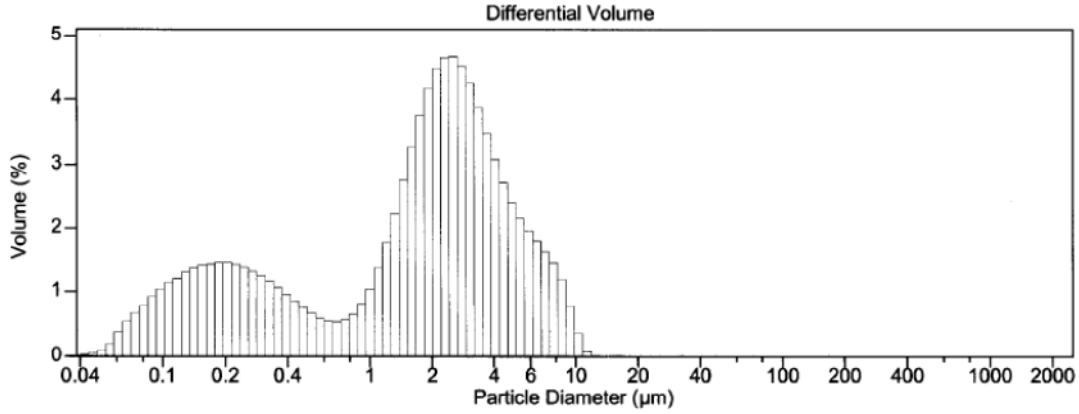

Volume Statistics (Arithmetic) 10023.$04

Calculations from 0.040 µm to 2,000 µm

Volume	100.0%		
Mean:	2.394 µm	S.D.:	2.149 µm
Median:	1.992 µm	C.V.:	89.8%
D(3,2):	0.493 µm		
Mode:	2.539 µm		

% <	10	25	50	75	90
Size µm	0.151	0.459	1.992	3.365	5.439

Figure B6. B_4C + 2Al (MW1-117B).

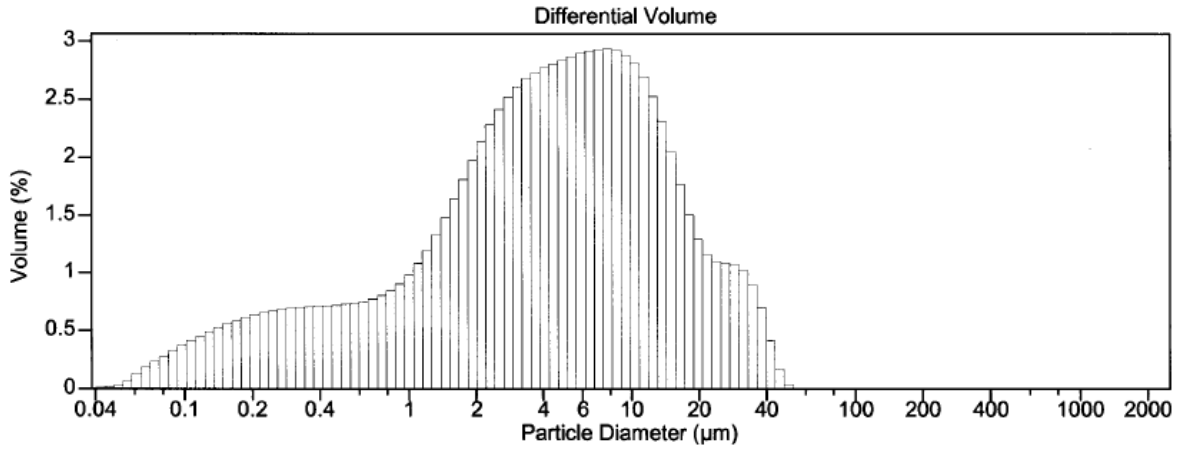

Volume Statistics (Arithmetic)			10025.$02
Calculations from 0.040 µm to 2,000 µm			
Volume	100.0%		
Mean:	7.202 µm	S.D.:	8.190 µm
Median:	4.335 µm	C.V.:	114%
D(3,2):	1.014 µm		
Mode:	7.776 µm		

Figure B7. -230 mesh AlB_3C + AlB_2 (MW1-117C).

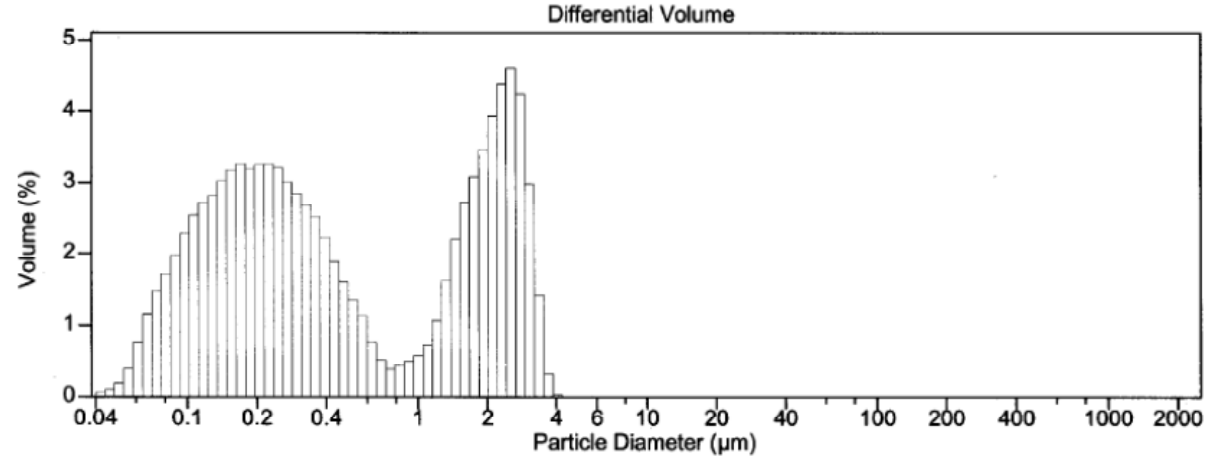

Volume Statistics (Arithmetic)			10026.$02
Calculations from 0.040 µm to 2,000 µm			
Volume	100.0%		
Mean:	0.970 µm	S.D.:	1.019 µm
Median:	0.354 µm	C.V.:	105%
D(3,2):	0.251 µm		
Mode:	2.539 µm		

% <	10	25	50	75	90
Size µm	0.101	0.165	0.354	1.856	2.611

Figure B8. Si + 6B (MW1-118A).

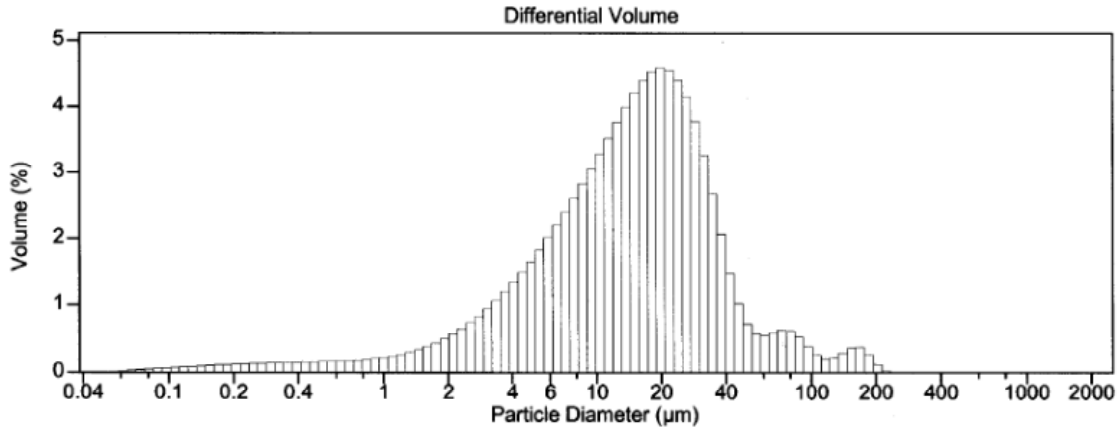

Volume Statistics (Arithmetic) 10031.$02

Calculations from 0.040 µm to 2,000 µm

Volume	100.0%		
Mean:	20.84 µm	S.D.:	24.82 µm
Median:	14.85 µm	C.V.:	119%
D(3,2):	3.974 µm		
Mode:	19.76 µm		

% <	10	25	50	75	90
Size µm	3.228	7.378	14.85	25.01	38.34

Figure B9. -230 mesh SiB_6 (MW1-118B).

Appendix C

(Paper Presented by Michael L. Whittaker at Fall MRS Meeting on 11-30-11)

Boride-Based Materials for Energetic Applications

Michael L. Whittaker,[1] Raymond A. Cutler,[2] and Paul E. Anderson[3]

[1] University of Utah, 122 S. Central Campus Drive, Salt Lake City UT, 84112
[2] Ceramatec, Inc., 2425 South 900 West, Salt Lake City, UT 84119
[3] Explosives Research and Development Branch, ARDEC, Picatinny Arsenal, NJ 07806

ABSTRACT

Metal borides (AlB_2, MgB_2, $Mg_{0.5}Al_{0.5}B_2$, AlB_{12}, SiB_6 and $MgAlB_{14}$) and boron carbide (B_4C) reacted with Al were compared to B, Mg, Al, Mg-Al and Si as potential energetic fuel additives. Stoichiometric physical mixtures of powders corresponding to unreacted boride compounds (Al+2B, Mg+2B, Mg-Al+2B, Al+12B, Si+6B, Mg-Al+14B, and B_4C+2Al) were also investigated in comparison to the compounds. Submicron boron was used, which resulted in very fine particle sizes for all materials studied. It was demonstrated that boride compounds were less sensitive to low-temperature oxidation in flowing air than physical mixtures or metallic fuels. Compounds with high mole fractions of boron were generally less sensitive, but their high temperature oxidation behavior showed no improvement over boron. Cylinder expansion testing of $MgAlB_{14}$ exposed its poor performance in an energetic mixture. However, aluminum and magnesium diborides (AlB_2, MgB_2 and $Mg_{0.5}Al_{0.5}B_2$) also had relatively low sensitivity and exhibited mechanisms to increase the rate of boron oxidation at high temperatures, showing promise as insensitive high-energy-density fuel additives. Detonation calorimetry of mixtures with AlB_2 or Al+2B suggested that the AlB_2 mixture released approximately 50% more heat per gram than Al +2B and underwent complete reaction. These results warrant further testing of the diboride compounds in energetic formulations. Due to the high cost of boron and acceptable performance of B_4C-Al mixtures, B_4C should also be investigated as a lower-cost alternative to boron.

INTRODUCTION

Boron has long been recognized as fuel for rocket boosters and other energetic applications where high energy density is required.[1,2] The heat of combustion for the oxidation of boron to boron oxide is highly exothermic on both a volumetric and gravimetric basis. The main problems with using boron have been obtaining complete combustion due to slow oxidation kinetics[1] and the high cost of the material. Metals like Al, Mg and Mg-Al have typically been used despite lower enthalpies of combustion and higher sensitivity to accidental discharge due to more favorable oxidation kinetics.

Mitani and Izumikawa[3] showed that the addition of micron sized Al to B increases its combustion efficiency in simple strand burner studies. Flower et al.[4] demonstrated a similar improvement in performance by bomb calorimetry for mechanically alloyed boron and Al powders. Hsia[2] measured ignition delay and burning time for 30-75 μm Al, Mg and Li borides in

air using optical techniques and came to the conclusion that the metal borides are superior to B for use in rocket propulsion systems due to faster ignition and complete combustion.

Mixtures of metal powders and submicron boron have not been previously tested, nor have metal borides less than 10 μm. These materials have not been compared side by side in any experimental setup. Problems associated with such fine powders include higher sensitivity and a higher concentration of inert oxide, but if boron can be made to combust completely the increase in energy density may compensate for higher oxide content. Due to the high cost of boron, alternative sources are desirable. Because B_4C is used in other industrial applications, it has the potential to be a less expensive source of boron. Recent studies by Sabatini et al.[5] showed that B_4C can work well in pyrolants. The objective of this work was to compare a variety of borides with similarly sized boron-metal mixtures for comparison in energetic mixtures.

EXPERIMENTAL PROCEDURE

Powder mixtures were made from amorphous B (H.C. Starck, 97% with 2% O and 0.8% Mg), spherical Al (Valimet H3, 99.9%), spherical Mg-Al alloy (Valimet Al-Mg alloy 55% Al-44% Mg with 0.4% Fe), Mg flake (Atlantic Equipment Engineers, 95%), atomized Si (Elkem Silgrain, 99%) and B_4C (UK Abrasives, 99%). Reacted compounds were synthesized at Ceramatec using proprietary processing.

Powder size was characterized by BET surface area and laser light scattering particle size analysis and particle morphology was investigated by scanning electron microscopy (SEM) and energy dispersive spectroscopy (EDS). Thermal gravimetric analysis (TGA) and differential thermal analysis (DTA) were used to characterize the response of the powders (50 mg samples) to oxidation in flowing air (~150cc/min). Detonation calorimetry was used to compare combustion behavior of AlB_2 and Al+2B mixtures. Cylinder expansion testing was conducted on $MgAlB_{14}$.[6] Impact, friction and shock sensitivity testing was performed on MgB_2 and AlB_2 powders by ATK.

RESULTS AND DISCUSSION

Table I gives surface area and particle size for the raw materials, mixtures, and borides. The average particle size was generally below 10 μm, although the agglomerated powders were above that size, as shown in Figure C1 for selected powders. The fine particle sizes contributed to rapid oxidation in air, with initiation between 500 and 950°C (see Table II). Increased initiation temperature is believed to be related to the sensitivity of the powder. In general, the powder mixtures were no less sensitive than the starting powders, but the reacted compounds didn't begin to oxidize until much higher temperatures.

TGA results for Al, B, Al+2B, and AlB_2 are shown in Table II. The high surface area boron exhibited faster initial oxidation kinetics than Al or AlB_2. At ≈50% conversion the oxidation of B was retarded by the formation of B_2O_3 and reached only 69% of its theoretical limit. This exemplifies the kinetic limitations of B oxidation at high temperatures. The oxidation of Al followed the general trend described in the literature[7] where polymorphic transformations in the Al_2O_3 shell gave rise to the step-like weight gain behavior. Despite the irregularity of the process, Al reached 100% of its theoretical limit. Al + 2B, with an approximately even weight distribution of Al and B, reached 85% of its theoretical weight gain, as expected. Surprisingly, AlB_2 reached 98% of its theoretical value despite having a much higher initiation temperature

Table I. Powder Size and Surface Area

Material	Surface Area (m^2/g)	Particle Size (μm) d_{10}	d_{50}	d_{90}	Mean	Calculated Particle Size (μm)*
B	10.88	0.1	0.2	3.2	1.2	0.2
Al	1.39	0.2	2.9	7.8	3.4	1.6
Mg	0.82	11.8	38.2	66.5	38.6	3.9
Mg-Al	0.40	2.0	10.0	25.9	12.4	6.8
Si	3.56	0.2	2.7	5.9	2.7	0.7
B_4C	6.92	0.1	1.4	3.8	1.7	0.3
Al + 2B	6.23	0.2	2.3	6.5	2.8	0.4
Al + 12B	9.11	0.1	0.4	3.2	1.3	0.3
Mg + 2B	6.73	0.3	8.6	65.4	24.0	0.4
½ Mg-Al + 2B	5.85	0.1	1.6	5.1	2.0	0.4
Al-Mg + 14B	7.75	0.1	1.3	4.4	1.8	0.3
Si + 6B	9.10	0.1	0.4	2.6	0.9	0.3
B_4C + 2Al	4.30	0.2	2.0	5.4	2.4	0.6
AlB_2	1.64	0.5	8.4	28.8	11.9	1.2
AlB_{12}	1.38	1.3	6.4	17.5	8.6	1.8
MgB_2	4.78	0.7	9.2	46.0	17.4	0.5
$Mg_{0.5}Al_{0.5}B_2$	2.30	0.9	7.3	27.5	11.4	0.9
$Mg_{0.78}Al_{0.75}B_{14}$	0.55	4.8	14.7	28.2	16.0	4.1
SiB_6	0.71	3.2	14.9	38.4	20.8	3.9
AlB_3C + AlB_2	2.60	0.3	4.3	17.7	7.2	0.9

*The calculated average particle size assumed monosized spheres ($d=6/(SA\cdot\rho)$).

than its constituent powders (see Figure C2). AlB_{12} and $MgAlB_{14}$, with high B contents, did not oxidize fully, although they showed the same benefits of increased insensitivity as AlB_2.

Oxidation in the Mg-B system was also promising. MgB_2 reached nearly the same extent of oxidation (90%) as the physical mixture (91%) and had a higher initiation temperature by

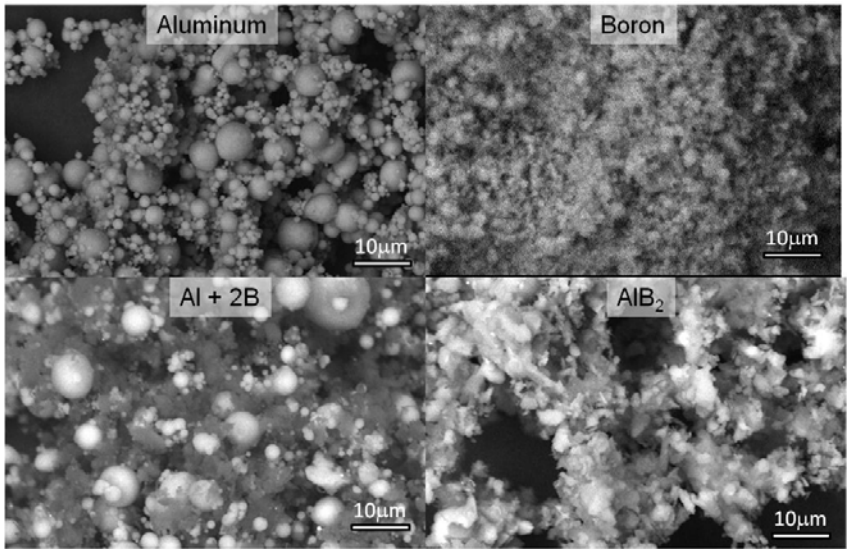

Figure C1. SEM backscattered images of selected powders. Markers are 10 μm.

Table II. Boride Powder Oxidation Characteristics

Material	Actual % Mass Change	Theoretical % Mass Change	% of Theoretical	Initiation Temp (^{0}C)*	T_{50} (^{0}C)**
B	152	222	69	563	906
Al	89	89	100	583	998
Mg	51	66	77	534	685
Mg-Al	78	78	100	527	735
Si	47	114	41	924	N/A
B_4C	100	152	65	522	825
Al + 2B	141	149	84	577	961
Al + 12B	147	199	71	543	968
Mg + 2B	126	139	91	597	802
½ Mg-Al+2B	122	146	92	596	848
Al-Mg + 14B	141	186	66	573	1088
Si + 6B	128	144	68	528	1225
$2Al + B_4C$	115	121	95	535	790
AlB_2	145	149	98	755	1074
AlB_{12}	146	199	72	746	1076
MgB_2	126	139	90	673	1107
$Mg_{0.5}Al_{0.5}B_2$	126	146	87	753	1051
$MgAlB_{14}$	135	186	64	890	1351
SiB_6	116	144	61	683	1464
AlB_3C+AlB_2	100	121	83	699	960

* Initiation temperature is reported as temperature at 5% mass gain.
** Temperature at which 50% of theoretical oxidation is reached

more than 80°C. The ternary diboride $Mg_{0.5}Al_{0.5}B_2$ was similar to MgB_2, reaching 87% of its theoretical value, while the mixture Mg-Al + 2B achieved 92% of its theoretical value.

The lowest extents of reaction were seen in Si, Si + 6B and SiB_6. Si oxidizes to SiO_2, which is more viscous than B_2O_3 and presents an even greater barrier to diffusion. When the two oxides are present concurrently they form borosilicate glassy oxides, which only exacerbate the

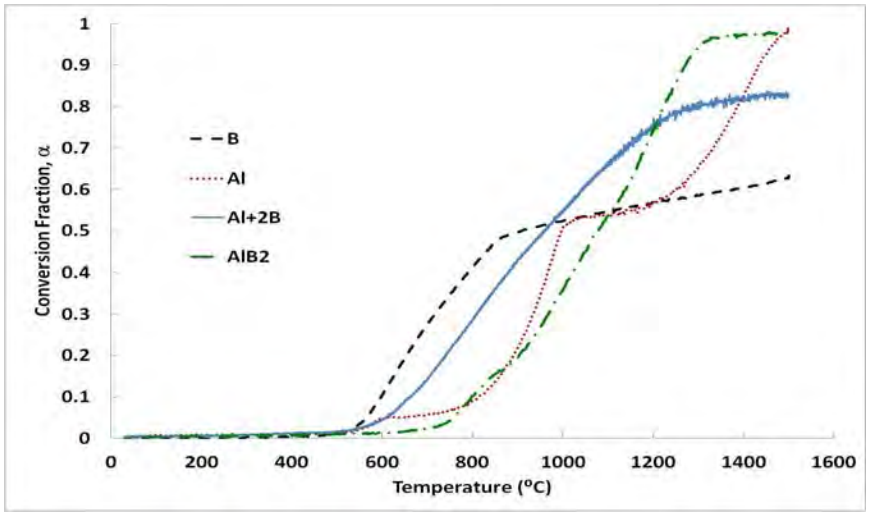

Figure C2. TGA in flowing air of B, Al, a physical mixture (Al+2B), and AlB_2.

diffusional limitations caused by B_2O_3. These materials are obviously not promising candidates for further testing.

Reaction products in the Al-B-O and Mg-B-O systems offered alternate mechanisms for oxidation that resulted in higher conversions. The main reaction products in these systems are $2Al_2O_3 \cdot B_2O_3$ ($Al_4B_2O_9$, see XRD pattern in Figure C3) and $3MgO \cdot B_2O_3$ ($Mg_3B_2O_6$), which produce solid, needle like structures on the surface of the oxidizing particle. These borates act to remove liquid B_2O_3 from the surface, exposing unoxidized material underneath and thereby increasing the rate of diffusion of oxidizer to the surface of the fuel particle. It can be seen from the stoichiometry of the borates that an Al:B or Mg:B molar ratio of 1:2 in the starting material (Al + 2B, Mg + 2B, Al-Mg + 2B, AlB_2, MgB_2 or $Mg_{0.5}Al_{0.5}B_2$) will allow for the removal of much of the B_2O_3 by Al_2O_3 or MgO through borate formation. Ratios of 1:7 and 1:12 (in Mg-Al + 14B, $MgAlB_{14}$, Al + 12B and AlB_2) do not provide significant decreases in B_2O_3 removal and because of the larger particle size of these materials they perform no better than boron.

When Al was intimately mixed with B_4C, results similar to those for Al + 2B were seen. Al greatly increased the extent of reaction for B_4C. Analysis of the reacted compound was more complicated. A 1:2 ratio of Al:B was maintained so that this system could be compared to AlB_2. The products of the reaction between Al and B_4C were Al_3BC, AlB_2 and unreacted Al and B_4C, which made determination of an oxidation mechanism more difficult. The reacted compound reached 83% of its theoretical value. Based on these results, and in light of the fact that B_4C is about 25% of the cost of boron, it is worthwhile to continue investigations into the use of B_4C as a precursor to boride compounds.

The similar extents of reaction for the diboride mixtures and compounds suggests that borate formation is not transport limited in the flowing air regime. This can be attributed to low glass transition temperature of B_2O_3, which is present as a liquid above 450°C. Subsequent tests have shown a similar situation in pure oxygen. However, in a rapid energetic event with many other components the borate formation mechanism may not provide a significant advantage if B_2O_3 is separated by more than a few nanometers from a metal oxide, as the time scale may not allow diffusion and reaction of the two oxides to occur. This gives boride compounds a distinct advantage over physical mixtures.

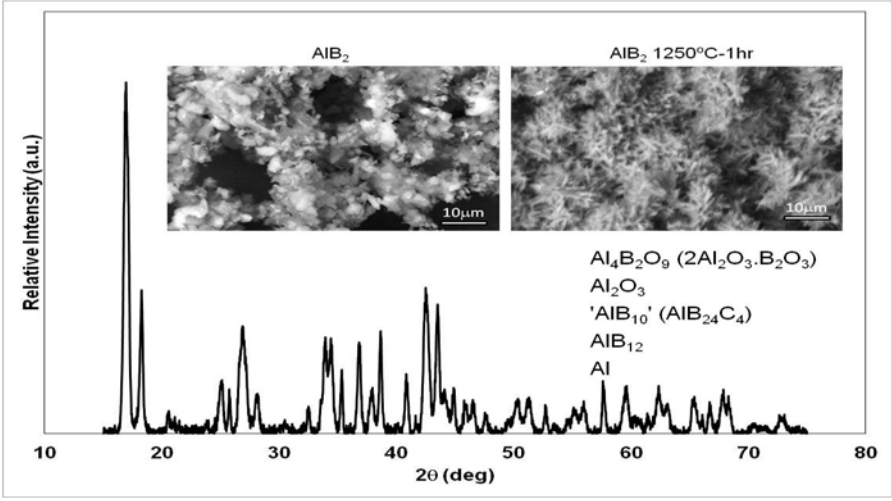

Figure C3. XRD pattern with SEM images inserted for AlB_2 oxidized in air at 1250°C for 1 hour showing needle-shaped $Al_4B_2O_9$ formation.

Detonation calorimetry was conducted on energetic mixtures containing either AlB_2 or Al + 2B to determine the effects of boride compound formation on heat release in an otherwise equivalent system. AlB_2 released about 50% more heat than Al + 2B in the proprietary energetic mixes evaluated. Cylinder expansion testing is the next step in assessing if the boride is an improvement over the metal boron mixture. Earlier cylinder expansion tests conducted on $MgAlB_{14}$ revealed that it did not perform as well as detonation models predicted. It is imperative that energetic testing, not 'static' oxidation testing, guide the development of new energetics.

Shock, impact and frication sensitivity data taken on AlB_2 and MgB_2 suggest that they are less sensitive than the conventional metal additives and are safe to handle. These borides are ready to be subjected to larger-scale testing.

CONCLUSIONS

At small particle sizes (200 nm) boron is more sensitive to low temperature oxidation in air than larger (3-40 μm) metallic fuels. At high temperatures, boron oxidation is retarded by the formation of B_2O_3, as expected, while Al and Al-Mg continue to oxidize to their theoretical limit by 1500°C.

The addition of Al, Mg and Al-Mg to B with high metal:boron ratios increases the extent of reaction of boron in flowing air. Using lower metal:boron ratios does not provide the same benefit. Silicon reduces the extent of reaction even further below that of boron due to the formation of viscous borosilicate glassy oxides. Forming boride compounds, however, decreases sensitivity to low temperature oxidation and increases the initiation temperature compared to intimate physical mixtures based on TGA testing.

Detonation calorimetry of AlB_2 and Al + 2B indicated that AlB_2 reacts completely in an energetic mixture while Al + 2B does not. AlB_2 had 50% higher heat output than Al + 2B in comparative testing. Cylinder expansion testing of these materials are needed since early testing of $MgAlB_{14}$ showed that it is not suitable for an energetic fuel additive.

While diboride materials appear promising, it is doubtful that 'static' oxidation in flowing air is any indicator of energetic performance since specific mixtures change the reaction products. Testing energetic mixtures of a wide variety of materials, such as those produced in this study, is therefore necessary to guide further development efforts. The addition of Al to B_4C to improve its oxidation characteristics is of specific interest due to the lower cost of B_4C compared to B.

REFERENCES

1. C. L. Yeh and K. K. Kuo, *Prog. Energy Comb. Sci.*, **22**[6] 511-41 (1996).
2. H. T.-S. Hsia, AFRTL-TR-71-80 (June 1971).
3. T. Mitani and M. Izumikawa, *J. Spacecraft* **28**[1] 79-84 (1991)
4. P.Q. Flower, P.A. Steward, L.R. Bates, A.J. Shakesheff, and P.W. Reip, Insensitive Munitions European Manufacturers Group (2006).
5. J. J. Sabatini, J. C. Poret, and R. N. Broad, *Angew. Chem. Int. Ed.*, **50** 4624-25 (2011).
6. M. L. Whittaker, R. A. Cutler, J. Campbell and J. LaSalvia, *Ceram. Eng. Sci. Proc.*, **31**[7] 239-250, (2010).
7. N. Eisenreich, H. Fietzek, M. d.M. Juez-Lorenzo, V. Kolarik, A. Koleczko, and V. Weiser, *Propellants Explos. Pyrotech.* **29**[3] (2004).